ABSTRACT

ERNSTBERGER, STACEY L. Sensitivity Methods for Dynamical Systems. (Under the direction of Professor H. T. Banks).

Sensitivity analysis is an important tool for researchers in a variety of fields, as it can be used in mathematical modeling to further the understanding of system dynamics. We review the usefulness of traditional and generalized sensitivity functions for general nonlinear dynamical systems for classical least squares parameter estimation problems. By analyzing the sensitivities of the logistic growth population model, we determine strengths and weaknesses of each technique when used in parameter estimation problems. We also employ sensitivity functions as tools in the formulation of data collection.

Next, we consider a hybrid biologically-based model, which couples the classical Sinko-Streifer size-structured population model to a multi-stage viral model. We model a population as the individuals move from states of healthy growth through various stages of infection. Further, partial differential equations (PDE) for sensitivities of solutions are derived with respect to rate functions associated with dynamics of the population or infection. Numerical results illustrating the use of these PDE systems are presented graphically. Additionally, we assess environmental conditions which affect the Pacific white shrimp for the growth portion of the hybrid model.

Sensitivity Methods for Dynamical Systems

by
Stacey Leigh Ernstberger

A dissertation submitted to the Graduate Faculty of
North Carolina State University
in partial fullfillment of the
requirements for the Degree of
Doctor of Philosophy

Computational Mathematics

Raleigh, North Carolina

2008

APPROVED BY:

Dr. R. H. Martin	Dr. Hien T. Tran
Dr. H. T. Banks Chair of Advisory Committee	Dr. Mansoor Haider

DEDICATION

This is dedicated to my loving husband, who has been my unwaivering support.

BIOGRAPHY

Stacey Leigh Ernstberger was born in Arlington, TX to parents Gale and Janie Lawler. She was raised in La Grange Park, IL, and decided at the age of six to (one day) become a mathematician. She later moved with her family to Franklin, TN and graduated from Centennial High School in 1999. Stacey attended Murray State University (MSU), where she earned her B.S. degree in Mathematics and Computer Science and graduated Summa Cum Laude. At MSU, Stacey met her future husband, Jon, in a mathematics reasoning class. Stacey and Jon later enrolled in graduate school at North Carolina State University (NCSU), and started the program in 2003. They were married in January 2004. While at NCSU, Stacey was awarded a fellowship from the Department of Homeland Security, and consequently interned at Oak Ridge National Laboratory under this program. The following year Stacey earned her M.S. degree in Applied Mathematics. Since that time, Stacey and her husband were blessed with a wonderful son, Lucas. All three will be relocating to LaGrange, Georgia, where Stacey and Jon have accepted positions at LaGrange College.

ACKNOWLEDGMENTS

I would like to begin by thanking Professor H. T. Banks, who has been such an amazing advisor. He has taught me to work with others, helped me grow as a person, and has provided extensive patience over these years. Without him as my advisor, I probably would have given up long ago.

Additionally at North Carolina State University (NCSU), I have learned so much from the post-doctoral researchers in the Center for Research in Scientific Computation (CRSC). In particular, Sava Dediu and Shuhua Hu have been irreplaceable. I would also like to thank the members of my doctoral committee, Professors H. T. Tran, R. H. Martin, and M. A. Haider, for graciously agreeing to devote their time and efforts, and for encouraging additional thought through questions, comments, and suggestions.

When I originally came to NCSU, I was given office space with my husband, Lara Dick and Sarah Muccio. Lara has been a wonderful friend - from the early days when we counted down until our weddings together, to the recent trips to the movies where I can escape from research for an afternoon! My other former officemate, Sarah, is one of the best friends I will ever have. We used to joke that if I wasn't with Jon, I was with her. I miss our closeness, and will visit as often as I can - she will always be family to me. Also, I want to thank Maura Chace for helping to keep me sane during my summer in Oak Ridge. I look forward to finally living near her again. I would be remiss if I did not additionally mention the wonderful support of a few others - Sarah Braun, Carrie Burns, Edna and Laddie Munger, as well as the rest of our Christian family at the Cary church of Christ. Their thoughts and prayers have meant so much to us.

I could not have made it this far in my academic career without the loving support of my family. My mom has provided me with countless hours of phone calls where I have vented, cried, and laughed about the entire process. She has even made last-minute trips to become a full-time babysitter so this degree could be possible. My dad has also supported me from the beginning, and has found a way to work a $20 into my suitcase or car everytime I see him! Someday I'll pay him back. I also want to mention my beautiful sister Carrie, who has provided guidance throughout my life. No matter where I am in life, I will always look up to her.

My grandparents have been lovingly supporting me throughout my entire life. I would like to add a special note to each one: Gramma - Thank you for all the orange slushes

and magic bars. I will never forget how much you delighted in Lucas. I miss our phone calls. Grampa - I look forward to hearing you play the harmonica next time I see you - I have a request this time: Pomp and Circumstance! Mema - I hope to one day continue my education in the ways of hypnotizing chickens. Maybe one day you can show me how it's done again! Papa - Thank you for carrying me up the stairs of the St. Louis Arch! I wish you could have met my little boy - one day I'll take him to the arch and carry him for you. And just because I know you would have asked - yes, I finally passed!

Additionally, I have had another family to call my own these last few years - my mother and father in-law (as well as the rest of the family!) have been such a blessing in my life. I didn't know how great a support group I was getting when I married Jon.

Above everyone, Jon has been my strongest supporter throughout my graduate career. He has helped me get through academic hurdles - including the dreaded qualifying exams - and has provided a balance to my life. I am a stressed person by nature, and Jon is the one who can calm and reassure me, in spite of myself. He is an amazing father to our little boy, and is my very best friend. I am blessed to have the opportunity to accompany him throughout life. In addition to Jon, there is one other smiling face to greet me every day - my little angel, Lucas. When life got hard, you came into our lives and blessed us so very much. I love you tremendously, and already dread the day that you will be too big to fall asleep in the rocking chair with me.

Thank you, Heavenly Father for life, for loving us all, for Your Son. Thank you for being in control. I look back at this list of people who have provided me with so much support in my pursuits, and know that every one of them is in my life because You put them there. I am truly blessed.

TABLE OF CONTENTS

LIST OF TABLES

LIST OF FIGURES

Chapter 1

Introduction

Sensitivity analysis of dynamical systems is of interest to numerous researchers because the resulting sensitivity functions have many applications in optimization and design [12, 24, 32, 37], computation of standard errors [5, 6, 17, 18, 35], information theory [15], and parameter estimation and inverse problems [2, 5, 6, 10, 38]. In recent years, due to a continuous need to better describe physical reality as well as a tremendous improvement in computing technology, these models have become more complex, with increased numbers of parameters. This has naturally introduced questions involving the determination of important parameters, the effects on model output due to changing parameters, etc., with answers that are not obvious for large, complex models [34]. Sensitivity analysis offers answers to these questions for problems of interest, yielding an improved understanding of the underlying mathematical model as well as better results.

General Methodology

In parameter identification studies, one typically wants to estimate model parameters from data measurements. One question of interest is the determination of which time point observations will carry the most information for the estimation of specific parameters. The information content with respect to parameter estimation may vary considerably between time measurements, and in this regard some measurements may be more informative than others. We assess and develop mathematical tools which can be used to improve the formulation of data collection, by specifying the duration and distribution of time sampling in the measurements to be taken. This improves the accuracy (i.e., reduces the uncertain-

ties) of the parameters to be estimated. In particular, we aim to determine the least final time T for successful parameter estimation. Further, we would like to find the optimal locations for a given number of data points in order to best recover the parameters. To carry this out, we assume that we have continuous time measurements and develop tools to quantify the information content with respect to our parameters.

We first address difficulties in parameter estimation problems, involving sampling data in regions of low parameter sensitivity. Then we show that the *traditional* and *generalized sensitivity functions* (GSF) can indicate regions of high information content, where if additional data points are sampled, the corresponding parameter estimates are improved [4, 38]. To present our ideas, we use the logistic growth population model as an example because it has an analytical solution, few parameters, and well-known dynamics (see [4, 6, 27]).

Hybrid Model

We next investigate sensitivities pertaining to the size-structured population model first studied by Sinko and Streifer [36] (additionally, see [27] and the related efforts of McKendrick [30] and von Forester [22]). Our motivation for investigating sensitivity for a size-structured population model originates from the study reported in [1], where a shrimp biomass production (growth) system and a related vaccine production system is modeled with a hybrid size-structured population model. The growth and mortality rates of the shrimp population are affected by several environmental factors such as temperature and salinity [26, 40]. Hence, the sensitivity of such a model with respect to the growth and mortality rates is an important factor in optimizing the entire production system.

The goal of the study pertaining to the hybrid system is to produce a maximum amount of vaccine by harvesting the shrimp population at a certain point in the infection process. Further, the population responds dramatically to changes in mortality and infection rates, and consequently we want to assess the sensitivity of the overall system to these rates. We thus derive and investigate sensitivity equations for both components of the hybrid model. The method of characteristics is a commonly used technique for establishing the existence and uniqueness of solutions to size-structured population models (see [8, 16, 25, 31]). We use this method in conjunction with the contraction mapping theorem to perform sensitivity analysis for the biomass portion of the hybrid model. We then apply the method

of characteristics to the vaccine production system to complete the sensitivity analysis of the hybrid model.

Organization

In Chapter 2 we discuss sensitivity analysis and apply the theory to the logistic growth population model. We present a short theoretical framework for least squares estimation problems, including a discussion in Section 2.1 pertaining to continuous time measurements. There we discuss *traditional* and *generalized sensitivity functions*. In Section 2.2 we relate sensitivity studies to the logistic model and perform numerical simulations to investigate the effectiveness of the GSF for improving accuracy of parameter estimates. We describe a strategy to determine the "optimal" duration time for an experiment based on the time evolution of the sensitivity functions and the condition number of the Fisher information matrix. We additionally consider sensitivity functions as tools in optimal design and present a new criterion based on finding the time distribution which gives the best discrete approximation for the continuous version of the Fisher information matrix.

In Chapter 3 we consider the hybrid biomass/vaccine production model and study the sensitivities pertaining to each model component, providing a detailed motivation for conducting the sensitivity analysis in Section 3.1. In Section 3.2 we give preliminary theoretical results that are essential to our sensitivity derivations. We perform the sensitivity analysis for the Sinko-Streifer size-structured population model used in the biomass portion of the hybrid model. Then, we formulate finite difference schemes to obtain numerical solutions of the model and sensitivities, and present numerical results. In Section 3.3 we derive the sensitivity equations pertaining to the vaccine production model, and similarly present a finite difference scheme and results of corresponding numerical simulations. Section 3.4 details the consideration of the effects of environmental conditions on the population density corresponding to the biomass model.

Finally, in Chapter 4 we give our concluding remarks and indicate directions for future work.

Chapter 2

General Methodology

We first give a general summary of the asymptotic theory for standard errors in the context of a parameter estimation problem for the general nonlinear dynamical system

$$\begin{aligned} \dot{x}(t) &= g(t, x(t), \theta) \\ x(t_0) &= x_0. \end{aligned} \tag{2.0.1}$$

We will then use this theory when investigating sensitivities for a problem of type (2.0.1), specifically we will consider the logistic growth population model as an example.

2.1 Theoretical Framework

Corresponding to system (2.0.1) is the following single-output model

$$y(t;\theta) = f(t,\theta) + \epsilon(t) = Cx(t,\theta) + \epsilon(t), \qquad 0 \le t \le T, \tag{2.1.1}$$

for the observation process. The nonlinear regression function f is assumed to be continuous and twice differentiable with respect to the parameter vector $\theta \in \mathbb{R}^p$, and C gives the observation data in terms of the components of the state variable x. Also, $\epsilon(t)$ represents the observation measurement error at time $t \in [0,T]$. The function y, which gives the measurements at any time t in $[0,T]$, is a realization of a stochastic process

$$Y(t) = f(t,\theta_0) + \mathcal{E}(t)$$

which governs the measurement process. Here, $f(t,\theta_0)$ is the (deterministic) model output corresponding to a "true" parameter θ_0, and $\mathcal{E}$ is a noisy random process. The measurement error $\epsilon(t)$ in (2.1.1) is simply a realization of $\mathcal{E}(t)$.

Standard assumptions on the noise process $\mathcal{E}(t)$ are the following:

(i) The random variables $\mathcal{E}(t)$, for $t \in [0,T]$, are independent and identically distributed.

(ii) $\mathrm{E}(\mathcal{E}(t)) = 0$ for $t \in [0,T]$.

(iii) The variance of $\mathcal{E}(t)$ is not dependent on θ, however it may be time-dependent: $\mathrm{var}(\mathcal{E}(t)) = \sigma(t)^2$, $t \in [0,T]$.

These assumptions imply that $\mathrm{E}(Y(t)) = f(t,\theta_0)$ and $\mathrm{var}(Y(t)) = \sigma(t)^2$, $t \in [0,T]$.

We now consider the case where we have n scalar longitudinal observations (with constant variance σ_0^2), and note that the extension to vectors is straightforward, see [4]. The measurements will be given as

$$y_j = f(t_j,\theta_0) + \epsilon_j, \qquad j = 1,\ldots,n$$

for "true" parameter value θ_0, and we use an ordinary least squares (OLS) approach to estimate θ_0. We seek to find a value $\hat{\theta}^n$ that minimizes the cost functional

$$J_n(\theta) = \sum_{j=1}^{n} \frac{1}{\sigma(t_j)^2}(y_j - f(t_j,\theta))^2 \tag{2.1.2}$$

over all admissible parameter vectors θ. Because $\{y_j\}$ is a realization of the random variable set $\{Y_j\}$, the estimate $\hat{\theta}^n$ we obtain by the minimization of J_n is a realization of some random variable $\hat{\Theta}^n$. Therefore, the accuracy of the parameter estimates $\hat{\theta}^n$ ultimately depends on the statistical properties of this random variable. We employ a standard error approach to qualitatively analyze the estimates.

From the asymptotic theory of statistical analysis,

$$\hat{\Theta}^n \sim \mathcal{N}_p(\theta_0,\Sigma_0) \quad \text{as} \quad n \to \infty,$$

where the covariance matrix Σ_0 is given by

$$\Sigma_0 = \sigma_0^2[\chi^T(\theta_0)\chi(\theta_0)]^{-1}, \tag{2.1.3}$$

and $\chi(\theta)$ is the $n \times p$ sensitivity matrix with elements

$$\chi_{jk}(\theta) = \frac{\partial f(t_j,\theta)}{\partial \theta_k}.$$

The covariance matrix Σ_0 is used in computing the standard errors for the estimates $\hat{\theta}^n$, which are given by

$$\mathrm{SE}_k = \sqrt{(\Sigma_0)_{kk}} = \sqrt{{\sigma_0}^2(\chi^T\chi)^{-1}_{kk}} \tag{2.1.4}$$

for $k = 1, \ldots, p$. Note that true parameter value θ_0 and variance σ_0^2 are generally unknown, and we use the approximation $\hat{\sigma}^2$ to σ_0^2 in (2.1.4) which is given by

$$\sigma_0^2 \approx \hat{\sigma}^2 = \frac{1}{n-p}\sum_{j=1}^{n} |f(t_j, \hat{\theta}^n) - y_j|^2. \tag{2.1.5}$$

Both $\hat{\sigma}^2$ and $\hat{\theta}^n$ are used in the approximation $\Sigma(\hat{\theta}^n)$ to Σ_0 in (2.1.3) with

$$\Sigma_0 \approx \Sigma(\hat{\theta}^n) = \hat{\sigma}^2[\chi^T(\hat{\theta}^n)\chi(\hat{\theta}^n)]^{-1}.$$

2.1.1 Traditional Sensitivity

Traditional sensitivity functions (TSF) are classically used in mathematical modeling to investigate how the output of a model changes when the parameters and the initial conditions vary. These functions are of interest in simulation studies (forward problems) where one must assess the degree of sensitivity of a model with respect to various parameters and to identify the parameters or the initial conditions to which the model is most/least sensitive.

We consider the dynamical system (2.0.1). In order to quantify the variation in the state variable $x(t)$ with respect to changes in the parameter θ or the initial condition $x(t_0) = x_0$, we are naturally led to consider the *traditional sensitivity functions (TSF)*

$$s_{\theta_k}(t, \theta) = \frac{\partial x}{\partial \theta_k}(t, \theta), \qquad k = 1, \ldots, p, \tag{2.1.6}$$

and

$$r_{x_{0l}}(t, \theta) = \frac{\partial x}{\partial x_{0l}}(t, \theta), \qquad l = 1, \ldots, N, \tag{2.1.7}$$

where x_{0l} is the l-th component of the initial condition x_0. When the function g (from (2.0.1)) is sufficiently regular in θ and x_0, the solution x is differentiable with respect to θ_k and x_{0l}, and therefore the sensitivity functions s_{θ_k} and $r_{x_{0l}}$ are well-defined.

Often, in practice, the model under investigation is simple enough to allow us to combine the sensitivity functions (2.1.6) and (2.1.7), as is the case with the logistic growth population example. However, when we deal with a more complex model, it is often preferable to consider these sensitivity functions separately for clarification purposes.

From sensitivity analysis theory for dynamical systems, we know $s = (s_{\theta_1}, \ldots, s_{\theta_p})$ is an $N \times p$ vector function that satisfies the ordinary differential equation (ODE) system

$$\begin{aligned} \dot{s}(t) &= g_x(t, x, \theta)s(t) + g_\theta(t, x, \theta), \\ s(t_0) &= 0_{N\times p}. \end{aligned} \tag{2.1.8}$$

Here we denote by $g_x = \partial g/\partial x$ and by $g_\theta = \partial g/\partial\theta$ the derivatives of g with respect to x and θ, respectively. Similarly, the sensitivity functions with respect to the components of the initial condition x_0 are represented by an $N \times N$ vector function $r = (r_{x_{01}}, \ldots, r_{x_{0N}})$, which satisfies

$$\begin{aligned} \dot{r}(t) &= g_x(t, x, \theta)r(t), \\ r(t_0) &= I_{N\times N}. \end{aligned} \tag{2.1.9}$$

Equations (2.1.8) and (2.1.9) are used in conjunction with system (2.0.1) to numerically compute the sensitivities s and r for general cases when the function g is complicated and a closed form solution is not easily obtained via direct integration.

In practice, parameters often have different units and state variables have varying orders of magnitude, making it more convenient in many ways to use the normalized version of the TSF, referred to as *relative sensitivity functions* (RSF). However, since we are using the standard error approach to analyze the performance of the least squares algorithm in estimating parameter values, we do not employ the RSF in most cases, and instead focus on the non-scaled sensitivities (TSF).

It is important to note that the traditional sensitivity functions depend on both t and θ, and these dependencies make the TSF suitable for use as optimal design tools. Like the partial derivatives through which they are defined, the TSF measure the rate of change of the output of a model with respect to parameters/initial conditions, but similarly have only *local character*.

For example, if the sensitivity $s_{\theta_k} = \frac{\partial x}{\partial \theta_k}(t, \theta_0)$ is near zero on a time subinterval $[\tilde{t} - \delta, \tilde{t} + \delta]$, then the model (2.0.1) and its solution are *insensitive* to the parameter θ_k on that particular interval. Hence, the state variable x will not change significantly on the time interval when the parameter θ_k varies in a neighborhood of the corresponding k-th component of θ_0. The same function, s_{θ_k}, can have large values on a different subinterval, indicating that the state variable x is *very sensitive* to θ_k on that subinterval. Intuitively, in

nonlinear regression problems where one wants to estimate θ_k from data, taking observations at time points which are within regions of high sensitivity with respect to θ_k should result in important improvements in the accuracy of the estimates for θ_k .

2.1.2 Generalized Sensitivity

Generalized sensitivity functions (GSF) were proposed by Thomaseth and Cobelli [38] as a tool in identification studies to analyze the distribution of the information content (with respect to the model parameters) of system output variables given a set of observations. However, the generalized sensitivity functions were only initially defined discretely as

$$\mathbf{gs}(t_l) = \sum_{i=1}^{l} \frac{1}{\sigma^2(t_i)} \left[F_D^{-1} \times \nabla_\theta f(t_i, \theta_0)\right] \bullet \nabla_\theta f(t_i, \theta_0), \tag{2.1.10}$$

where $\{t_l\}$, $l = 1, \ldots, n$ is the time distribution where the measurements are taken, and

$$F_D = \sum_{j=1}^{n} \frac{1}{\sigma^2(t_j)} \nabla_\theta f(t_j, \theta_0) \nabla_\theta f(t_j, \theta_0)^T \tag{2.1.11}$$

is the corresponding Fisher information matrix (FIM), denoted F_D to acknowledge that it is here defined in a discrete manner. The symbol "$\bullet$" represents element-by-element vector multiplication and for the motivation and details which led to the definition above, the interested reader may consult [10] and [38].

We note that the generalized sensitivity functions (2.1.10) are vector-valued functions having the same length as θ. The k-th component of the vector function **gs** represents the generalized sensitivity function with respect to θ_k, and we denote this $\mathbf{gs}_{\theta_k}$. The GSF are defined only at the discrete time points $\{t_j, j = 1, \ldots, n\}$. They are cumulative functions at each time point t_j, taking into account only the contributions of the measurements prior to t_j. This shows how the information associated with each measurement for the parameter estimates is distributed throughout the simulation.

From (2.1.10) it follows that all the components of **gs** equal one at the end of the time interval, i.e., $\mathbf{gs}(t_n) = \mathbf{1}$, and initially $\mathbf{gs}(t) = \mathbf{0}$ for $t < t_1$ (**gs** is zero when no measurement is collected). Then each component of **gs** varies from 0 to 1 during the experiment, not necessarily monotonically or with values remaining within $[0, 1]$. According to [38], the time subinterval during which the rate of change of $\mathbf{gs}_{\theta_k}$ has the *sharpest increase* corresponds to measurements which provide the most information on possible variations in

the corresponding true model parameter θ_k. Thus, the amount of information with respect to a parameter θ_k is directly related to the rate of change of the corresponding GSF, where regions of sharp increases in $\mathbf{gs}_{\theta_k}$ indicate a high concentration of information about θ_k.

The numerical implementation of the generalized sensitivity functions (2.1.10) is straightforward, because the gradient of f with respect to θ is simply the Jacobian of x with respect to θ multiplied by C, see (2.1.1). These Jacobian matrices can be obtained by numerically solving the sensitivity ODE system (2.1.8) or (2.1.9) coupled with (2.0.1). In many cases, the ODE is simple enough to be solved analytically.

General Formulation

It is often advantageous to consider more general measurement procedures than just a finite number of discrete time instances. We introduce the measurement density $m(t)$ at time $t \in [0,T]$, i.e., $\int_0^t m(s)\,ds$ is the number of measurements in the interval $[0,t]$. Then the cost functional (or the total weighted error) $J(y,\theta)$ can be rewritten as

$$J(y,\theta) = \int_0^T \frac{m(t)}{\sigma(t)^2}(y(t) - f(t,\theta))^2\,dt \tag{2.1.12}$$

and can be viewed as an integral of the error function

$$t \to \frac{1}{\sigma(t)^2}(y(t) - f(t,\theta))^2$$

with respect to a measure $\mathcal{P}$ on $[0,T]$ with density $m(\cdot)$ for the Lebesgue measure [21]. More generally, we shall consider least squares errors of the form

$$J(y,\theta) = \int_0^T \frac{1}{\sigma(t)^2}(y(t) - f(t,\theta))^2\,d\mathcal{P}(t) \tag{2.1.13}$$

where $\mathcal{P}$ is a general nonnegative measure on $[0,T]$. Since the minima of $J(y,\theta)$ as defined in (2.1.13) are not affected if we replace $\mathcal{P}$ with $k\mathcal{P}$ for $k > 0$, we can assume without loss of generality that $\mathcal{P}$ in (2.1.13) is a probability measure on $[0,T]$. For points $0 \le t_1 < \cdots < t_n \le T$, if we take

$$\mathcal{P} = \frac{1}{n}\sum_{i=1}^{n} \delta_{t_i} \tag{2.1.14}$$

where δ_a denotes the delta distribution with support a, then

$$J(y,\theta) = \frac{1}{n}\sum_{i=1}^{n} \frac{1}{\sigma(t)^2}(y(t_i) - f(t_i,\theta))^2 \tag{2.1.15}$$

which only varies from (2.1.2) by the normalizing factor $(n)^{-1}$.

We now consider parameter vectors θ in a neighborhood $\mathcal{U}$ about some fixed θ_0, and impose the following condition concerning local identifiability:

(iv) For any θ in a neighborhood of θ_0, the functional $\Theta \to J(f(t,\theta)+\mathcal{E}(t),\Theta)$ has a unique minimum for each realization $\epsilon(t)$ of $\mathcal{E}(t)$.

The estimator $\hat{\Theta}$ is then defined as

$$\hat{\Theta} = \arg \min_{\Theta} J(Y,\Theta),$$

and we note that $\hat{\Theta}$ is also a random variable, dependent on $Y(t)$, with estimates

$$\hat{\theta} = \arg \min_{\tau} J(y,\tau),$$

where $Y(t)$ and consequently $y(t)$ are generated based on the parameter θ in a neighborhood of θ_0. Then, for θ in a neighborhood of θ_0, assumption (iv) implies that

$$\nabla_\theta J(y,\hat{\theta}) = \nabla_\theta J(f(t,\theta)+\epsilon(t),\hat{\theta}(\theta)) = 0,$$

$$\nabla^2_{\theta\theta} J(y,\hat{\theta}) = \nabla^2_{\theta\theta} J(f(t,\theta)+\epsilon(t),\hat{\theta}(\theta)) > 0.$$

Further, $\hat{\Theta}$ satisfies the conditions

$$H_1(\theta) = \nabla_\theta J(Y,\hat{\Theta}) = \nabla_\theta J(f(t,\theta)+\mathcal{E}(t),\hat{\Theta}(\theta)) = 0,$$

$$H_2(\theta) = \nabla^2_{\theta\theta} J(Y,\hat{\Theta}) = \nabla^2_{\theta\theta} J(f(t,\theta)+\mathcal{E}(t),\hat{\Theta}(\theta)) > 0.$$

Moreover,

$$\begin{aligned} H_1(\theta) &= \nabla_\theta J(Y(t),\hat{\Theta}) \\ &= \nabla_\theta \left[\int_0^T \frac{1}{\sigma^2(t)}(Y(t)-f(t,\hat{\Theta}))^2\, d\mathcal{P}(t)\right] \\ &= -2\int_0^T \frac{1}{\sigma^2(t)}\nabla_\theta f(t,\hat{\Theta})\left[Y(t)-f(t,\hat{\Theta})\right]\, d\mathcal{P}(t) \end{aligned}$$

and

$$\begin{aligned} H_2(\theta) &= \nabla^2_{\theta\theta} J(Y(t),\hat{\Theta}) \\ &= -2\int_0^T \frac{1}{\sigma^2(t)}\left[\nabla^2_{\theta\theta} f(t,\hat{\Theta})\big(Y(t)-f(t,\hat{\Theta})\big) - \nabla_\theta f(t,\hat{\Theta})\nabla_\theta f(t,\hat{\Theta})^T\right]\, d\mathcal{P}(t), \end{aligned}$$

which we can simply write as

$$\begin{aligned} H_2(\theta) &= 2\int_0^T \frac{1}{\sigma^2(t)} \nabla_\theta f(t,\hat{\Theta}) \nabla_\theta f(t,\hat{\Theta})^T \, d\mathcal{P}(t) \\ &\quad -2\int_0^T \frac{1}{\sigma^2(t)} \nabla^2_{\theta\theta} f(t,\hat{\Theta}) \big(Y(t) - f(t,\hat{\Theta})\big) \, d\mathcal{P}(t). \end{aligned} \tag{2.1.16}$$

Recall that assumptions (i) and (ii) imply

$$\mathrm{E}[Y(t)] = \mathrm{E}[f(t,\hat{\Theta}) + \mathcal{E}(t)] = f(t,\theta),$$

as we are considering θ in a neighborhood of θ_0. Also, from asymptotic statistical theory we have that the estimator $\hat{\Theta}$ is unbiased, i.e., $\mathrm{E}[\hat{\Theta}] = \theta$. Then we note that if a given function g is linear, then $\mathrm{E}[g(\theta)] = g(\mathrm{E}[\theta])$, but this is true only to a first-order approximation when g is a general nonlinear function. In general, we only have $\mathrm{E}[g(\theta)] \approx g(\mathrm{E}[\theta])$. This linearization argument applies with regard to $\dfrac{\partial f}{\partial \theta}$, and hence the expected value of the first integral in (2.1.16) is exactly

$$2\int_0^T \frac{1}{\sigma^2(t)} \nabla_\theta f(t,\theta) \nabla_\theta f(t,\theta)^T \, d\mathcal{P}(t)$$

if we have linearity. Next, we make the tacit assumption that the scalar random variable $\big(Y(t) - f(t,\hat{\Theta})\big)$ and the elements of the random variable matrix $\nabla^2_{\theta\theta} f(t,\hat{\Theta})$ are independent, and hence the expected values of the quantities multiplied together are the product of the expected values of each component. This is the property

$$\mathrm{E}[X \cdot Y] = \mathrm{E}[X] \cdot \mathrm{E}[Y] \tag{2.1.17}$$

for independent random variables X and Y. Applying these assumptions, we see that

$$\begin{aligned} \mathrm{E}[H_2(\theta)] &\approx 2\int_0^T \frac{1}{\sigma^2(t)} \nabla_\theta f(t,\theta) \nabla_\theta f(t,\theta)^T \, d\mathcal{P}(t) \\ &\quad -2\int_0^T \frac{1}{\sigma^2(t)} \nabla^2_{\theta\theta} f(t,\theta) \big(f(t,\theta) - f(t,\theta)\big) \, d\mathcal{P}(t) \\ &= 2\int_0^T \frac{1}{\sigma^2(t)} \nabla_\theta f(t,\theta) \nabla_\theta f(t,\theta)^T \, d\mathcal{P}(t) \\ &= 2F(T) \end{aligned}$$

where F is the Fisher information matrix for a general continuum observation formulation. We now note that $H_1'(\theta) = 0$, which can be written as

$$H_1'(\theta) = \nabla^2_{\theta\theta} J(Y,\hat{\Theta}) \frac{\partial \hat{\Theta}}{\partial \theta}(\theta) + \nabla^2_{\theta y} J(Y,\hat{\Theta}) \frac{\partial Y}{\partial \theta}(\theta) = 0,$$

which (assuming the invertibility from condition (iv)) implies that

$$\frac{\partial\hat{\Theta}}{\partial\theta}(\theta) = -(\nabla^2_{\theta\theta}J(Y,\hat{\Theta}))^{-1}\nabla^2_{\theta y}J(Y,\hat{\Theta})\frac{\partial Y}{\partial\theta}(\theta). \tag{2.1.18}$$

We next argue that the second derivative $\nabla^2_{\theta y}J(Y,\hat{\Theta})$ is a Fréchet derivative, and use this to rewrite (2.1.18).

Definition 2.1.1. *The linear operator A is a Fréchet derivative of $\nabla_\theta J$ with respect to y if*

$$\lim_{h\to 0}\frac{1}{\|h\|}\left\|\nabla_\theta J(Y+h,\hat{\Theta}) - \nabla_\theta J(Y,\hat{\Theta}) - A(h)\right\| = 0.$$

We have that

$$\begin{aligned}
&\lim_{h\to 0}\frac{1}{\|h\|}\left\|\nabla_\theta\left[\int_0^T \frac{1}{\sigma^2(t)}(Y(t)+h(t)-f(t,\hat{\Theta}))^2\,d\mathcal{P}(t))\right]\right. \\
&\qquad\left. - \nabla_\theta\left[\int_0^T \frac{1}{\sigma^2(t)}(Y(t)-f(t,\hat{\Theta}))^2\,d\mathcal{P}(t))\right] - A(h)\right\| \\
= &\lim_{h\to 0}\frac{1}{\|h\|}\left\|-2\int_0^T \frac{1}{\sigma^2(t)}\nabla_\theta f(t,\hat{\Theta})\left[Y(t)+h(t)-f(t,\hat{\Theta})\right]\,d\mathcal{P}(t)\right. \\
&\qquad\left. +2\int_0^T \frac{1}{\sigma^2(t)}\nabla_\theta f(t,\hat{\Theta})\left[Y(t)-f(t,\hat{\Theta})\right]\,d\mathcal{P}(t) - A(h)\right\|
\end{aligned}$$

which further reduces to

$$\lim_{h\to 0}\frac{1}{\|h\|}\left\|-2\int_0^T \frac{1}{\sigma^2(t)}\nabla_\theta f(t,\hat{\Theta})h(t)\,d\mathcal{P}(t) - A(h)\right\|$$

and is zero when

$$A(h) = -2\int_0^T \frac{1}{\sigma^2(t)}\nabla_\theta f(t,\hat{\Theta})h(t)\,d\mathcal{P}(t).$$

Therefore,

$$\nabla^2_{\theta y}J(Y,\hat{\Theta})[h] = A(h),$$

and we see that $\nabla^2_{\theta y}J(Y,\hat{\Theta})$ is in fact a Fréchet derivative. Then we see that

$$\begin{aligned}
\nabla^2_{\theta y}J(Y,\hat{\Theta})\left[\frac{\partial Y}{\partial\theta}(\theta)\right] &= -2\int_0^T \frac{1}{\sigma^2(t)}\nabla_\theta f(t,\hat{\Theta})\cdot\left(\frac{\partial Y}{\partial\theta}(\theta)\right)^T d\mathcal{P}(t) \\
&= -2\int_0^T \frac{1}{\sigma^2(t)}\nabla_\theta f(t,\hat{\Theta})\nabla_\theta f(t,\theta)^T\,d\mathcal{P}(t),
\end{aligned}$$

and, again using a first order approximation,

$$\begin{aligned}
\mathrm{E}\left[\nabla^2_{\theta y}J(Y,\hat{\Theta})\frac{\partial Y}{\partial\theta}(\theta)\right] &\approx -2\int_0^T \frac{1}{\sigma^2(t)}\nabla_\theta f(t,\theta)\nabla_\theta f(t,\theta)^T\,d\mathcal{P}(t) \\
&= -2F(T).
\end{aligned}$$

Next we take the expected value of (2.1.18), but must first assume that $\left(\nabla^2_{\theta\theta}J\big(Y,\hat{\Theta}\big)\right)^{-1}$ and $\nabla^2_{\theta y}J\big(Y,\hat{\Theta}\big)\left[\frac{\partial Y}{\partial\theta}(\theta)\right]$ are independent $p\times p$ random variables. Then, by (2.1.17), we have

$$\begin{aligned}
\mathrm{E}\left[\frac{\partial\hat{\Theta}}{\partial\theta}(\theta)\right] &= \mathrm{E}\left[-(\nabla^2_{\theta\theta}J(Y,\hat{\Theta}))^{-1}\nabla^2_{\theta y}J(Y,\hat{\Theta})\left[\frac{\partial Y}{\partial\theta}(\theta)\right]\right]\\
&= -\mathrm{E}\left[(H_2(\theta))^{-1}\nabla^2_{\theta y}J(Y,\hat{\Theta})\left[\frac{\partial Y}{\partial\theta}(\theta)\right]\right]\\
&= -\mathrm{E}\left[(H_2(\theta))^{-1}\right]\mathrm{E}\left[\nabla^2_{\theta y}J(Y,\hat{\Theta})\left[\frac{\partial Y}{\partial\theta}(\theta)\right]\right]\\
&\approx -(2F(T))^{-1}(-2F(T))\\
&= F^{-1}(T)F(T)\\
&= I_{p\times p}.
\end{aligned}$$

We can now consider the expected values of $\dfrac{\partial\hat{\Theta}}{\partial\theta}$ for all $t\in[0,T]$,

$$\begin{aligned}
\mathrm{E}\left[\frac{\partial\hat{\Theta}}{\partial\theta}(\theta)\right](t) &= \mathrm{E}\left[(H_2(\theta))^{-1}\cdot 2\int_0^t\frac{1}{\sigma^2(t)}\nabla_\theta f(t,\hat{\Theta})\nabla_\theta f(t,\theta)^T\,d\mathcal{P}(t)\right]\\
&\approx (2F^{-1}(T))\cdot 2\int_0^t\frac{1}{\sigma^2(t)}\nabla_\theta f(t,\theta)\nabla_\theta f(t,\theta)^T\,d\mathcal{P}(t)\\
&= F^{-1}(T)F(t),
\end{aligned}$$

where the above arguments are heuristic in that tacit assumptions (generally unverifiable) of independence have been made. If the θ_i values are independent, $\mathrm{E}\left[\frac{\partial\hat{\Theta}}{\partial\theta}\right]$ is just a diagonal matrix. Although this is generally not the case, this provides motivation for looking at the diagonal components of $\mathrm{E}\left[\frac{\partial\hat{\Theta}}{\partial\theta}\right](t)$:

$$\begin{aligned}
gs_k(t) &= \left(F^{-1}(T)\int_0^t\frac{1}{\sigma^2(t)}\nabla_\theta f(t,\theta)\nabla_\theta f(t,\theta)^T\,d\mathcal{P}(t)\right)_{kk}\\
&= \big(F^{-1}(T)F(t)\big)_{kk}
\end{aligned}$$

for $k=1,\ldots,p$, which are the *generalized sensitivity functions* for the general continuum case.

2.2 Application to Logistic Model

In order to illustrate traditional and general sensitivities in applications to an ODE system, we start by considering the logistic growth (Verhulst-Pearl) equation, which

approximates the evolution of a population size over time [27], i.e.,

$$\frac{dx}{dt} = rx\left(1 - \frac{x}{K}\right). \tag{2.2.1}$$

The constants K and r represent the carrying capacity and the intrinsic growth rate, respectively. The solution $x(t)$ of (2.2.1), representing the population number at time t, is given by

$$x(t) = \frac{K}{1 + \left(\frac{K}{x_0} - 1\right)e^{-rt}}, \tag{2.2.2}$$

where $x_0 = x(0)$ is the initial population size. The solution $x(t)$ approaches an asymptote at $x = K$ when $t \to \infty$, as can be seen in the graph of $x(t)$ in Figure 2.1.

The Verhulst-Pearl logistic equation is a relatively simple example with clear dynamics that can be used to demonstrate the utility of the traditional sensitivity functions as well as the generalized sensitivity functions in parameter estimation problems. Unless data is sampled from regions with changing dynamics, it is possible that there will be difficulty estimating some of the parameters. The parameters that are obtainable may have high standard errors as a result of introducing redundancy to the sampling region [6]. In order to demonstrate this phenomenon for the logistic growth problem, we will examine varying behavior in the model depending on the region from which t_j is sampled. We consider points τ_1 and τ_2, as depicted in Figure 2.1, partitioning the curve into three distinct regions: $0 < t_j < \tau_1$, $\tau_1 < t_j < \tau_2$, and $\tau_2 < t_j < T$, for T sufficiently large for the solution to closely approximate its steady state. We expect differences in the ability to estimate parameters based upon solution dynamics in these differing regions of observation.

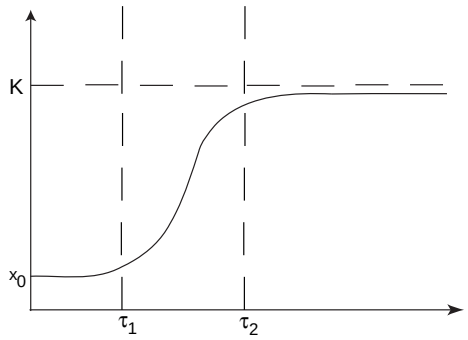

Figure 2.1: Partition of solution curve into distinct regions.

2.2.1 Traditional Sensitivity

We perform estimation procedures for $\theta = (K, r, x_0)$ in the logistic growth population model using ordinary least square procedures with both exact (no-noise) and noisy simulated data. We created a simulated data set $\{y_j\}_{j=1}^n$ by evaluating the solution (2.2.2) at t_j with the "true" value parameters θ_0. We minimize the cost functional

$$J_n(\theta) = \sum_{j=1}^{n} |f(t_j, \theta) - y_j|^2 \tag{2.2.3}$$

with respect to θ, using an initial estimate θ^0 for the optimization algorithm. Because we have a small dimension parameter space, a Nelder-Mead optimization routine is sufficient for this problem. In order to avoid what is typically called an inverse crime, we evaluate f in the cost function using a numerical ODE solver, which returns the numerical approximation to the solution $f(t, \theta) = x(t; K, r, x_0)$, rather than using the analytical solution. We consider a specific example [6], with $\theta_0 = (K, r, x_0) = (17.5, 0.7, 0.1)$.

As stated earlier, we consider an ordinary least squares problem for the parameters $\theta = (K, r, x_0)$ in (2.2.2) with the corresponding estimate of the standard error

$$\mathrm{SE}_k = \sqrt{\hat{\sigma}^2 (\chi^T \chi)^{-1}_{kk}}, \qquad k = 1, 2, 3. \tag{2.2.4}$$

The approximate covariance matrix is given by

$$\begin{aligned} \Sigma &= \hat{\sigma}^2 \big(\chi^T \chi\big)^{-1} \\ &= \frac{1}{n-p} \sum_{j=1}^{n} \big(f\big(t_j, \hat{\theta}\big) - y_j\big)^2 \big(\chi^T \chi\big)^{-1}, \end{aligned} \tag{2.2.5}$$

where $\sum_{j=1}^{n} (f(t_j, \hat{\theta}) - y_j)^2$ is the residual sum of squares (RSS). The partial derivatives

$$\begin{aligned} \frac{\partial x}{\partial K} &= \frac{x_0^2 (1 - e^{-rt})}{(x_0 + (K - x_0)e^{-rt})^2}, \\ \frac{\partial x}{\partial r} &= \frac{K x_o (K - x_0) t e^{-rt}}{(x_0 + (K - x_0)e^{-rt})^2}, \\ \frac{\partial x}{\partial x_0} &= \frac{K^2 e^{-rt}}{(x_0 + (K - x_0)e^{-rt})^2}, \end{aligned} \tag{2.2.6}$$

are the traditional sensitivity functions s_K, s_r and s_{x_0}. The matrix χ is composed of these

partial derivatives evaluated at points $t = t_1, \ldots, t_n$, i.e.,

$$\chi = \begin{pmatrix} \frac{\partial x(t_1)}{\partial K} & \frac{\partial x(t_1)}{\partial r} & \frac{\partial x(t_1)}{\partial x_0} \\ \vdots & \vdots & \vdots \\ \frac{\partial x(t_n)}{\partial K} & \frac{\partial x(t_n)}{\partial r} & \frac{\partial x(t_n)}{\partial x_0} \end{pmatrix}.$$

Then

$$\chi^T\chi = \sum_{j=1}^{n} \begin{pmatrix} \left(\frac{\partial x(t_j)}{\partial K}\right)^2 & \frac{\partial x(t_j)}{\partial K}\frac{\partial x(t_j)}{\partial r} & \frac{\partial x(t_j)}{\partial K}\frac{\partial x(t_j)}{\partial x_0} \\ \frac{\partial x(t_j)}{\partial r}\frac{\partial x(t_j)}{\partial K} & \left(\frac{\partial x(t_j)}{\partial r}\right)^2 & \frac{\partial x(t_j)}{\partial r}\frac{\partial x(t_j)}{\partial x_0} \\ \frac{\partial x(t_j)}{\partial x_0}\frac{\partial x(t_j)}{\partial K} & \frac{\partial x(t_j)}{\partial x_0}\frac{\partial x(t_j)}{\partial r} & \left(\frac{\partial x(t_j)}{\partial x_0}\right)^2 \end{pmatrix}$$

can be used in the approximation (2.2.5).

Analytical Considerations

We examine varying model behavior and the resulting statistical analysis based on the region from which t_j is sampled. To this end, we divide the entire sampling region into three sections: where $t \in [0, \tau_1]$, $t \in [\tau_1, \tau_2]$, and $t \in [\tau_2, \infty)$ as depicted in Figure 2.1, and will consider each section separately. We expect differences in the ability to estimate parameters depending on the region in which the solution is observed. In order to consider the problem for data in different regions, we use the explicit solution of (2.2.1), given by (2.2.2), and then examine the partial derivatives $\frac{\partial x}{\partial K}$, $\frac{\partial x}{\partial r}$, and $\frac{\partial x}{\partial x_0}$. We readily see that $x(t) \to K$ as $t \to \infty$ and $x(t) \to x_0$ as $t \to 0$. The process is as follows:

1. We analyze the TSF corresponding to each parameter in the initial region of the curve, where the solution approaches x_0. When we consider this region, where $0 < t_j < \tau_1$ for $j = 1, \ldots, n$, we have

$$\frac{\partial x(t_j)}{\partial K} \approx 0, \qquad \frac{\partial x(t_j)}{\partial r} \approx 0, \qquad \frac{\partial x(t_j)}{\partial x_0} \approx 1,$$

as a result of taking the limits of the sensitivity functions (2.2.6) as $t \to 0$. Based on the above analytical findings, which indicate low sensitivities with respect to K and r on $[0, \tau_1]$, we expect to have no accuracy in determining these parameters; however, we should be able to estimate x_0. Also note that

$$\sum_{j=1}^{n} \frac{\partial x(t_j)}{\partial x_0}\frac{\partial x(t_j)}{\partial x_0} \approx \sum_{j=1}^{n} 1 = n$$

for $t_j < \tau_1$, and hence, in this region we can make the approximation

$$\chi^T\chi \approx \begin{pmatrix} 0 & 0 & 0 \\ 0 & 0 & 0 \\ 0 & 0 & n \end{pmatrix}. \tag{2.2.7}$$

As additional data points are sampled from $[0, \tau_1]$, we expect that SE_K and SE_r will increase because the first two diagonal elements of $(\chi^T\chi)^{-1}$ become unbounded.

2. We next consider the region of the curve which has an asymptote at $x = K$, where $\tau_2 < t_j < T$ for $j = 1, \ldots, n$. Here we find that by taking the limits as $t \to \infty$, we may make the approximations

$$\frac{\partial x(t_j)}{\partial K} \approx 1, \qquad \frac{\partial x(t_j)}{\partial r} \approx 0, \qquad \frac{\partial x(t_j)}{\partial x_0} \approx 0.$$

Based on these approximations, we expect to be able to estimate K when we sample data from $[\tau_2, T]$. However, in this region we do not expect to be able to estimate x_0 or r using this data only. Again, we note that

$$\sum_{j=1}^{n} \frac{\partial x(t_j)}{\partial K} \frac{\partial x(t_j)}{\partial K} \approx \sum_{j=1}^{n} 1 = n$$

for $\tau_2 < t_j < T$, and hence when sampling in this region

$$\chi^T\chi \approx \begin{pmatrix} n & 0 & 0 \\ 0 & 0 & 0 \\ 0 & 0 & 0 \end{pmatrix}. \tag{2.2.8}$$

The ill-posedness (ill-conditioning) of $\chi^T\chi$ can be expected to become more severe and SE_{x_0} and SE_r will increase as more data points are sampled from $[\tau_2, T]$.

3. Finally we consider the part of the solution curve that has changing dynamics, where $\tau_1 < t_j < \tau_2$ for $j = 1, \ldots, n$. We note that the partial derivative values differ greatly from the values in regions $[0, \tau_1]$ and $[\tau_2, T]$, and in general the matrix $\chi^T\chi$ is well-conditioned. Also, estimating θ with reasonable standard errors is possible, and using more data (within reason) will improve reliability (i.e., the corresponding standard errors). When $[\tau_1, \tau_2]$ is included in the sampling region we should be able to recover good estimates for all three parameters.

Correlation

Before we perform the supporting numerical simulations, we add a note regarding the significance of the correlation coefficients for the parameter set. Recall that correlation coefficients range from -1 to 1, where higher magnitudes indicate stronger correlation between the corresponding parameters. Positive values indicate that the parameters vary together; likewise, negative coefficients indicate that the parameters vary in opposite directions. The correlation coefficients displayed in Table 2.1 were computed using the standard definition

$$\operatorname{corr}(X,Y) = \frac{\operatorname{cov}(X,Y)}{\sigma_X \sigma_Y}$$

where X and Y are two random variables with variances σ_X^2 and σ_Y^2. From the asymptotic theory of statistical analysis for the least square algorithm, the parameter estimates $\hat{\theta}^n$ can be interpreted as realizations of a random variable $\hat{\Theta}^n$, which has a normal distribution when $n \to \infty$, i.e. $\hat{\Theta}^n \sim \mathcal{N}_p\left(\theta_0, \sigma_0^2 \left(\chi^T \chi\right)^{-1}\right)$. Then the correlation coefficient between two components of θ is given by

$$\operatorname{corr}(\theta_k, \theta_l) = \frac{\operatorname{cov}(\theta_k, \theta_l)}{\sigma_{\theta_k} \sigma_{\theta_l}}.$$

Using the definition of the covariance matrix, $\operatorname{cov}(\theta_k, \theta_l)$ is simply the (k,l)-th element of $\sigma_0^2 \left(\chi^T \chi\right)^{-1}$ and the standard deviations σ_{θ_k} and σ_{θ_l} are the square roots of the (k,k)-th and (l,l)-th diagonal entries.

In [6], the logistic model was considered and analyzed with regard to traditional sensitivity functions, however the model was set up with a different parameterization: instead of $\theta = (K, r, x_0)$, the parameter set was given by $\beta = (a, b, x_0) = \left(r, \frac{r}{K}, x_0\right)$. By studying the TSF curves with the β parameterization, there was no difficulty in predicting the regions in which the state was sensitive to each parameter with no consideration given to the correlation coefficients. With the original parameterization, $\theta = (K, r, x_0)$, the correlation between the coefficients has a direct affect on our ability to predict the sensitivity corresponding to each parameter. In particular, we note that the correlation is very high

Table 2.1: Correlation coefficients for each parameter

	K	r	x_0
K	1.0000	-0.34339	0.28546
r	-0.34339	1.0000	-0.97714
x_0	0.28546	-0.97714	1.0000

between r and x_0, see Table 2.1. We observe the significance of the correlation between the parameters in the following numerical simulations.

Numerical Simulations with Noise-Free Data

To illustrate our previous analytical arguments in a computational sense, we perform several simulations using the example of the logistic equation with $\theta_0 = (K, r, x_0) = (17.5, 0.7, 0.1)$, and we see this curve plotted in Figure 2.2.

Our analytical observations are supported by the graphs of the TSF and RSF illustrated in Figure 2.3 for $T = 25$. We use s_{θ_k} and rs_{θ_k}, respectively, to denote the traditional and relative sensitivities of the solution with respect to θ_k. We note that

$$rs_{\theta_k} = \frac{\partial x}{\partial \theta_k} \cdot \frac{\theta_k}{x} = s_{\theta_k} \cdot \frac{\theta_k}{x}.$$

We observe in Figure 2.3(a) that the curve s_K slowly increases with time and the solution appears insensitive to K until the inflection point of the logistic curve (which occurs shortly after $t = 7$). Also, we notice that s_{x_0} and s_r are nearly zero in [15,25], suggesting that we will be unable to recover x_0 or r there. In Figure 2.3(b) we have the graphs of the sensitivities relative to the parameter sizes. We now see that the sensitivities rs_K and rs_r are both small when t is close to zero, and we deduce that K and r will be difficult (or impossible) to recover in that region. This is consistent with our previous estimation to the sensitivity matrix $\chi^T\chi$, see (2.2.7). We again notice that rs_{x_0} and rs_r are nearly zero in

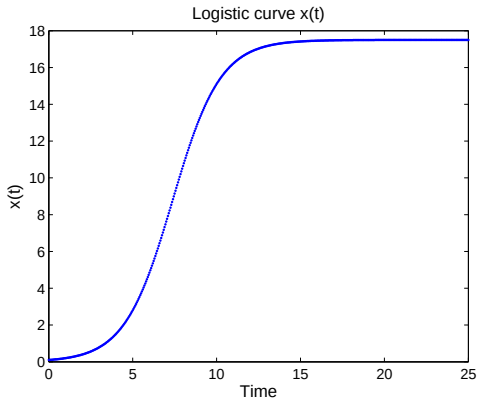

Figure 2.2: Logistic curve with $\theta_0 = (17.5, 0.7, 0.1)$.

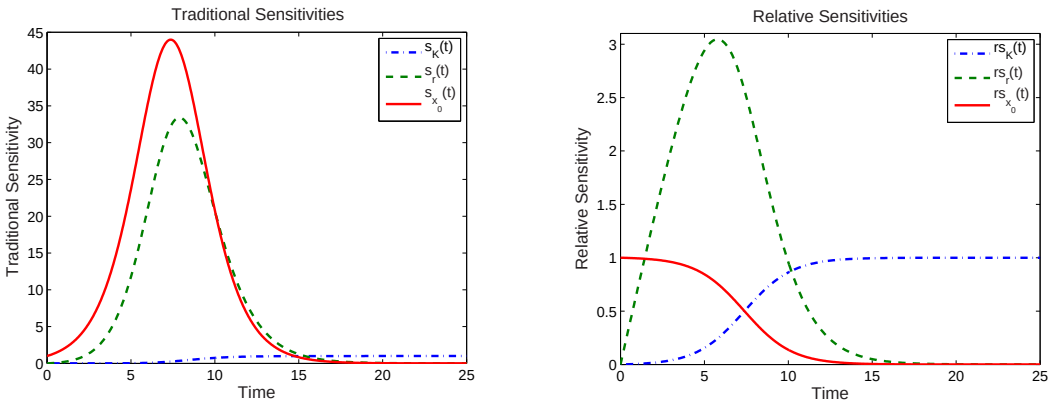

(a) (b)

Figure 2.3: (a) TSF and (b) RSF corresponding to each parameter for the logistic curve with $\theta_0 = (17.5, 0.7, 0.1)$.

[15,25], indicating that we will be unable to identify x_0 or r in that region. Again, this is consistent with the approximation (2.2.8).

Results

In order to computationally illustrate how the traditional sensitivity theory applies to our logistic growth problem, we use exact (no-noise) simulated data. We also restricted the time domain from which we sample data points to the region of interest $[0, \tau_1]$, $[\tau_1, \tau_2]$ or $[\tau_2, T]$ for each simulation. Then we determine the standard errors of each parameter set in order to analyze the success of the algorithm at approximating the components of θ.

We first sampled data where the solution curve is close to x_0, and for this example we considered the region $[0, 1]$. We passed several initial estimates to the optimization routine, and expected with each estimate that we would be able to recover x_0, but not r or K, based on the approximation (2.2.7). In actuality we were able to obtain close estimates for both r and x_0, see Table 2.2. Upon further examination we learned that r and x_0 are highly correlated, which is evident by the magnitude of their correlation coefficients, given in Table 2.1, and clearly seen in Figure 2.3(a). By studying each iteration of the optimization routine, we observed that x_0 is easily identified, and due to the high correlation between r and x_0, r is eventually obtained each time. However, as predicted, K is never reasonably estimated. In Figure 2.4(a), when $\theta^0 = (15, 1.4, 1)$, the simulation demonstrates the poor

Table 2.2: Optimized $\hat{\theta}$ and corresponding standard errors for $\theta_0 = (17.5, 0.7, 0.1)$ on the given intervals. Model fit to exact data.

$\boldsymbol{\theta^0}$	$\hat{\boldsymbol{\theta}}$	**Standard Error**
Values corresponding to the interval $[0, 1]$		
(5,0.2,0.5)	(8.3127,0.70674,0.099955)	$(2.1916, 0.0034321, 3.3265 \cdot 10^{-5})$
(8,1,0.3)	(11.2296,0.70339,0.099976)	$(2.0616, 0.0017523, 1.6981 \cdot 10^{-5})$
(15,1.4,1)	(26.881,0.6979,0.10001)	$(6.8706, 0.0010032, 9.7196 \cdot 10^{-6})$
(19,0.4,0.8)	(19.0481,0.69951,0.1)	$(0.67786, 0.00019803, 1.9188 \cdot 10^{-6})$
(25,0.8,2)	(32.3378,0.69724,0.10002)	$(13.2303, 0.0013323, 1.2908 \cdot 10^{-5})$
Values corresponding to the interval $[1, 15]$		
(5,0.2,0.5)	(17.4983,0.69987,0.10003)	$(0.00018458, 2.7386 \cdot 10^{-5}, 1.9253 \cdot 10^{-5})$
(8,1,0.3)	(17.4983,0.69986,0.10003)	$(0.0001847, 2.7405 \cdot 10^{-5}, 1.9267 \cdot 10^{-5})$
(15,1.4,1)	(17.4984,0.69985,0.10004)	$(0.00018483, 2.7422 \cdot 10^{-5}, 1.928 \cdot 10^{-5})$
(19,0.4,0.8)	(17.4983,0.69986,0.10004)	$(0.00018458, 2.7385 \cdot 10^{-5}, 1.9253 \cdot 10^{-5})$
(25,0.8,2)	(17.4983,0.69987,0.10003)	$(0.00018453, 2.738 \cdot 10^{-5}, 1.9248 \cdot 10^{-5})$
Values corresponding to the interval $[15, 25]$		
(5,0.2,0.5)	(17.5025,0.53639,1.1724)	(0.00056618,0.019696,0.3311)
(8,1,0.3)	(17.4878,1.1452,0.048662)	(0.0031974,135.8319,100.6793)
(15,1.4,1)	(17.4877,1.28,0.89893)	(0.0031185,22996.6125,298995.5609)
(19,0.4,0.8)	(17.5018,0.57375,0.6752)	(0.00040349,0.01542,0.15394)
(25,0.8,2)	(17.4877,0.8672,2.1698)	(0.0035097,75.9155,2213.0856)

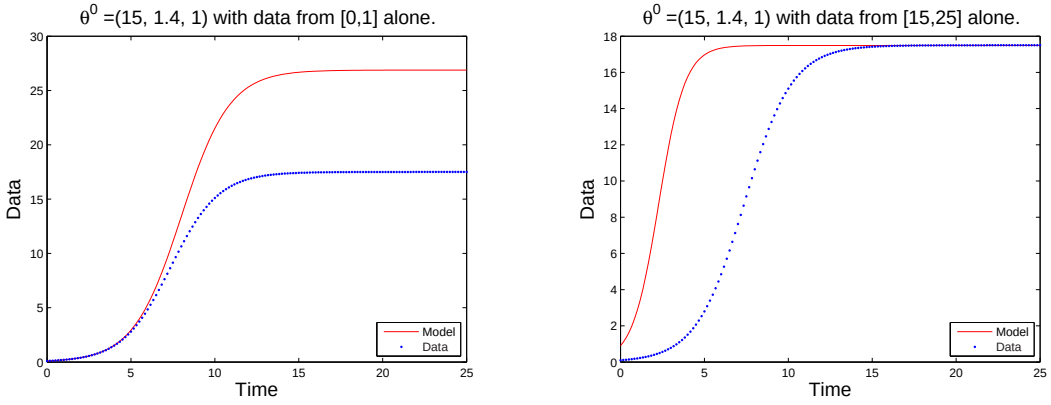

(a) (b)

Figure 2.4: The logistic curve with $\theta_0 = (17.5, 0.7, 0.1)$, and optimal curves using $\theta^0 = (15, 1.4, 1)$ with data sampled only from (a) $[0, 1]$ and (b) $[15, 25]$.

estimate of K when using data from only this region $[0, 1]$. Note that the predicted value for K is 26.881, which is nowhere near the true value of 17.5.

We next considered the region where the dynamics of the curve changed, and for our example this region is the interval $[1, 15]$. As expected, regardless of the initial estimate that is passed to the optimization routine, we obtained reasonable estimations for K, r and x_0 as can be seen in Table 2.2.

Lastly, we sampled data where the curve approaches an asymptote at K. For this example we considered the region $[15, 25]$. We passed several initial estimates to the optimization algorithm, and expected that with each estimate we would be able to identify K, but not for r or x_0, based on the approximation (2.2.8). This occurred with every initial estimate, although we note that in some cases the standard errors are significantly larger than others, see Table 2.2. We observe that when the optimized r is larger than the true value $r = 0.7$, the corresponding standard errors for r and x_0 are very large. This is due to the dependency of the sensitivities on r. This results in the sensitivity matrix $\chi^T\chi$ approaching singularity at a much faster rate than when r is small. For example, we notice that the largest standard errors that are represented in Table 2.2 are from the optimized parameters associated with $\theta^0 = (15, 1.4, 1)$ when data was sampled from the interval $[15, 25]$ alone. The sensitivity matrix for this example is given as

$$\chi^T\chi = \begin{pmatrix} 61 & 1.21008 \cdot 10^{-4} & 9.0382 \cdot 10^{-6} \\ 1.21008 \cdot 10^{-4} & 1.48107 \cdot 10^{-9} & 1.1335 \cdot 10^{-10} \\ 9.0382 \cdot 10^{-6} & 1.1335 \cdot 10^{-10} & 8.68057 \cdot 10^{-12} \end{pmatrix}. \tag{2.2.9}$$

For these simulations a step size of $1/6$ was used, resulting in 61 data points for the region $[15, 25]$. Hence, we see that (2.2.9) is a close approximation of the predicted sensitivity matrix (2.2.8). We see the results from this simulation in Figure 2.4(b), and note the poor approximation for both r and x_0.

These results help us see that the TSF, used in conjunction with the correlation coefficients, provided enough information to predict which parameters would be able to be determined in each region.

2.2.2 Generalized Sensitivity

To display the effectiveness of generalized sensitivity functions for parameter estimation problems, we again consider the logistic growth population model (2.2.1) as an example. We start by numerically computing the GSF using (2.1.10) with $\sigma = 1$ and $T = 25$ with true parameter value $\theta_0 = (K, r, x_0) = (17.5, 0.7, 0.1)$. The plots of these functions are

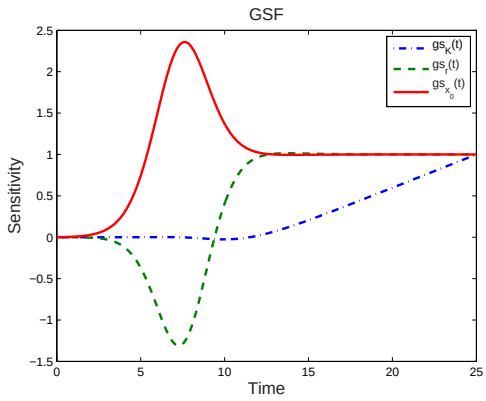

Figure 2.5: GSF for the logistic curve with $\theta = (17.5, 0.7, 0.1)$.

shown in Figure 2.5 where one can notice clear regions of steep increase in each curve. For the curves $gs_{x_0}(t)$, $gs_r(t)$ and $gs_K(t)$, we find (by visual inspection) that these regions are approximately $[4.5, 7.5]$, $[7, 11]$ and $[12, 25]$ respectively. By the aforementioned generalized sensitivity theory, if we increase the number of data points sampled in one of these regions, the estimation of the corresponding parameter is expected to improve.

We note that generally the GSF would be applied to models with more parameters, and in these cases a uniform distribution of time points is reasonable. Hence, we will initially consider a uniform time grid for these simulations.

Numerical Simulations with Noisy Data

For the numerical simulations, we initially sample n data points uniformly over $[0, T]$, and then sample an additional m points pertaining to the GSF regions of interest. By including data points from the entire region $[0, T]$, we will be able to recover the exact parameter values when using noise-free data, as seen in Table 2.2. Hence, for these simulations we must consider noisy data, and consequently add Gaussian noise to the logistic curve with $\epsilon_j \overset{i.i.d.}{\sim} \mathcal{N}(0, \sigma_0^2)$ for $j = 1, \ldots, n + m$.

Each parameter in θ has an interval of steepest increase for each corresponding GSF, and the m additional points are sampled according to those regions. We first consider the time grid $t_{uniform}$, which refers to n uniform time points over [0,25] with m additional points added as uniformly as possible over the entire region. The results using this grid are displayed in Table 2.3, and are used as a basis of comparison for the remaining results in

Table 2.3: Standard errors ($\mathrm{SE}_K, \mathrm{SE}_r, \mathrm{SE}_{x_0}$) corresponding to the addition of m additional uniformly distributed points throughout $[0, 25]$.

n	m	$t_{uniform}$
50	0	(0.10748,0.029371,0.021604)
50	25	(0.086565,0.023623,0.017374)
50	50	(0.077352,0.021049,0.01548)
125	0	(0.061814,0.016807,0.01236)
125	25	(0.057056,0.015504,0.011401)
125	50	(0.053388,0.014502,0.010664)
125	125	(0.047175,0.012805,0.0094158)
250	0	(0.047175,0.012805,0.0094158)
250	50	(0.043685,0.011854,0.0087166)
250	100	(0.0404,0.01096,0.0080592)
250	250	(0.034008,0.0092229,0.0067818)

this section. Then in each of Tables 2.4, 2.5, and 2.6, we consider two alternate time grids:

- t_{GSF} consists of n uniform time points over [0,25] with m points added in the area of steepest increase according to the GSF for each parameter, and
- t_{nonGSF} consists of n uniform time points over [0,25] with m points added everywhere except the area of steepest increase according to the GSF for each parameter.

For example, in Table 2.4, the t_{GSF} column refers to the standard errors generated by optimizing θ over n uniformly distributed data points in [0,25] with m additional data points sampled from the interval of gs_K with the steepest increase, which is $[12, 25]$. The standard errors in the t_{nonGSF} column refer to the same n initial data points, with the additional m points sampled from outside the "GSF region" for K. We expect SE_K to be the standard error which is most affected by additional points sampled with respect to this region, and hence it is the component of interest in Table 2.4. Similarly Tables 2.5 and 2.6 are based on the GSF regions corresponding to r and x_0 respectively, with SE_r and SE_{x_0} as the respective values of interest.

We expect that for each parameter, the corresponding standard errors in the t_{GSF} column will generally improve as m increases. In actuality, the corresponding standard errors show improvement when m additional points are sampled in *all three grids* for each parameter. However, we get better results with the t_{GSF} grid than with the $t_{uniform}$ grid, with the worst results from the t_{nonGSF} grid.

Table 2.4: Standard errors ($\mathrm{SE}_K, \mathrm{SE}_r, \mathrm{SE}_{x_0}$) corresponding to the addition of m extra points within and excluding [12,25], the period of steepest increase in gs_K.

n	m	t_{GSF}	t_{nonGSF}
50	0	(0.10748,0.029371,0.021604)	(0.10748,0.029371,0.021604)
50	25	(0.077068,0.027991,0.020752)	(0.10441,0.021464,0.015622)
50	50	(0.059962,0.025752,0.019184)	(0.099866,0.01754,0.012632)
125	0	(0.061814,0.016807,0.01236)	(0.061814,0.016807,0.01236)
125	25	(0.053069,0.016569,0.012234)	(0.061051,0.014428,0.010561)
125	50	(0.046431,0.016095,0.011919)	(0.06453,0.013726,0.010003)
125	125	(0.037958,0.016276,0.012124)	(0.061772,0.010767,0.0077615)
250	0	(0.047175,0.012805,0.0094158)	(0.047175,0.012805,0.0094158)
250	50	(0.039627,0.012356,0.009123)	(0.046264,0.010884,0.0079648)
250	100	(0.035866,0.012422,0.009198)	(0.045259,0.0095868,0.0069842)
250	250	(0.027388,0.011737,0.0087426)	(0.04239,0.0073602,0.0053052)

Table 2.5: Standard errors ($\mathrm{SE}_K, \mathrm{SE}_r, \mathrm{SE}_{x_0}$) corresponding to the addition of m extra points within and excluding [7,11], the period of steepest increase in gs_r.

n	m	t_{GSF}	t_{nonGSF}
50	0	(0.10748,0.029371,0.021604)	(0.10748,0.029371,0.021604)
50	25	(0.097735,0.021034,0.016379)	(0.085987,0.025298,0.01814)
50	50	(0.10215,0.019931,0.015575)	(0.071516,0.022395,0.015627)
125	0	(0.061814,0.016807,0.01236)	(0.061814,0.016807,0.01236)
125	25	(0.061485,0.014585,0.011165)	(0.055069,0.0155,0.011258)
125	50	(0.063405,0.013979,0.010842)	(0.052744,0.015359,0.011012)
125	125	(0.062507,0.012136,0.009478)	(0.043153,0.013462,0.0093937)
250	0	(0.047175,0.012805,0.0094158)	(0.047175,0.012805,0.0094158)
250	50	(0.046673,0.011057,0.0084657)	(0.043127,0.012158,0.0088167)
250	100	(0.045837,0.010087,0.0078221)	(0.038498,0.01117,0.0080133)
250	250	(0.043884,0.0085094,0.0066447)	(0.032496,0.010137,0.0070706)

We further observe that SE_r and SE_{x_0} both improve greatly when we consider the t_{GSF} grid corresponding to each parameter r and x_0, (see Tables 2.5 and 2.6). This observation inclines us to investigate the theory regarding the regions of "steepest increase" providing the most information for parameter identification. At each time point, the corresponding Fisher information matrix does not necessarily have only positive entries, resulting in the non-monotonicity of the GSF. However, contrary to the idea of "steepest increase" proposed by Thomaseth and Cobelli [38], we have no reason to assume that the positive entries are of greater value than any of the negative entries. Hence, we consider another time grid, corresponding to regions of steep increase *or decrease* in the GSF. By visual

Table 2.6: Standard errors $(\mathrm{SE}_K, \mathrm{SE}_r, \mathrm{SE}_{x_0})$ corresponding to the addition of m extra points within and excluding [4.5,7.5], the period of steepest increase in gs_{x_0}.

n	m	t_{GSF}	t_{nonGSF}
50	0	(0.10748,0.029371,0.021604)	(0.10748,0.029371,0.021604)
50	25	(0.10338,0.021906,0.014617)	(0.081923,0.02323,0.017621)
50	50	(0.099638,0.018577,0.012139)	(0.07291,0.021106,0.016235)
125	0	(0.061814,0.016807,0.01236)	(0.061814,0.016807,0.01236)
125	25	(0.064238,0.015175,0.010452)	(0.056836,0.015457,0.011486)
125	50	(0.059416,0.012951,0.0086999)	(0.052824,0.01476,0.011091)
125	125	(0.05867,0.010902,0.0071197)	(0.043777,0.012942,0.0099389)
250	0	(0.047175,0.012805,0.0094158)	(0.047175,0.012805,0.0094158)
250	50	(0.046931,0.011043,0.0076218)	(0.043069,0.011892,0.0088565)
250	100	(0.046695,0.010136,0.006819)	(0.040509,0.011467,0.0086329)
250	250	(0.043801,0.0081056,0.0052964)	(0.031893,0.0095317,0.0073385)

Table 2.7: Standard errors $(\mathrm{SE}_K, \mathrm{SE}_r, \mathrm{SE}_{x_0})$ corresponding to the addition of m extra points within and excluding [4.5,11], the period of most significant change in the GSF for the parameters x_0 and r.

n	m	t_{GSF}	t_{nonGSF}
50	0	(0.10748,0.029371,0.021604)	(0.10748,0.029371,0.021604)
50	25	(0.10801,0.020384,0.014864)	(0.089544,0.028147,0.020721)
50	50	(0.10407,0.016495,0.011929)	(0.066204,0.022516,0.01656)
125	0	(0.061814,0.016807,0.01236)	(0.061814,0.016807,0.01236)
125	25	(0.066803,0.015054,0.011051)	(0.056917,0.016377,0.012)
125	50	(0.063829,0.012666,0.0092624)	(0.049834,0.015145,0.011094)
125	125	(0.059484,0.00939,0.0067894)	(0.045552,0.015425,0.011285)
250	0	(0.047175,0.012805,0.0094158)	(0.047175,0.012805,0.0094158)
250	50	(0.04625,0.010394,0.0076238)	(0.041199,0.011995,0.0088246)
250	100	(0.045683,0.0090403,0.0066069)	(0.038051,0.011663,0.0085602)
250	250	(0.044083,0.006944,0.0050191)	(0.030519,0.01041,0.0076278)

inspection of Figure 2.5, we see that these regions are approximately $[4.5, 11]$, $[4.5, 11]$, and $[12, 25]$ for the curves $gs_{x_0}(t)$, $gs_r(t)$ and $gs_K(t)$, respectively. Notice that the new GSF region for K is $[12, 25]$ as before, however the GSF regions corresponding to r and x_0 have changed. In fact, these regions are equal, which is not unexpected based on the correlation we have already observed in Table 2.1.

In Table 2.7 we consider the same structure for our numerical simulations as before, adding m additional points in (and excluding) the region $[4.5, 11]$. The resulting standard errors for r and x_0 are generally lower in Table 2.7 than in the corresponding entries in

Tables 2.5 and 2.6 (for the t_{GSF} grid). Thus, we see that the decreasing regions in the GSF curves also appear to be useful (as with the the increasing regions) when recovering parameters and improving standard errors.

By utilizing the regions that are indicated by the GSF, we obtain better standard errors for the corresponding parameters than by merely increasing the number of points uniformly sampled over the entire region. Further, we postulate that sampling additional points from the regions with steepest increase/decrease will result in better standard errors than if we only consider the regions with steepest increase.

Forced-to-One Artifact

We note that the shape of the TSF curves remains the same regardless of the amount of data that is sampled, whereas the GSF curves are data dependent and change shape with varying amounts of data. We see in Figures 2.6(a) and 2.6(b) that when we restrict the data set for the logistic growth population model to $[0, 2]$, the TSF curves look the same as when we merely zoom in to $[0, 2]$ after sampling data over the entire region: $[0, 25]$. However, the GSF curves look very different when the sampled data is only from the interval $[0, 2]$ in Figure 2.7(a) than when the data is sampled from $[0, 25]$ and scaled to $[0, 2]$ as shown in Figure 2.7(b).

If an insufficient amount of data is used for parameter estimations, the GSF curves

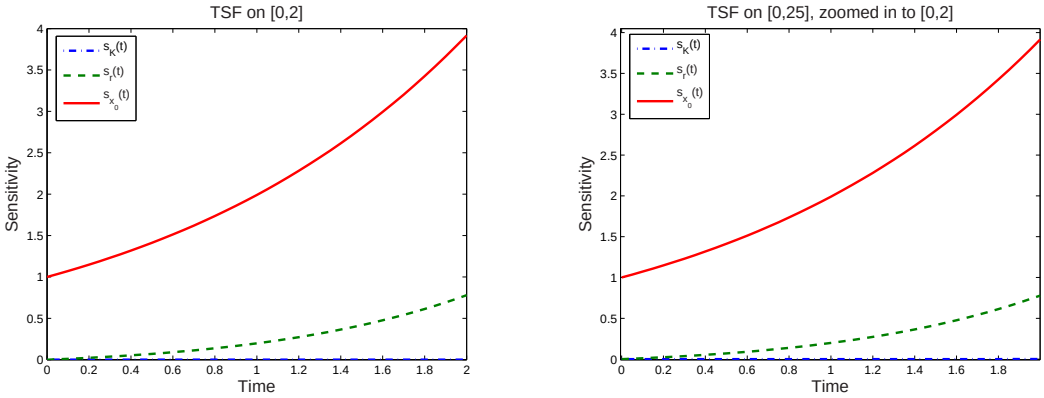

(a) (b)

Figure 2.6: (a) TSF for the logistic equation when sampling data in [0,2], (b) the scaled portion when data is observed from the entire region [0,25].

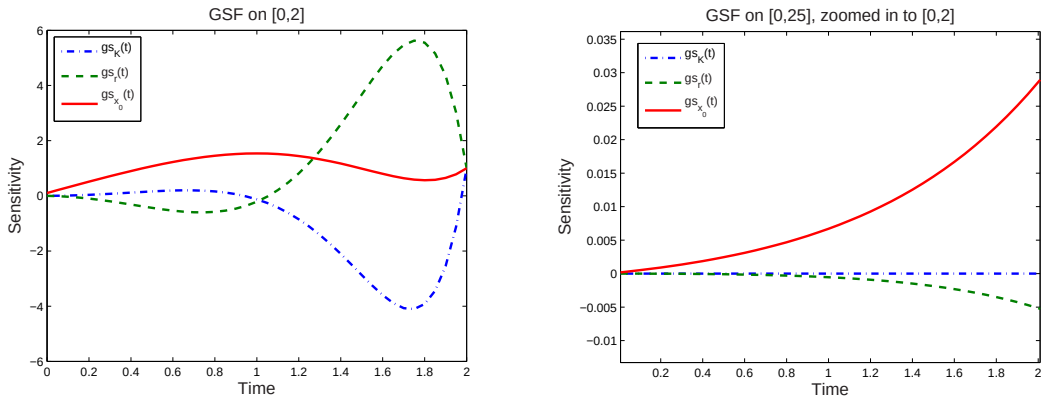

(a) (b)

Figure 2.7: (a) GSF for the logistic equation when sampling data in [0,2], (b) the scaled portion [0,2] when data was observed from the entire region [0,25].

can be misleading because by definition the GSF are forced to be equal to one by the end of the data set. This so-called "forced-to-one" artifact can cause false regions of steep increase in the GSF curves as can be seen in the curve gs_K when $t \in [1.7, 2]$ in Figure 2.7(a). Notice that in Figure 2.6 we can see that the state is clearly not sensitive to the K parameter in region $[0, 2]$, and hence sampling additional data points in the period of false increase would merely increase standard error. We see another example of this phenomenon in Figure 2.8 where we compare the GSF curves generated from data sampled on $[0, 0.2]$ to the curves generated when data is sampled on $[0, 25]$. In Figure 2.8(b) it is clear that there is no significant period of increase for either K or r, however in Figure 2.8(a) it appears that the corresponding GSF curves both have distinct regions of (false) increase. Therefore, it is important to note that while the GSF curves can be misleading when a limited portion of data is obtainable, the TSF curves can still be used appropriately in sensitivity studies.

Although there is improvement when the GSF regions are considered, the amount of additional points sampled to garner the improved standard errors needs to be taken into consideration. Depending on the problem, the cost may be too high to sample additional data points for the slightly improved results. However, in other cases the additional sampling may be worth the improvement. While a useful tool, the GSF may not be an efficient choice in all parameter estimation problems.

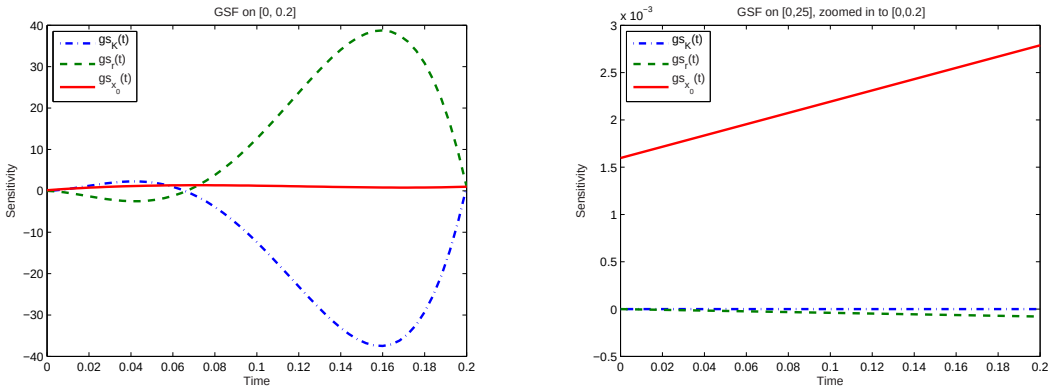

(a) (b)

Figure 2.8: (a) GSF for the logistic equation when sampling data in [0,0.2], (b) we have the scaled portion [0,0.2] when data was observed from the entire region[0,25].

2.2.3 Usefulness in formulating data collection

We now consider several mathematical tools to assist in the formulation of data collection. We begin by analyzing the usefulness of the condition number of F, the Fisher information matrix for a general continuum observation, and use this tool in combination with traditional sensitivity functions to determine an optimal final time. Next, we strive to use the Fisher information matrix in determining the optimal placement of longitudinal data points.

Condition number of the Fisher information matrix

In this subsection we establish the theoretical basis for using the condition number of the generalized Fisher information matrix F to indicate an optimal stopping time. As we have seen, the FIM relates the variation in parameter estimates to variations in collected data. Also, F^{-1} is an important component in the definition of the generalized sensitivity functions. Consequently, the condition number of F, which we denote $\rho(F)$, is expected to contribute to the statistical properties of the estimate $\hat{\theta}$, and numerical stability issues suggest that it is important to have the sampling interval $[0, T]$ chosen appropriately. The following theorem gives a theoretical basis for using the condition number of the Fisher information matrix as an optimal design tool.

Theorem 2.2.1. *Assume that* $\det(F(T)) \neq 0$. *Then* $\det(F(T+\Delta)) \neq 0$ *for all* $\Delta \geq 0$ *and*

the spectral norm of the covariance matrix F^{-1} is a nonincreasing function of the final time T, i.e.,

$$\left\|F(T+\Delta)^{-1}\right\|_2 \leq \left\|F(T)^{-1}\right\|_2$$

for all $\Delta \geq 0$ (here $\|\cdot\|_2$ denotes the spectral norm of a matrix).

Proof. The matrix $F(T)$ is positive definite. Let $\lambda_{\min}(T)$ and $\lambda_{\max}(T)$ denote the smallest and the largest eigenvalue of $F(T)$. Then we have

$$\lambda_{\min}(T)\|a\|_2^2 \leq a^T F(T) a \leq \lambda_{\max}(T)\|a\|_2^2, \quad a \in \mathbb{R}^p.$$

For $a \in \mathbb{R}^p$ and $\Delta > 0$ we have

$$\begin{aligned}\lambda_{\min}(T)\|a\|^2 + \int_T^{T+\Delta} \frac{1}{\sigma^2(t)}\|\nabla_\theta f(t;\theta_0)a\|^2 dt &\leq a^T F(T+\Delta)a \\ &\leq \lambda_{\max}(T)\|a\|^2 + \int_T^{T+\Delta} \frac{1}{\sigma^2(t)}\|\nabla_\theta f(t;\theta_0)a\|^2 dt.\end{aligned}$$

The left side of this inequality implies

$$\lambda_{\min}(T+\Delta) \geq \lambda_{\min}(T). \tag{2.2.10}$$

If we choose a as an eigenvector of $F(T)$ corresponding to $\lambda_{\max}(T)$ then we obtain

$$a^T F_G(T+\Delta)a = \lambda_{\max}(T)\|a\|^2 + \int_T^{T+\Delta} \frac{1}{\sigma^2(t)}\|\nabla_\theta f(t;\theta_0)a\|^2 dt \leq \lambda_{\max}(T+\Delta)\|a\|^2,$$

which implies

$$\lambda_{\max}(T) \leq \lambda_{\max}(T+\Delta). \tag{2.2.11}$$

The largest and smallest eigenvalues of $F(T+\Delta)^{-1}$ are respectively $1/\lambda_{\min}(T+\Delta)$ and $1/\lambda_{\max}(T+\Delta)$. Then (2.2.10) implies that $\det F(T+\Delta) \neq 0$. The result on the spectral norms is a consequence of (2.2.10). Note that $\|F(T+\Delta)^{-1}\|_2 = 1/\lambda_{\min}(T+\Delta)$, because $F(T+\Delta)^{-1}$ is symmetric and consequently the spectral radius of $\left(F(T+\Delta)^{-1}\right)^T F(T+\Delta)^{-1}$ is $\lambda_{\min}(T+\Delta)^{-2}$. □

One might think a natural consequence of this theorem is that the condition number of the generalized Fisher information matrix is a nonincreasing function of the final time T, i.e.

$$\rho_F(T) \geq \rho_F(T+\Delta). \tag{2.2.12}$$

Table 2.8: The minimum eigenvalue, maximum eigenvalue, and condition number of the FIM corresponding to the logistic equation, with increasing final time T.

T	$\lambda_{\min}(T)$	$\lambda_{\max}(T)$	$\rho_F(T)$
15	2.6112	11403.3913	4367.0612
20	7.3132	11404.9422	1559.5081
25	12.2328	11404.9461	932.3246
30	17.1568	11404.9467	664.7493

Indeed, when we increase the final time in the logistic equation, we see that the minimum and maximum eigenvalues both increase while the condition number decreases. The numerical values in Table 2.8 and the plot in Figure 2.9(a) support this idea. We observe that the minimum eigenvalue increases at a significantly faster rate than the maximum eigenvalue, see Table 2.8. Upon closer examination, we see that the eigenvalues and the rate at which they increase appear to be directly related to the traditional sensitivity equations. We use this observation to construct another example which also has increasing eigenvalues (of the FIM), but where the maximum value increases faster than the minimum value.

The differential equation

$$\dot{x} = -\mu_1 \exp(-t) + \frac{\mu_2}{t+1}$$

has solution

$$x = \mu_1 \exp(-t) + \mu_2 \ln(t+1)$$

and corresponding sensitivity equations

$$\frac{\partial x}{\partial \mu_1} = \exp(-t) \quad \text{and} \quad \frac{\partial x}{\partial \mu_2} = \ln(t+1).$$

As t increases, $\frac{\partial x}{\partial \mu_1}$ will become close to zero, however $\frac{\partial x}{\partial \mu_2}$ will stay relatively large.

As recorded in Table 2.9, both eigenvalues of the corresponding FIM increase, with the maximum value increasing at a faster rate than the minimum value. For these computations we used the values $\mu_1 = 2$, $\mu_2 = 4$, and $\delta t = 0.1$. It is important to note that the condition number of the Fisher information matrix increases in this case.

Thus, we conclude that Theorem 2.2.1 does not always imply a nonincreasing condition number of the corresponding Fisher information matrix. However, for the example of the logistic model, the condition number of the FIM is nonincreasing, and this will be useful when analyzing the system.

Table 2.9: The minimum eigenvalue, maximum eigenvalue and condition number of the FIM corresponding to the counterexample, with increasing final time T.

T	$\lambda_{\min}(T)$	$\lambda_{\max}(T)$	$\rho_F(T)$
10	0.6941	306.2346	441.2221
15	0.7217	644.9540	893.6955
20	0.7316	1070.8184	1463.6838
25	0.7364	1569.4112	2131.3063
30	0.7391	2130.7878	2883.1087

Determining an Optimal Final Time

The choice of an optimal interval $[0, T]$ for data sampling is important to parameter estimation problems for dynamical systems. Specifically, we consider an "optimal interval" as one that satisfies the two following criteria:

1. All data on $[0, T]$ is relevant to the estimation of θ (i.e., more accurate estimates are obtained when sampling data on $[0, T]$ than on $[0, T - \Delta T]$ for $\Delta T > 0$).

2. Data outside $[0, T]$ is irrelevant with respect to the quality of parameter estimates (i.e., improvements in parameter estimates are negligible when the interval is enlarged to $[0, T + \Delta T]$ for $\Delta T > 0$).

The choice of an optimal final time T reaps particular benefit in applications where the collection of data is prohibitively expensive.

In practice, experimentalists commonly use prior knowledge to choose the stopping time. For numerical simulations, we want T to be sufficiently large to guarantee that the state variable reaches any possible steady state. Here, we use the evolution of the condition number of the FIM (as function of final time T) and the traditional sensitivity functions to indicate the optimal final time.

From Figure 2.2 we estimate that the steady state is reached by approximately $t = 20$ for the logistic model with $\theta_0 = (17.5, 0.7, 0.1)$. If we look at the traditional sensitivity functions of Figure 2.3(a), we observe that the TSF for r and x_0 are compactly supported in the interval $[0, 20]$ and they vanish elsewhere. Also, the TSF for K increases from zero and reaches one (the steady state) slightly before $t = 20$. Therefore, for the logistic model with $\theta_0 = (17.5, 0.7, 0.1)$, the interval $[0, 20]$ appears to be the minimum interval for sampling data. Sampling data from a smaller interval may prove unwise. The elimination

of data points where the model exhibits sensitivity to a specific parameter would render their identification difficult (or impossible).

To quantify the final time, we look at each sensitivity function individually and locate the time point after which there is no transitional behavior, i.e., to find T_K, T_r and T_{x_0} given by

$$\begin{aligned} T_K &= \max\{t : |s_K(u) - s_K(v)| > \varepsilon, \text{ for } u, v \in [t, t+h]\}, \\ T_r &= \max\{t : |s_r(u) - s_r(v)| > \varepsilon, \text{ for } u, v \in [t, t+h]\}, \\ T_{x_0} &= \max\{t : |s_{x_0}(u) - s_{x_0}(v)| > \varepsilon, \text{ for } u, v \in [t, t+h]\}, \end{aligned} \tag{2.2.13}$$

where s_K, s_r and s_{x_0} are the traditional sensitivity functions with respect to the corresponding parameters, ε is a small tolerance, and $h > 0$ is the length of the time window used. Note that a smaller ε results in a larger final time T_{θ_i} for $i = 1, \ldots, p$. The final time T is simply the maximum of the previous times, given as

$$T = \max\left(T_K, T_r, T_{x_0}\right).$$

In Figures 2.9(a), 2.9(b) and 2.9(c), the condition number of the Fisher information matrix (FIM) for the logistic model is described as a function of the final time T, as well as the same time evolution of the first and second time derivatives. Here, we consider the integral version of the FIM which incorporates all three parameters. The FIM initially has a large condition number which decreases exponentially on the interval $[0, 15]$, after which it decreases at a slow rate. In order to better understand the rate of change and concavity of the condition number of the FIM, we look at the first and second derivatives.

The condition number of the FIM decreases sharply on $[0, 15]$, followed by a slower rate of decrease, as seen in Figure 2.9(a). Also we observe that the second derivative (of the base ten logarithm of the condition number) approaches zero near $T = 7$, corresponding with the change of inflection of the logistic model. This implies that we cannot estimate all three parameters if we sample data only from $[0, 7]$, regardless of the number of points sampled. This is due to the data in $[0, 7]$ carrying little to no information about K. In fact, we know that the value of the curve when the inflection changes is precisely half of the carrying capacity, K. Until this point is reached, we can only estimate r and x_0. However, the continuous improvement in the condition number of the FIM after $T = 20$ is due to the sensitivity with respect to K which approaches the steady state of one (the sensitivities with respect to r and x_0 approach zero after $T = 20$). This results in the adding of nontrivial

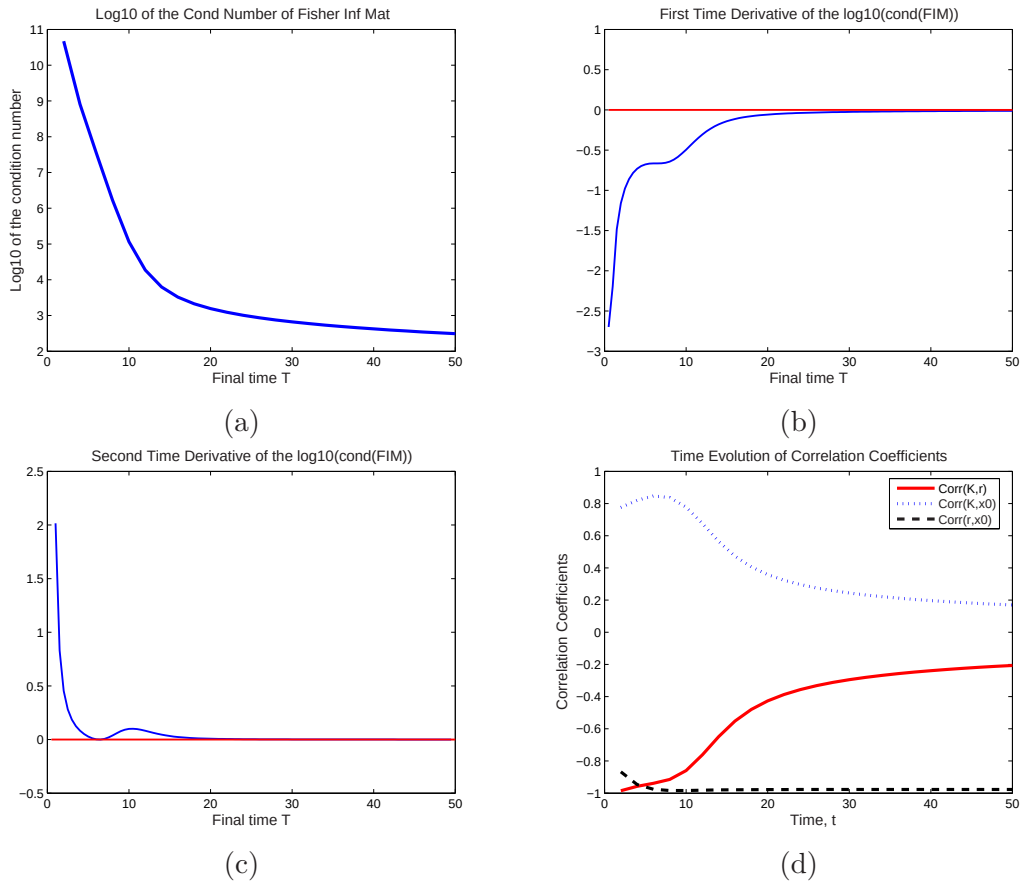

Figure 2.9: (a) Log10 of the condition number of the FIM, (b) first and (c) and second derivatives of the log10 of the condition number of the FIM, and (d) correlation coefficients. All figures plotted for the true parameter value $\theta_0 = (17.5, 0.7, 0.1)$.

rank one matrices to the FIM, slightly improving its condition number. As a consequence (in agreement with the TSF and the time derivative of the GSF), Figures 2.9(a)–(c) suggest that most of the relevant information is contained in the interval $[0, 20]$ and little is left outside this interval.

The behavior of the condition number of the Fisher information matrix illustrated in Figure 2.9(a) agrees with the theoretical results (see Theorem 2.2.1) and coincides with our insight about the logistic model. Intuitively, if T is larger, we have more information about the logistic curve and thus we can estimate the parameters which control the shape of the curve more accurately. Hence, it is perfectly reasonable for the condition number of the FIM to decrease as T gets larger. A smaller condition number for the FIM is desirable,

resulting in a "smaller" dispersion matrix (the inverse of the FIM) and smaller standard errors for the estimates.

Also of interest is the evolution of the correlation coefficients for this problem, (see Figure 2.9(d) for the corresponding plots). In general, it is more difficult to estimate parameters which are strongly correlated than those which are moderately correlated. By looking at the evolution of the correlation coefficients we conclude that $T = 20$ is a reasonable choice, as the correlation has strongly decreased between K and r, as well as the correlation between K and x_0. Note that the correlation between r and x_0 remains high, as we observed in Table 2.1, which is unavoidable regardless of the final time chosen.

It is very important to note that all the curves plotted in Figure 2.9 depend on the true value $\theta_0 = (17.5, 0.7, 0.1)$ which in practice is not known *a priori* (θ_0 is the parameter we want to estimate). Hence, we use mathematical tools to indicate an optimal stopping time. However, these tools depend on the values of the parameters we want to find making the use of prior knowledge is necessary. In optimal design literature ([12, 24, 32, 37]), it is assumed that a reasonable initial estimate for θ_0 is available. We assume that we have a range of values from prior knowledge for the components of θ which is a weaker assumption than having a reasonable initial estimate for θ_0. Instead of using the one-dimensional curves plotted in Figure 2.9, we will plot and use the 2D maps of these functions depending on T and the corresponding parameter (see Figure 2.10 to establish the sampling intervals).

We then choose a stopping time T with conditions involving ranges of acceptable values, and use a "worst-case scenario" approach as before. However, this time we will consider the two-dimensional maps of Figure 2.10. Specifically, we choose a minimum stopping time after which both the TSF and the condition number of FIM do not exhibit any significant transient behavior.

In Figure 2.10(a) we include the (traditional) sensitivity plots corresponding to the interval $[K-\delta_1 K, K+\delta_1 K]$ with $\delta_1 = 0.5$, instead of just considering $K = 17.5$. We see that for smaller values of K, the solution is insensitive to changes in K until approximately $t = 7$, where for larger values the change occurs slightly higher at around $t = 10$. This is a relatively subtle change, especially when compared to the changes in sensitivity when we vary r. In Figure 2.10(b), we consider the TSF corresponding to r over the range $[r - \delta_2 r, r + \delta_2 r]$, with $\delta_2 = 0.5$. Here we see that for lower values of r, the solution is sensitive to changes for a longer period of time than when considering larger values of r. In Figure 2.10(c) we observe the TSF corresponding to x_0 over the range $[x_0 - \delta_3 x_0, x_0 + \delta_3 x_0]$ with $\delta_3 = 0.5$, and

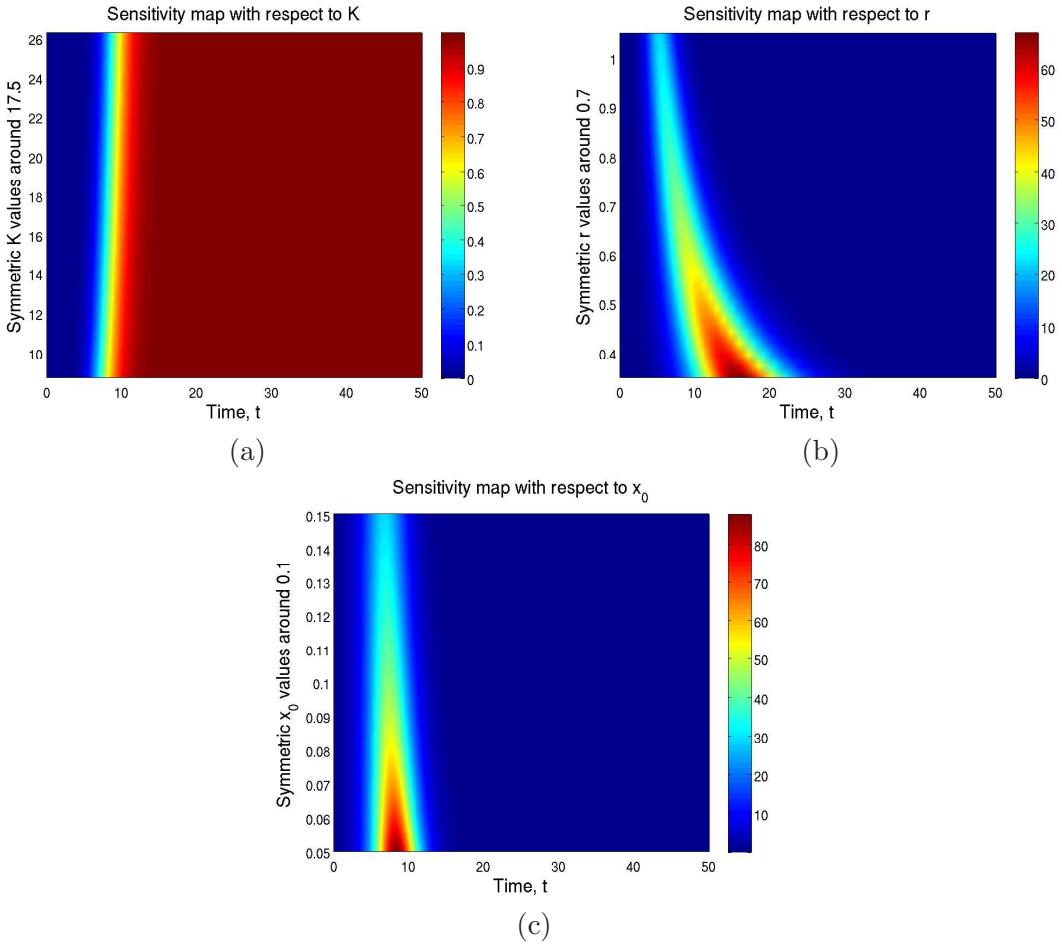

Figure 2.10: TSF maps for (a) K centered around 17.5, (b) r centered around 0.7, and (c) x_0 centered around 0.1.

notice that there are small changes, just as we observed with the sensitivities corresponding to K. We now consider the maximum time pertaining to all three sensitivities,

$$T_D = \max\left[\max_{\theta\in D} T_K(\theta), \max_{\theta\in D} T_r(\theta), \max_{\theta\in D} T_{x_0}(\theta)\right]$$

where D refers to the interval $[\theta_k - \delta_k\theta_k, \theta_k + \delta_k\theta_k]$ for each parameter θ_k, and $T_{\theta_k}(\theta)$ are defined as in (2.2.13). We consider the ranges $[K - \delta_1 K, K + \delta_1 K]$, $[r - \delta_2 r, r + \delta_2 r]$, and $[x_0 - \delta_3 x_0, x_0 + \delta_3 x_0]$ with $\delta = \delta_1 = \delta_2 = \delta_3$. The resulting optimal final time points T_D can be seen in Table 2.10 for various values of δ and ε.

As expected, we see that better *a priori* knowledge yields a closer estimate to the final time value corresponding to the true value parameter θ_0 with no uncertainty. However,

Table 2.10: The optimal duration time, T_D, for several values of δ and ε, based on the TSF with non-noisy data.

$\boldsymbol{\delta}$	$\boldsymbol{T_D(\varepsilon{=}10^{-3})}$	$\boldsymbol{T_D(\varepsilon{=}10^{-4})}$	$\boldsymbol{T_D(\varepsilon{=}10^{-5})}$
0	15.3	17.6	20.9
0.25	21.0	23.0	27.4
0.4	26.9	28.2	33.7
0.5	32.8	33.4	39.9
0.6	41.9	41.9	49.2

in practice there will be noisy data, which we currently do not take into account. Rather, this indicates the final time which best includes *any usable information* for determining optimal parameter values, regardless of noise level.

Numerical Simulations

Numerical simulations verify the analysis carried out in the previous subsection which demonstrates that the traditional sensitivity functions, when used in conjunction with the condition number of the Fisher information matrix, are efficient tools in determining a sufficient final experiment time. We set up and evaluate an inverse problem in which we optimize the parameter $\hat{\theta}$ over an increasing time interval. We use standard errors to indicate the accuracy of $\hat{\theta}$, and our goal is to determine a sufficient stopping time T based on when the standard errors for θ_k, $k = 1, \ldots, p$ reach a steady state.

To conduct this experiment, we consider a data set (created by solving the logistic ODE with a "true" parameter θ_0, and then adding Gaussian noise to the obtained solution), and set up an inverse problem using the solution of the logistic equation in order to obtain the optimal parameter set based on an ordinary least squares cost functional. Next, we add an additional data point to the existing data set, and again perform the inverse problem. We continue to add additional data points and solve the inverse problem until the data set reaches a predetermined final stopping time. Each time we perform the simulations, we compute the standard errors for each of the parameters. We consider average values over many simulations as opposed to values from an individual data set. Because we note that each data set $y(\cdot)$ is a realization of a random variable $Y(\cdot)$, we want to look for characteristics of the random variable (i.e., similarities among all the realizations) as opposed to just a single realization. We repeat the entire process 100 times, averaging the standard errors (for each final time T) over all the data sets in order to obtain the mean values.

Due to the small number of parameters to estimate, we use the Nelder-Mead optimization algorithm, implemented with *fminsearch* in MATLAB. We consider $T = 10$ as the starting value for the final time, because the standard errors (and condition number) are very large for the parameters when there is an insufficient amount of information for the computations, as is the case with a lower stopping time. We allow T to increase by one unit at a time until 50, a value sufficiently large for the purposes of these simulations. By increasing T in this manner, we create a uniform grid for each simulation. We generate noisy data by adding Gaussian noise with mean zero and variance $\sigma_0^2 = 0.16$ to a deterministic solution to the logistic ODE with true parameter $\theta_0 = (17.5, 0.7, 0.1)$. The optimization algorithm also requires an initial estimate for the parameter set, which we give as $\theta^0 = 1.4 \cdot \theta_0 = (24.5, 0.98, 0.14)$.

We observe the results of the simulations in Figure 2.11 and note that the standard errors for r and x_0 remain consistently low after $T \approx 20$, as shown in Figures 2.11(b) and 2.11(c). The standard error for K is higher, but continues to decrease even after reaching $T = 20$, as seen in Figure 2.11(a). However, we observe that by $T \approx 25$, SE_K is relatively low, and additional data points sampled beyond this point will contribute very little to the optimization of K. Also, we consider the condition number of the corresponding Fisher information matrix, $\rho(F)$, and we can see in Figure 2.9(a) that $\rho(F)$ is relatively low by $T = 15$. Hence, any final time chosen beyond this point would be reasonable. We note that in many problems, the condition number may not be steadily decreasing in this manner, and may require further consideration. Thus, by examining the evolution of condition number obtaining as well as the decreasing standard errors, a final time of $T = 25$ should be sufficient for low standard errors for the parameter set. However, depending on the cost of data collection it may be necessary to be less conservative with the final time choice, and hence a final time of $T = 20$ should be sufficient.

We note that in Table 2.10, the suggested final time, corresponding to prior knowledge of up to 40% of the true parameter value, is $T_D = 26.9$ for $\varepsilon = 10^{-3}$. This indicates that we should be able to obtain a sufficiently optimized parameter set from data in an interval no larger than $[0, 26.9]$ with the initial estimate of $1.4 \cdot \theta_0$. Note that the data to which the model is compared is noiseless. Nonetheless, we see from computational results that choosing a final time of $T = 26.9$, as suggested by the initial TSF analysis, seems to be decent although slightly conservative in this case. This indicates that the traditional sensitivity functions are a useful tool in determining a sufficient (or "optimal") final time.

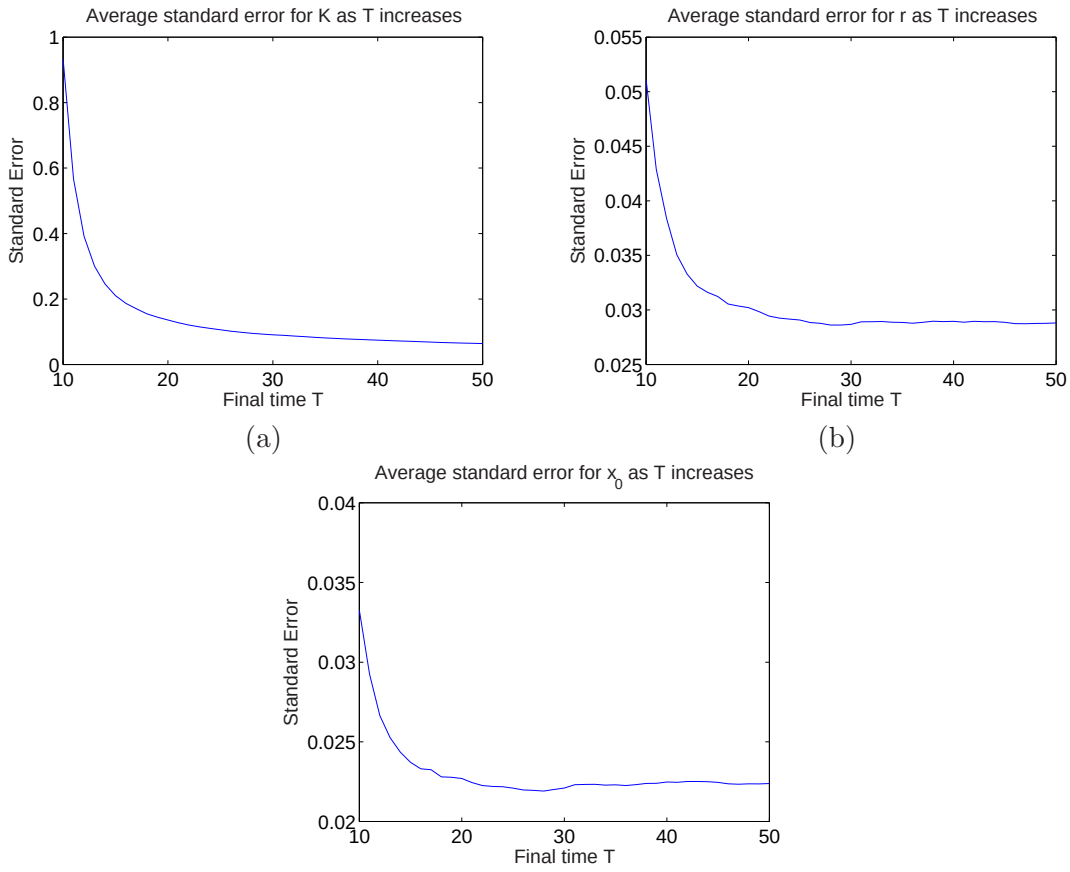

Figure 2.11: As the final time T increases, we have the averages over 100 sets of noisy data with $\sigma_0^2 = 0.16$ of (a) SE_K, (b) SE_r, and (c) SE_{x_0}.

Sampling Distribution

As discussed in Section 2.1.2, it is typical to consider discrete time measurements and minimize the residual sum of squares (2.1.15) when solving parameter estimation problems. However, when modeling a physical or biological phenomenon, we assume that the mathematical model $f(t, \theta)$ approximates the phenomenon for all t in some interval $[0, T]$ and for all θ in a neighborhood of the true value θ_0. In other words, in the absence of measurement noise, the model $f(t, \theta)$ should accurately predict the behavior of the physical system for an entire time interval and not just for some particular instances $t_1 < t_2 < \cdots < t_n$ in the interval $[0, T]$. Therefore, when solving a parameter estimation problem for θ, it seems logical to consider continuous time observations, i.e., to find the estimate $\hat{\theta}$ which minimizes

(2.1.13). Due to constraints/restrictions imposed by real world applications, the continuous cost functional (2.1.13) is rarely feasible in practice, and we are often forced to use (2.1.15). However, from a theoretical point of view, the approach (2.1.13) is perfectly legitimate, and the idea of using continuous time measurements comes naturally, when considering that the model itself is continuous.

Recall that each cost functional is associated with a probability measure $\mathcal{P}(t)$. When $\mathcal{P}$ is taken in the form (2.1.14), we see that it governs the location of the discrete time points. Then we naturally can extend this idea to Fisher information matrices, where we consider the amount of information in the measurements at those time points supported in the measure $\mathcal{P}$. It follows intuitively that the continuous formulation of the Fisher information matrix, F, carries the maximum amount of information for each of the parameters. However, since gathering data that is longitudinally continuous is rarely possible, our goal is to determine the longitudinal placement of n given data points which yields the most information toward parameter identification. We assume there is an optimal $\mathcal{P}^\star$ (associated with an optimal $F_D^\star$) which is the probability measure producing a placement of data points yielding the most information. Given n, we then assume that there is some $\hat{\mathcal{P}}^n$ which best approximates $\mathcal{P}^\star$. The Fisher information matrix $\hat{F}_D^n$ which corresponds to this measurement $\hat{\mathcal{P}}^n$ is the argument which minimizes

$$J(F_D^n) = \sum_{i=1}^{p} \sum_{j=1}^{p} \left| F_{ij} - F_{Dij}^n \right|^2, \tag{2.2.14}$$

for a system with p parameters. That is, we seek the discrete measure $\hat{\mathcal{P}}^n$ that gives the best discrete approximation $\hat{F}_D^n$ to the continuous Fisher information matrix F in the Frobenius norm.

Numerical simulations implementing this data formulation technique are currently underway.

2.2.4 Concluding Methodology Remarks

Through our analysis and application to the logistic growth population model, we have established that the traditional and generalized sensitivities are both essential tools in parameter estimation and inverse problems. Additionally, the consideration of the Fisher information matrix, both with respect to its condition number and usefulness in

measurement of information content, is helpful in the formulation of data collection for these types of problems.

We will continue efforts in numerically implementing the optimal time point distribution methodology as outlined in Section 2.2.3.

Chapter 3

Sinko-Streifer Hybrid Model

We model a system in which shrimp are used as a scaffold organism to produce biological countermeasures. First, shrimp postlarvae would be stocked in a controlled environment, and allowed to grow normally. The shrimp would then be infected with a recombinant viral vector (e.g., recombinant Taura Syndrome Virus or rTSV) expressing a foreign antigen, resulting in vaccine production in live infected shrimp. To mathematically represent this approach, we consider a hybrid model of the shrimp biomass/vaccine production system as found in [1], which has two components: (uninfected) biomass production, and vaccine/antibody production. The output of the biomass production model is used as input to the vaccine production model, as depicted in Figure 3.1, from [1]. We make the initial assumption that the amount of vaccine produced equals the total infected biomass, which we seek to model. The model we employ is based upon the McKendrick-von-Foerster/Sinko-Streifer size-structured population models (see [27, 31, 36]), where we consider mass rather than size.

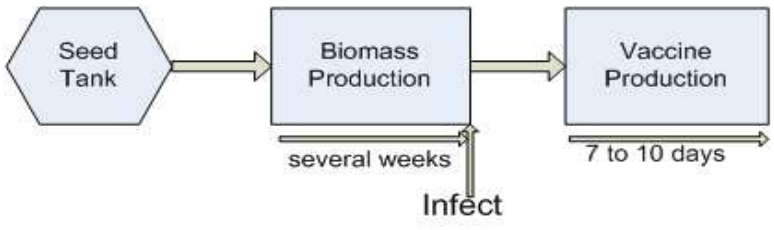

Figure 3.1: Flow of the hybrid model.

3.1 Motivation for Sensitivity Analysis

Our ultimate goal is to maximize the total amount of live infected biomass, which directly corresponds to the amount of vaccine produced. Hence, we focus on the parameters which directly impact the total amount of infected biomass. We begin by considering the biomass component of the hybrid model.

As previously stated, a certain density of shrimp postlarvae are initially placed into a controlled growth environment. Then, after the shrimp have reached a sufficient size, they are infected with a recombinant viral vector. In Figure 3.2(a) we see an example of the progression of the shrimp from the initial stocking time until the time of infection. In Figure 3.2(b) we see the output from the biomass model, which is the input into the vaccine production model. The model output is highly dependent on the growth, mortality and reproduction rates of the individual shrimp. Since this output is also the input into the vaccine production model, we see that these rates affect the amount of total infected biomass. Hence, we investigate the sensitivity of the biomass model with respect to each of these functions.

Next, we motivate the need to conduct sensitivity analysis for the vaccine production component of the hybrid model. As we will discuss in detail in Section 3.3, the infected shrimp move through several states of infection in our model: susceptible, latent, and acute. After exposure to the infection, the shrimp are said to be in the *susceptible* state. When

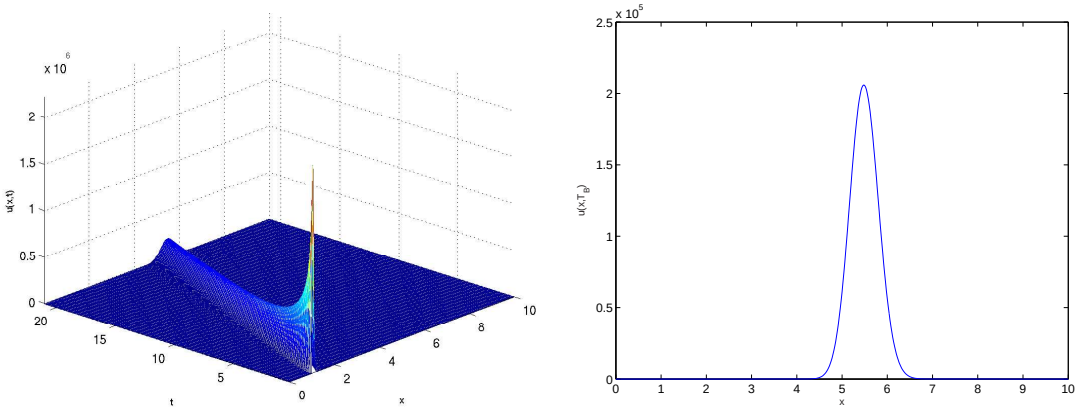

(a) (b)

Figure 3.2: (a) Example of the biomass simulation, and (b) output from the biomass model, used as input to the vaccine production model.

the shrimp have become infected, but show few signs of infection and are not yet producing the vaccine, we say the shrimp are in the *latent* state. Lastly, the latently infected shrimp progress into the *acute* state, where they show severe signs of infection and produce the vaccine.

The cumulative latent-to-acute rate function governs the rate of progression of the shrimp population from the latent to the acute state, of which several examples are displayed in Figure 3.3(a). Then in Figure 3.3(b), we see the total amount of acutely infected shrimp as a function of time, where each population density corresponds to one of the rate functions shown in Figure 3.3(a). It is evident that the latent-to-acute rate function is significant in determining the optimal harvest time (when the total acutely infected biomass is at a maximum). The details regarding the generation of the plots in Figure 3.2 and Figure 3.3 can be found in [1].

We have established the need to investigate the sensitivity of each component of the hybrid model with respect to the rates which govern the population size. Consequently, we derive the necessary sensitivities and then show the results of numerical simulations.

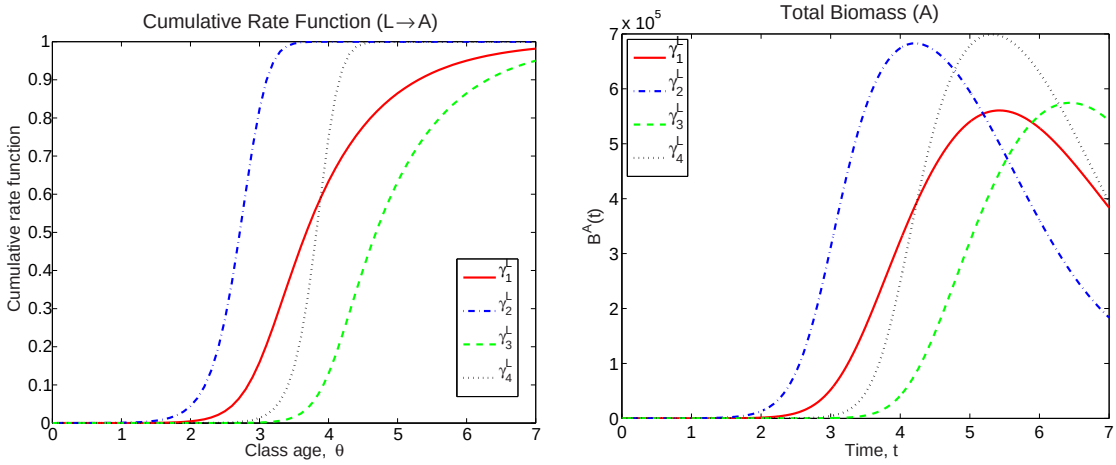

(a) (b)

Figure 3.3: (a) Several examples of cumulative latent-to-acute rate functions. (b) The corresponding acutely infected total population densities.

3.2 Biomass Model

We present a classical size-structured population model with mass as the structure variable. The factors that we consider which affect the total biomass of normal shrimp are the growth and mortality rates. We do not include reproduction in the model, as the amount of time required for shrimp to grow from the postlarval stage until they are ready for vaccination is insufficient for reproduction. At present, we consider a controlled environment for biomass production and assume that the growth and morality rates of normal shrimp are indifferent to changes in environmental factors such as temperature and salinity.

Shrimp growth is characterized by molting and "intermolting" (no external growth) periods [14]. However over a long period of time, the growth can be approximated by a continuous process. Consequently, the growth rate $g(x)$ is assumed to be a continuous function of mass x. We likewise consider mortality as a function of mass x only.

The biomass production model is given by

$$\begin{aligned} &u_t(x,t) + (g(x)u(x,t))_x + m(x)u(x,t) = 0, \\ &u(0,t) = 0, \\ &u(x,0) = u_0(x). \end{aligned} \tag{3.2.1}$$

for $(x,t) \in [0, x_{max}] \times [0, T_B]$. The function $u(x,t)$ denotes the population density with size x at time t, g is the size-dependent growth rate, m represents the size-dependent mortality rate, and u_0 is the initial population density. T_B denotes the final time considered in the biomass portion of the model, and the maximum size individuals may obtain in the time interval $[0, T_B]$ is x_{max}. The well-posedness of this model is proven in [9] using weak formulations, while existence and uniqueness are proven in [8].

3.2.1 Sensitivity Analysis

In this section, we derive and investigate the sensitivity equations for the more general linear size-structured population model

$$\begin{aligned} &u_t(x,t) + (g(x)u(x,t))_x + m(x)u(x,t) = 0, \\ &g(0)u(0,t) = \int_0^{\bar{x}} \beta(x)u(x,t)dx, \\ &u(x,0) = u_0(x), \end{aligned} \tag{3.2.2}$$

which has only minor differences from the biomass production model (3.2.1). Notice that we have incorporated reproduction in (3.2.2), because we want to investigate the sensitivities for the general formulation as opposed to restricting the analysis to the shrimp biomass model. Here $(x,t) \in [0,\bar{x}] \times [0,T]$, $u(x,t)$ denotes the population density with size x at time t, g is the size-dependent growth rate, m represents the size-dependent mortality rate, β is the size-dependent reproduction rate, and u_0 is the initial population density. The maximum size individuals may obtain in their lifetime is $\bar{x}$. Although our objective is to derive the sensitivity equations of u with respect to the functions β, g, m, and u_0, here we consider only the sensitivity with respect to mortality m as an example of the process required for each function. We note that this derivation, as well as the others, can be found in [7].

For traditional finite-dimensional parameter-dependent systems of ordinary differential equations

$$\dot{x}(t) = f(x(t),\theta), \qquad x(0) = x_0,$$

one finds that the heuristic differentiation of the system (using the chain rule) with respect to a parameter θ, provides the correct sensitivity equations for $y(t) = \dfrac{\partial x}{\partial \theta}(t)$,

$$\dot{y}(t) = \frac{\partial f}{\partial x} y(t) + \frac{\partial f}{\partial \theta}, \qquad y(0) = 0.$$

Differentiation of (3.2.2) with respect to the functions β, g, m, or u_0 is somewhat more delicate. However, we establish that a formal, heuristic differentiation also results in the correct sensitivity equations and that this heuristic derivation can be made rigorous.

The method of characteristics is commonly used (see [8, 16, 25]) to establish the existence and uniqueness of the solution to size-structured population models. Using this approach one obtains an *implicit* representation of the solution which can be used to transform the partial differential equation into an integral equation. Then, we apply the contraction mapping theorem to complete the sensitivity analysis for m in (3.2.2).

Preliminary Results

In order to develop the sensitivity formulations, the following assumptions are imposed on our model parameters and initial conditions in (3.2.2):

(A1) $g \in \mathcal{W}^{1,\infty}(0,\bar{x})$, $g > 0$ on $[0,\bar{x})$, and $g(\bar{x}) = 0$, and

(A2) $m \in \mathcal{L}^\infty(0, \bar{x})$, and $m \geq 0$ on $[0, \bar{x}]$.

We will use $\|\cdot\|_\infty$ to denote the norm $\|\cdot\|_{\mathcal{L}^\infty(0,\bar{x})}$, and $\|\cdot\|_1$ to denote the norm $\|\cdot\|_{\mathcal{L}^1(0,\bar{x})}$ for the rest of the section. Note that assumption (A1) implies that g is in a convex subset of $\mathcal{W}^{1,\infty}(0, \bar{x})$. Assumption (A2) shows that m is in a convex subset of $\mathcal{L}^\infty(0, \bar{x})$. Consequently, we can formulate the sensitivity equations for (3.2.2) using a directional (Gateaux) derivative of u with respect to m. The directional derivative is defined in Definition 3.2.1.

Definition 3.2.1. *Let Θ be a convex subset in some topological vector space, and $f : \mathbb{R}_+ \times \Theta \to R$. Given θ and ϑ in Θ, we define the derivative $f_\theta(t; \theta, \vartheta)$ of a function f at θ in the direction ϑ to be*

$$f_\theta(t; \theta, \vartheta - \theta) = \lim_{\varepsilon \to 0+} \frac{f(t; \theta + \varepsilon(\vartheta)) - f(t; \theta)}{\varepsilon}, \tag{3.2.3}$$

provided this limit exists.

The existence and uniqueness of the solution to (3.2.2), as well as the sensitivity equations, are carried out using the method of characteristics. The equations are reduced to a *renewal equation* (a Volterra equation of convolution type), and the existence and uniqueness of the solution to this integral equation are established with the result of Theorem 3.2.4 from [11].

Theorem 3.2.2. *If $\Psi(t)$ is bounded on $[0, T]$, and $\int_0^T |\phi(s)|ds < \infty$, then the equation*

$$\Phi(t) = \int_0^t \phi(s)\Phi(t - s)ds + \Psi(t) \tag{3.2.4}$$

has a unique bounded solution in $[0, T]$. If we further assume that $\Psi(t)$ is continuous, then $\Phi(t)$ is also continuous.

Suppose that ϕ and Ψ in equation (3.2.4) are both dependent on parameter θ in a convex subset Θ of some topological space. Then the integral equation (3.2.4) becomes

$$\Phi(t; \theta) = \int_0^t \phi(s; \theta)\Phi(t - s; \theta)ds + \Psi(t; \theta). \tag{3.2.5}$$

We first give a sensitivity result for (3.2.5) because the sensitivity results for (3.2.2) are heavily dependent upon it. We state this formally as a theorem because it is fundamental to the subsequent results in this section.

Theorem 3.2.3. *Suppose that for some $\theta \in \Theta$, the functions $\phi(t;\theta)$ and $\Psi(t;\theta)$ are both bounded on $[0,T]$. We assume that for $\theta, \vartheta \in \Theta$, ϕ has a bounded directional derivative $\phi_\theta(t;\theta,\vartheta)$ on $[0,T]$ with respect to $\theta \in \Theta$ in the direction ϑ, and Ψ has a bounded directional derivative $\Psi_\theta(t;\theta,\vartheta)$ on $[0,T]$ with respect to $\theta \in \Theta$ in the direction ϑ. Then the directional derivative $\Phi_\theta(t;\theta,\vartheta)$ of Φ with respect to θ in the direction ϑ exists. Let $z(t) = \Phi_\theta(t;\theta,\vartheta)$, then it satisfies the following equation*

$$z(t) = \int_0^t \phi(s;\theta) z(t-s) ds + \int_0^t \phi_\theta(s;\theta,\vartheta)\Phi(t-s;\theta) ds + \Psi_\theta(t;\theta,\vartheta). \tag{3.2.6}$$

See [7] for arguments which establish these results.

Sensitivity Equation with Respect to Mortality Rate

In this section, we conduct the sensitivity analysis of u with respect to m. We will use the method of characteristics to obtain the renewal equation for (3.2.2) and show that there exists a unique solution to this equation. The following notation will be used throughout this section:

$$G(x) = \int_0^x \frac{1}{g(\xi)} d\xi \quad \text{and} \quad B(t) = \int_0^{\bar{x}} \beta(x) u(x,t) dx,$$

where u is the unique solution of (3.2.2) which is guaranteed to exist (see [8, 25]). By assumption (A1), we find that for $\xi \in [0, \bar{x})$,

$$0 < g(\xi) = g(\xi) - g(\bar{x}) \leq \|g'\|_\infty (\bar{x} - \xi).$$

Hence, we have

$$G(x) \geq \frac{1}{\|g'\|_\infty} \int_0^x \frac{1}{\bar{x} - \xi} d\xi,$$

which implies that

$$\lim_{x \to \bar{x}} G(x) = \infty.$$

G is a strictly increasing function due to the fact that $g > 0$ on $[0, \bar{x})$. Thus, G^{-1} exists and is a strictly increasing map from $[0,\infty) \to [0, \bar{x})$. Therefore, the requirement that $g(\bar{x}) = 0$ in (A1) guarantees that the size of an individual always remains less than $\bar{x}$. In addition, to simplify the expressions, we let:

$$\pi(x,t) = G^{-1}(G(x) - t), \quad \varrho(t,\xi) = G^{-1}(t - \xi), \quad \rho(x,t,\xi) = 2t - G(x) - \xi.$$

Using the method of characteristics, we see that the solution of (3.2.2) is given implicitly as follows:

If $x \geq G^{-1}(t)$, then

$$u(x,t) = u_0(G^{-1}(G(x)-t))\frac{g(G^{-1}(G(x)-t))}{g(x)} \exp\left(-\int_{G^{-1}(G(x)-t)}^{x} \frac{m(\xi)}{g(\xi)}d\xi\right), \quad (3.2.7)$$

and if $x < G^{-1}(t)$, then

$$u(x,t) = \frac{B(t-G(x))}{g(x)} \exp\left(-\int_0^x \frac{m(\xi)}{g(\xi)}d\xi\right). \quad (3.2.8)$$

Hence, we have

$$\begin{aligned} B(t) = & \int_0^{G^{-1}(t)} \beta(x)\frac{B(t-G(x))}{g(x)} \exp\left(-\int_0^x \frac{m(\xi)}{g(\xi)}d\xi\right) dx \\ & + \int_{G^{-1}(t)}^{\bar{x}} \beta(x)u_0(\pi(x,t))\frac{g(\pi(x,t))}{g(x)} \exp\left(-\int_{\pi(x,t)}^{x} \frac{m(\xi)}{g(\xi)}d\xi\right) dx. \end{aligned} \quad (3.2.9)$$

Let $\eta = G(x)$, then $x = G^{-1}(\eta)$ and $d\eta = \dfrac{1}{g(x)}dx$. Consequently, the first term of (3.2.9) can be rewritten as

$$\begin{aligned} & \int_0^{G^{-1}(t)} \beta(x)\frac{B(t-G(x))}{g(x)} \exp\left(-\int_0^x \frac{m(\xi)}{g(\xi)}d\xi\right) dx \\ & = \int_0^t \beta(G^{-1}(\eta)) \exp\left(-\int_0^{G^{-1}(\eta)} \frac{m(\xi)}{g(\xi)}d\xi\right) B(t-\eta)d\eta \\ & = \int_0^t \beta(G^{-1}(\eta)) \exp\left(-\int_0^{\eta} m(G^{-1}(\sigma))d\sigma\right) B(t-\eta)d\eta. \end{aligned} \quad (3.2.10)$$

Letting $\eta = G^{-1}(G(x)-t)$ yields $x = G^{-1}(G(\eta)+t)$ and $\dfrac{1}{g(\eta)}d\eta = \dfrac{1}{g(x)}dx$. These relations imply that $dx = \dfrac{g(G^{-1}(G(\eta)+t))}{g(\eta)}d\eta$. Recall that $\lim\limits_{\tau\to\infty} G^{-1}(\tau) = \bar{x}$, and hence

$$\lim_{x\to\bar{x}} G^{-1}(G(x)-t) = \bar{x} \ \text{ for all } \ t \in [0,T]. \quad (3.2.11)$$

We then use (3.2.11) to rewrite the second term of (3.2.9) as

$$\begin{aligned} & \int_{G^{-1}(t)}^{\bar{x}} \beta(x)u_0(G^{-1}(G(x)-t))\frac{g(G^{-1}(G(x)-t))}{g(x)} \exp\left(-\int_{G^{-1}(G(x)-t)}^{x} \frac{m(\xi)}{g(\xi)}d\xi\right) dx \\ & = \int_0^{\bar{x}} \beta(G^{-1}(G(\eta)+t))u_0(\eta) \exp\left(-\int_{\eta}^{G^{-1}(G(\eta)+t)} \frac{m(\xi)}{g(\xi)}d\xi\right) d\eta. \end{aligned} \quad (3.2.12)$$

Now, let $\sigma = G(\xi) - G(\eta)$, which implies that $\xi = G^{-1}(G(\eta) + \sigma)$ and $d\sigma = \dfrac{1}{g(\xi)} d\xi$. Then we have

$$\exp\left(-\int_{\eta}^{G^{-1}(G(\eta)+t)} \frac{m(\xi)}{g(\xi)} d\xi\right) = \exp\left(-\int_0^t m(G^{-1}(G(\eta)+\sigma)) d\sigma\right). \tag{3.2.13}$$

Following from (3.2.13) and (3.2.12), we see that

$$\begin{aligned}\int_{G^{-1}(t)}^{\bar{x}} \beta(x) u_0(G^{-1}(G(x)-t)) \frac{g(G^{-1}(G(x)-t))}{g(x)} \exp\left(-\int_{G^{-1}(G(x)-t)}^{x} \frac{m(\xi)}{g(\xi)} d\xi\right) dx \\ = \int_0^{\bar{x}} u_0(\eta)\beta(G^{-1}(G(\eta)+t)) \exp\left(-\int_0^t m(G^{-1}(G(\eta)+\sigma)) d\sigma\right) d\eta.\end{aligned} \tag{3.2.14}$$

Therefore, by (3.2.9), (3.2.10) and (3.2.14) we obtain the renewal equation

$$B(t) = \int_0^t k(\eta) B(t-\eta) d\eta + F(t), \tag{3.2.15}$$

where

$$k(\eta) = \beta(G^{-1}(\eta)) \exp\left(-\int_0^{\eta} m(G^{-1}(\sigma)) d\sigma\right) \tag{3.2.16}$$

and

$$F(t) = \int_0^{\bar{x}} u_0(\eta)\beta(G^{-1}(G(\eta)+t)) \exp\left(-\int_0^t m(G^{-1}(G(\eta)+\sigma)) d\sigma\right) d\eta. \tag{3.2.17}$$

Note that $0 \le F(t) \le \|\beta\|_\infty \|u_0\|_1$ and $0 \le k(t) \le \|\beta\|_\infty$ on $[0, T]$. Hence, by Theorem 3.2.2 we are guaranteed the existence of a unique bounded nonnegative solution to (3.2.15). Thus, the solution of (3.2.15) is the same B used in the unique nonnegative solution to (3.2.2), given in equations (3.2.7) and (3.2.8).

We observe from equation (3.2.8) that the representation for $u(x,t)$ in the region

$$\left\{(x,t) \,\middle|\, 0 \le x < G^{-1}(t), t > 0\right\}$$

is dependent on B. Hence, in order to derive the sensitivity equation of u with respect to m, we need to investigate the sensitivity for B. To simplify notation, we use h to denote a given direction in the corresponding parameter space when we take a directional derivative with respect to m. Then, for example, the sensitivity of B with respect to m in the direction h is written as $B_m(t; m, h)$.

We first consider the sensitivity of B with respect to m. Using the chain rule, we find that $k_m(\eta; m, h)$ satisfies

$$\begin{aligned} k_m(\eta; m, h) &= -\beta(G^{-1}(\eta)) \exp\left(-\int_0^\eta m(G^{-1}(\sigma))d\sigma\right)\left(\int_0^\eta h(G^{-1}(\sigma))d\sigma\right) \\ &= -k(\eta)\left(\int_0^\eta h(G^{-1}(\sigma))d\sigma\right), \end{aligned} \tag{3.2.18}$$

and $F_m(t; m, h)$ is given by

$$F_m(t; m, h) = -\int_0^{\bar{x}} u_0(\eta)\beta(\pi(\eta, -t)) \exp\left(-\int_0^t m(\pi(\eta, -\sigma)d\sigma\right)\left(\int_0^t h(\pi(\eta, -\sigma)d\sigma\right)d\eta. \tag{3.2.19}$$

Then,

$$|k_m(\eta; m, h)| \leq T\|h\|_\infty\|\beta\|_\infty \text{ for } \eta \in [0, T]$$

and

$$|F_m(t; m, h)| \leq T\|h\|_\infty\|\beta\|_\infty\|u_0\|_1 \text{ for } t \in [0, T].$$

Theorem 3.2.3 guarantees that $B_m(t; m, h)$ is the unique bounded solution to

$$B_m(t; m, h) = \int_0^t k(\eta)B_m(t-\eta; m, h)d\eta + \int_0^t k_m(\eta; m, h)B(t-\eta)d\eta + F_m(t; m, h). \tag{3.2.20}$$

Based on the above discussion of the sensitivity analysis for B with respect to m, we can now obtain the sensitivity of u with respect to m using (3.2.7) and (3.2.8). Equations (3.2.7)–(3.2.8) coupled with the existence of $B_m(t; m, h)$ for $t \in [0, T]$ imply that the directional derivative $u_m(x, t; m, h)$ satisfies:

If $x \geq G^{-1}(t)$, then

$$u_m(x, t; m, h) = -u(x, t)\int_{G^{-1}(G(x)-t)}^x \frac{h(\tau)}{g(\tau)}d\tau, \tag{3.2.21}$$

and if $x < G^{-1}(t)$, then

$$\begin{aligned} u_m(x, t; m, h) = \; & \frac{B_m(t - G(x); m, h)}{g(x)} \exp\left(-\int_0^x \frac{m(\tau)}{g(\tau)}d\tau\right) \\ & -\frac{B(t - G(x))}{g(x)} \exp\left(-\int_0^x \frac{m(\xi)}{g(\xi)}d\xi\right)\int_0^x \frac{h(\tau)}{g(\tau)}d\tau. \end{aligned} \tag{3.2.22}$$

Differential equations are typically easier to numerically approximate than integral equations. Hence, we show that $u_m(x, t; m, h)$ is the solution to a first-order hyperbolic partial

differential equation. Then, we use this partial differential equation to obtain the numerical solution for the sensitivity of u with respect to m instead of using an integral equation as in (3.2.20).

Let w be the unique solution to

$$\begin{aligned} &w_t(x,t) + (g(x)w(x,t))_x + m(x)w(x,t) + h(x)u(x,t) = 0, \\ &g(0)w(0,t) = \int_0^{\bar{x}} \beta(x)w(x,t)dx, \\ &w(x,0) = 0. \end{aligned} \tag{3.2.23}$$

We wish to show that $w = u_m(x,t;m,h)$. Using the method of characteristics, we find that the solution to (3.2.23) is given by

If $x \geq G^{-1}(t)$, then

$$w(x,t) = -\int_0^t h(\pi(x,\xi))u(\pi(x,\xi),t-\xi)\frac{g(\pi(x,\xi))}{g(x)}\exp\left(-\int_{\pi(x,\xi)}^x \frac{m(\tau)}{g(\tau)}d\tau\right)d\xi, \tag{3.2.24}$$

and if $x < G^{-1}(t)$, then

$$\begin{aligned} w(x,t) = \quad & \frac{W(t-G(x))}{g(x)}\exp\left(-\int_0^x \frac{m(\tau)}{g(\tau)}d\tau\right) \\ & -\int_{t-G(x)}^t h(\varrho(t,\xi))u(\varrho(t,\xi),\rho(x,t,\xi))\frac{g(\varrho(t,\xi))}{g(x)}\exp\left(-\int_{\varrho(t,\xi)}^x \frac{m(\tau)}{g(\tau)}d\tau\right)d\xi, \end{aligned} \tag{3.2.25}$$

where $W(t) = \int_0^{\bar{x}} \beta(x)w(x,t)dx$.

We begin by simplifying (3.2.24). Note that $x \geq G^{-1}(t)$ implies that

$$G(\pi(x,\xi)) = G(x) - \xi \geq t - \xi,$$

and further, $G^{-1}(G(\pi(x,\xi)) - (t-\xi)) = \pi(x,t)$. Hence, by (3.2.7),

$$u(\pi(x,\xi),t-\xi) = u_0(\pi(x,t))\frac{g(\pi(x,t))}{g(\pi(x,\xi))}\exp\left(-\int_{\pi(x,t)}^{\pi(x,\xi)} \frac{m(\tau)}{g(\tau)}d\tau\right), \tag{3.2.26}$$

and thus, when $x \geq G^{-1}(t)$,

$$w(x,t) = -u_0(\pi(x,t))\frac{g(\pi(x,t))}{g(x)}\exp\left(-\int_{\pi(x,t)}^x \frac{m(\tau)}{g(\tau)}d\tau\right)\int_0^t h(\pi(x,\xi))d\xi. \tag{3.2.27}$$

Next we simplify (3.2.25). Together, (3.2.8) and the relation

$$2t - G(x) - \xi - G(G^{-1}(t-\xi)) = t - G(x)$$

imply that

$$u(G^{-1}(t-\xi), 2t - G(x) - \xi) = \frac{B(t-G(x))}{g(G^{-1}(t-\xi))} \exp\left(-\int_0^{G^{-1}(t-\xi)} \frac{m(\tau)}{g(\tau)} d\tau\right) \tag{3.2.28}$$

when $x < G^{-1}(t)$. Using (3.2.25) and (3.2.28), we see that

$$\begin{aligned} w(x,t) = \quad & \frac{W(t-G(x))}{g(x)} \exp\left(-\int_0^x \frac{m(\tau)}{g(\tau)} d\tau\right) \\ & - \frac{B(t-G(x))}{g(x)} \exp\left(-\int_0^x \frac{m(\tau)}{g(\tau)} d\tau\right) \int_{t-G(x)}^t h(G^{-1}(t-\xi)) d\xi. \end{aligned} \tag{3.2.29}$$

Then from (3.2.27) and (3.2.29), we find that when $x < G^{-1}(t)$

$$\begin{aligned} W(t) = \quad & \int_0^{G^{-1}(t)} \beta(x) \frac{W(t-G(x))}{g(x)} \exp\left(-\int_0^x \frac{m(\xi)}{g(\xi)} d\xi\right) dx \\ & - \int_0^{G^{-1}(t)} \beta(x) \frac{B(t-G(x))}{g(x)} \exp\left(-\int_0^x \frac{m(\xi)}{g(\xi)} d\xi\right) \left(\int_{t-G(x)}^t h(G^{-1}(t-\xi)) d\xi\right) dx \\ & - \int_{G^{-1}(t)}^{\bar{x}} \beta(x) u_0(\pi(x,t)) \frac{g(\pi(x,t))}{g(x)} \exp\left(-\int_{\pi(x,t)}^x \frac{m(\xi)}{g(\xi)} d\xi\right) \left(\int_0^t h(\pi(x,\xi)) d\xi\right) dx. \end{aligned}$$

Using the same transformation as derived for $B(t)$, we obtain

$$\begin{aligned} W(t) = \quad & \int_0^t \beta(G^{-1}(\eta)) \exp\left(-\int_0^\eta m(G^{-1}(\sigma)) d\sigma\right) W(t-\eta) d\eta \\ & - \int_0^t \beta(G^{-1}(\eta)) \exp\left(-\int_0^\eta m(G^{-1}(\sigma)) d\sigma\right) \left(\int_0^\eta h(G^{-1}(\sigma)) d\sigma\right) B(t-\eta) d\eta \\ & - \int_0^{\bar{x}} u_0(\eta) \beta(\pi(\eta,-t)) \exp\left(-\int_0^t m(\pi(\eta,-\sigma) d\sigma\right) \left(\int_0^t h(\pi(\eta,-\sigma) d\sigma\right) d\eta. \end{aligned} \tag{3.2.30}$$

From equations (3.2.18), (3.2.19), and (3.2.30), we see that

$$W(t) = \int_0^t k(\eta) W(t-\eta) d\eta + \int_0^t k_m(\eta; m, h) B(t-\eta) d\eta + F_m(t; m, h). \tag{3.2.31}$$

Hence, equation (3.2.31) and the uniqueness of the solution to (3.2.20) imply that

$$W(t) = B_m(t; m, h) \quad \text{for any } t \in [0, T]. \tag{3.2.32}$$

Next we argue that $\dfrac{\partial u}{\partial m}[h] = w$, which shows that $u_m(x,t;m,h)$ satisfies (3.2.23). Let $\tau = G^{-1}(G(x)-\xi)$. Then $d\xi = -\dfrac{1}{g(\tau)}d\tau$, and hence,

$$\int_0^t h(G^{-1}(G(x)-\xi))d\xi = \int_{G^{-1}(G(x)-t)}^{x} \frac{h(\tau)}{g(\tau)}d\tau. \tag{3.2.33}$$

From equations (3.2.7), (3.2.27) and (3.2.33), we observe that

$$w(x,t) = -u(x,t)\int_{G^{-1}(G(x)-t)}^{x} \frac{h(\tau)}{g(\tau)}d\tau, \tag{3.2.34}$$

if $x \geq G^{-1}(t)$. Therefore, by (3.2.21) and (3.2.34) we see that $\dfrac{\partial u}{\partial m}[h] = w$ in the region defined by

$$\left\{(x,t)\,\middle|\,\bar{x} > x \geq G^{-1}(t),\ t \geq 0\right\}.$$

Now let $\tau = G^{-1}(t-\xi)$. Then $d\xi = -\dfrac{1}{g(\tau)}d\tau$, and hence,

$$\int_{t-G(x)}^{t} h(G^{-1}(t-\xi))d\xi = \int_0^x \frac{h(\tau)}{g(\tau)}d\tau. \tag{3.2.35}$$

From equations (3.2.29), (3.2.32) and (3.2.35) we see that if $x < G^{-1}(t)$ then we have the following

$$\begin{aligned} w(x,t) = \ & \frac{B_m(t-G(x);m,h)}{g(x)}\exp\left(-\int_0^x \frac{m(\tau)}{g(\tau)}d\tau\right) \\ & -\frac{B(t-G(x))}{g(x)}\exp\left(-\int_0^x \frac{m(\xi)}{g(\xi)}d\xi\right)\int_0^x \frac{h(\tau)}{g(\tau)}d\tau. \end{aligned} \tag{3.2.36}$$

By (3.2.22) and (3.2.36) we have $\dfrac{\partial u}{\partial m}[h] = w$ when $x < G^{-1}(t)$. Therefore, $u_m(x,t;m,h)$ satisfies the initial boundary value problem (3.2.23), and we can use this system to determine $u_m(x,t;m,h)$.

3.2.2 Numerical Scheme and Results

We now illustrate the ease of computations for the sensitivity of u with respect to m. We use an implicit finite difference scheme to approximate the population density $u(x,t)$ as well as $w(x,t) = u_m(x,t;m,h)$. Let $\Delta x = \bar{x}/n$ and $\Delta t = T/l$ be the spatial and time mesh sizes, respectively. The mesh points are then given by $x_j = j\Delta x$ for $j = 0,1,\ldots,n$, and $t_k = k\Delta t$ for $k = 0,1,\ldots,l$. We denote by u_j^k the finite difference approximation of

$u(x_j, t_k)$, and we let $u_j^0 = u_0(x_j)$, $g_j = g(x_j)$, $m_j = m(x_j)$, and $\beta_j = \beta(x_j)$, $j = 0, 1, \ldots, n$. The finite difference scheme used to approximate the solution $u(x,t)$ to (3.2.2) is now given as

$$\begin{aligned} &\frac{u_j^{k+1} - u_j^k}{\Delta t} + \frac{g_j u_j^{k+1} - g_{j-1} u_{j-1}^{k+1}}{\Delta x} + m_j u_j^{k+1} = 0, \quad 1 \le j \le n, \\ &g_0 u_0^{k+1} = \sum_{i=1}^{n} \beta_i u_i^k \Delta x. \end{aligned} \tag{3.2.37}$$

We denote the finite difference approximation of $w(x_j, t_k)$ by w_j^k, and let $w_j^0 = 0$ and $h_j = h(x_j)$. The scheme used to approximate the solution $w(x,t)$ to (3.2.23) is then given by

$$\begin{aligned} &\frac{w_j^{k+1} - w_j^k}{\Delta t} + \frac{g_j w_j^{k+1} - g_{j-1} w_{j-1}^{k+1}}{\Delta x} + m_j w_j^{k+1} + h_j u_j^{k+1} = 0, \quad 1 \le j \le n, \\ &g_0 w_0^{k+1} = \sum_{i=1}^{n} \beta_i w_i^k \Delta x. \end{aligned} \tag{3.2.38}$$

In this example, we assume a maximum size of $\bar{x} = 1$ unit of mass and a final time of $T = 5$ units of time. The initial condition and model parameters are given as

$$u^0(x) = 10x^3(1-x), \quad g(x) = 0.2(1-x), \quad m(x) = 0.4, \quad \beta(x) = 0.$$

Then, by (3.2.7) and (3.2.8), we can solve analytically for $u(x,t)$:

$$u(x,t) = \begin{cases} 10(1-x)[1-(1-x)e^{0.2t}]^3 & x \ge 1 - e^{-0.2t} \\ 0 & x < 1 - e^{-0.2t}. \end{cases}$$

Note that m is a constant, and hence we allow the direction $h = 1$ when we take the directional derivative of u with respect to m. Then, by (3.2.34) and (3.2.36), the analytical solution for $w(x,t)$ is given as

$$w(x,t) = \begin{cases} -10t(1-x)[1-(1-x)e^{0.2t}]^3 & x \ge 1 - e^{-0.2t} \\ 0 & x < 1 - e^{-0.2t}. \end{cases}$$

The numerical solutions to (3.2.37) and (3.2.38) with $\Delta x = 10^{-4}$ and $\Delta t = 10^{-3}$ are shown in Figures 3.4(a) and 3.5(a), respectively. Figures 3.4(b) and 3.5(b) depict the analytical solutions, and we see the difference between the analytical and approximate solutions for $u(x,t)$ and $w(x,t)$ in Figures 3.4(c) and 3.5(c). These figures demonstrate that numerical solutions for $u(x,t)$ and $w(x,t)$ provide reasonable approximations to the

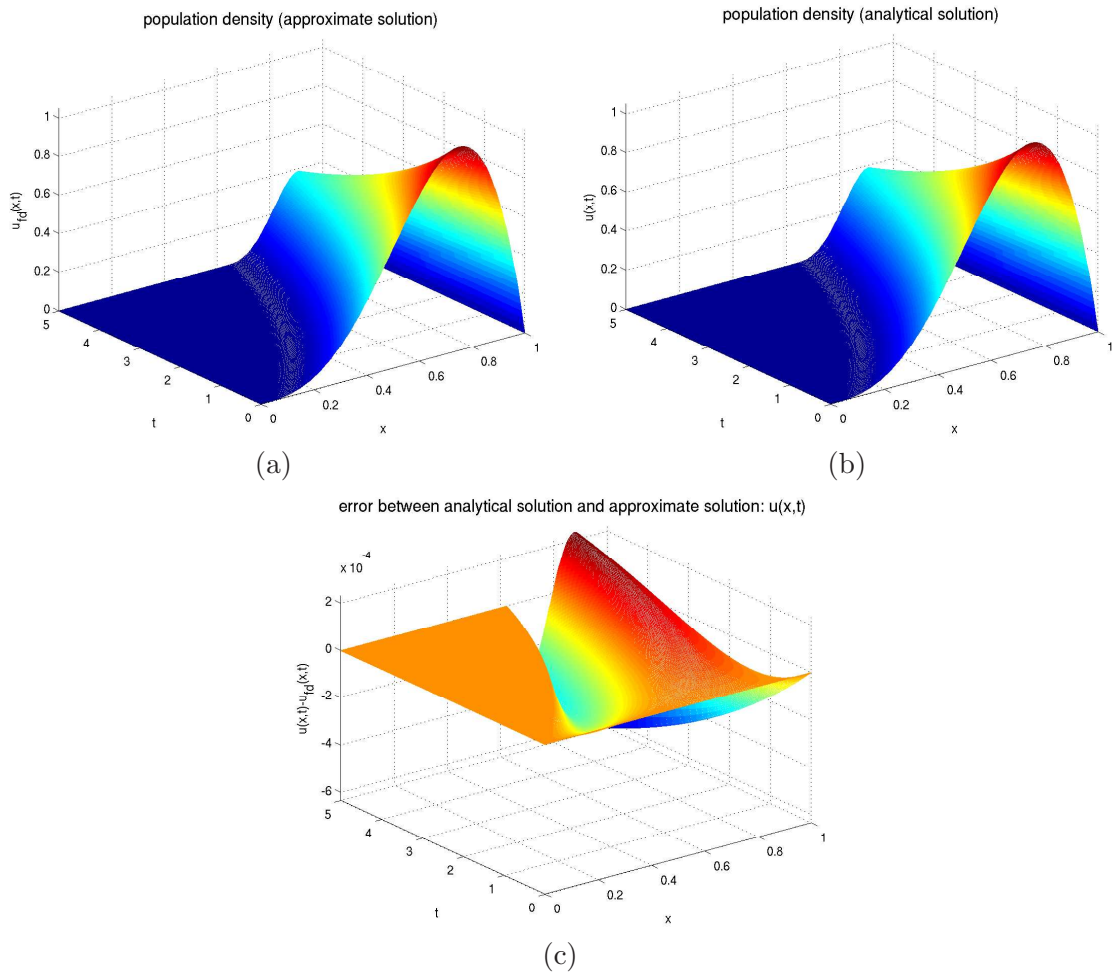

Figure 3.4: (a) The finite difference approximation $u_{fd}(x,t)$ of $u(x,t)$, (b) analytical solution for $u(x,t)$, and (c) error between the analytical solution and the finite difference approximation.

analytical solutions. However, we observe in Figures 3.6(b) and 3.7(b) that the magnitude of the error increases with time, due to a change in the shape of the population distribution curve (see Figures 3.6(a) and 3.7(a)). In particular, the decreasing growth rate causes the population distribution to become more narrow and steep with time. Notice also that the mortality rate directly affects the magnitude of the density.

The error for the population density is on the order of 10^{-4}, and the error for the sensitivity is on the order of 10^{-3}, as seen in Figures 3.6(b) and 3.7(b). Hence, the finite difference schemes seem to sufficiently approximate the analytical solution, as well as the

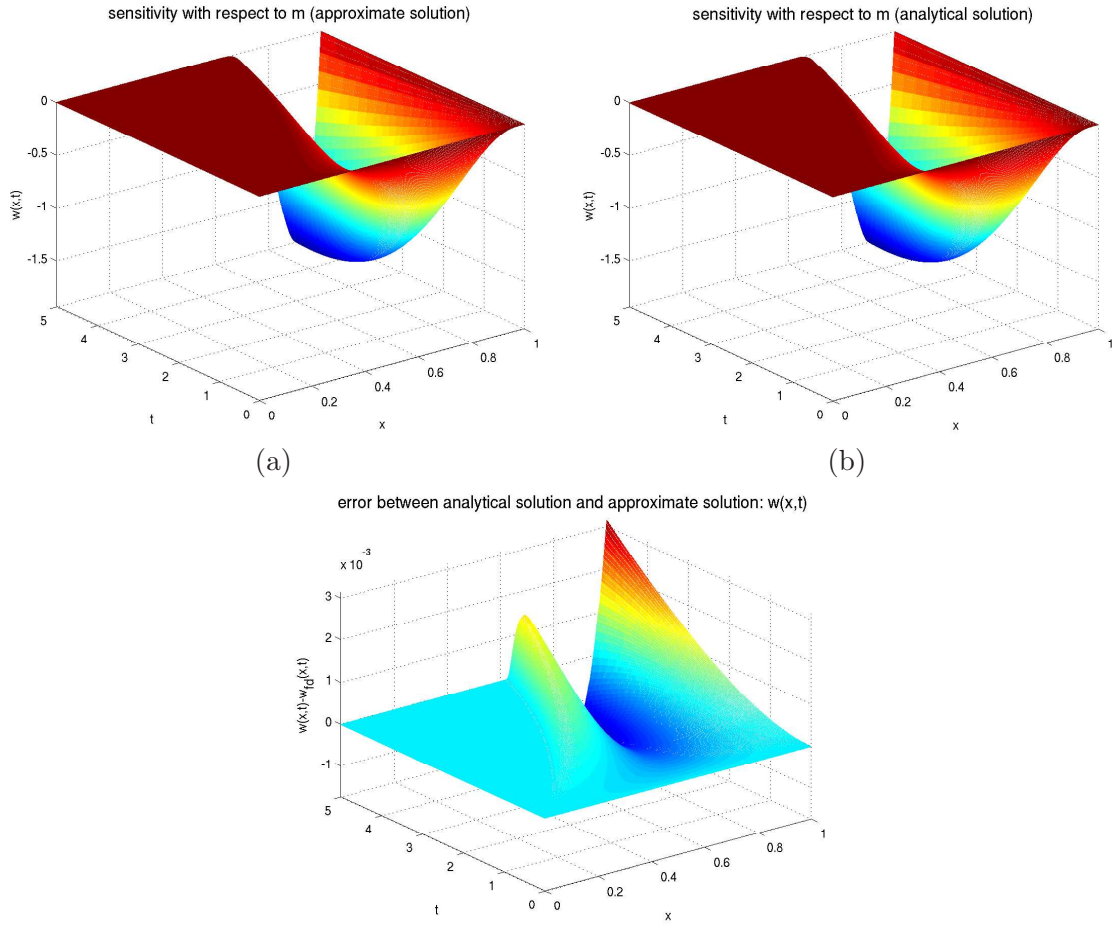

Figure 3.5: (a) The finite difference approximation $w_{fd}(x,t)$ of $w(x,t)$, (b) analytical solution for $w(x,t)$, and (c) error between the analytical solution and the finite difference approximation.

sensitivity, for this problem. If a more precise approximation is sought, one could refine the mesh with respect to mass and/or time in order to decrease the error.

3.2.3 Concluding Biomass Remarks

In this section, we considered the Sinko-Streifer/McKendrick-von Foerster equations for size-structured populations (3.2.1). First, we rigorously derived the partial differential equations for the sensitivity of the population density with respect to mortality m. Then, we verified that the systems of differential equations could be numerically represented

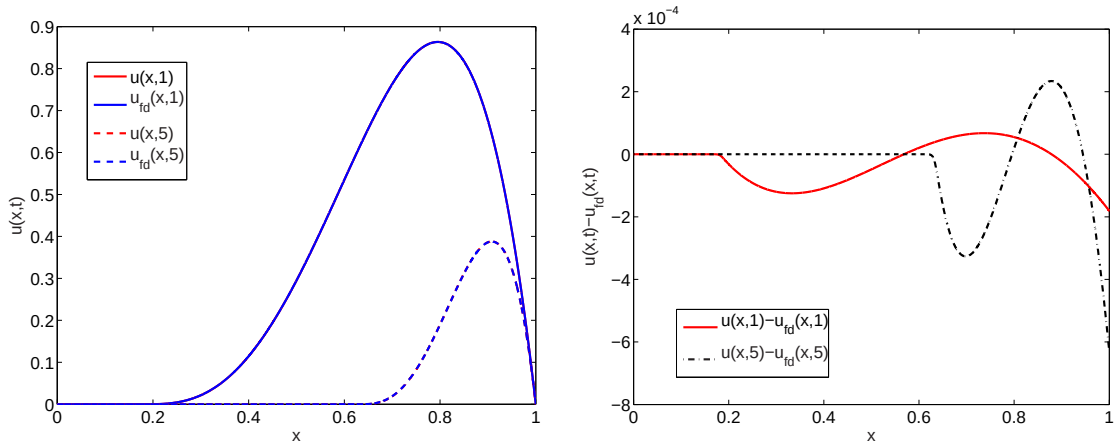

(a) (b)

Figure 3.6: (a) The analytical and approximate solutions for population density at $t = 1$ and $t = 5$, and (b) error between analytical and approximate solutions at $t = 1$ and $t = 5$.

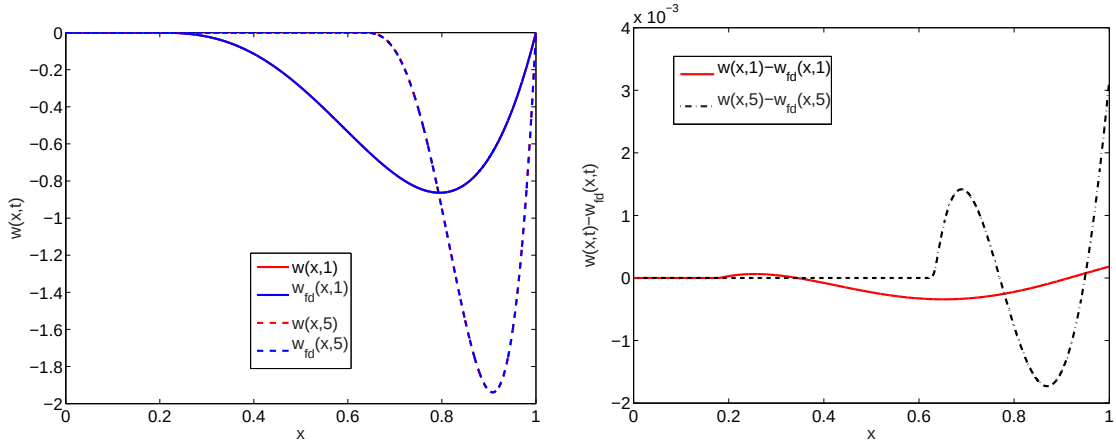

(a) (b)

Figure 3.7: (a) The analytical and approximate solutions for sensitivity with respect to m at $t = 1$ and $t = 5$, and (b) error between analytical and approximate solutions at $t = 1$ and $t = 5$.

with finite difference schemes in order to sufficiently approximate the analytical solutions, which in many cases might be difficult or impossible to procure.

Due to our investigations, we see that the correct sensitivity equations can be formally obtained by differentiating the population equation of interest with respect to the function m. This is also seen to be true when we consider the functions μ_0, g and β, see [7].

3.3 Vaccine Production Model

Now we consider the vaccine production model, which is the second component of the biomass/vaccine production hybridization. Healthy shrimp are exposed to infection by ingesting dead transfected biomass, and it is assumed that all the shrimp are equally likely to become infected within a reasonable amount of time. Once infected, we generally consider only a time interval of seven to ten days, due to the nature of the infection (see [1, 20, 29]). Beyond this time frame, the shrimp will typically either become resistant to the virus (entering into a *chronic* state) or expire. In our model, the infected shrimp move through several states of infection: *susceptible*, *latent*, and *acute*. When initially exposed to the infection, the shrimp are in the susceptible state. Then, the shrimp become latently infected, and show few signs of infection and are not yet producing the vaccine. Lastly, the latently infected shrimp move into the acute state, showing severe signs of infection and producing the vaccine. Recall that we make the assumption that the amount of vaccine produced equals the total live infected biomass, which we model.

The vaccine production model [1] is given by

$$\begin{aligned}
&S_t(x,t) + (g^S(x)S(x,t))_x + m^S(x)S(x,t) = -\lambda S(x,t),\\
&L_t(x,t,\theta) + (g^L(x)L(x,t,\theta))_x + L_\theta(x,t,\theta) + m^L(x)L(x,t,\theta) = -\gamma^L(\theta)L(x,t,\theta),\\
&A_t(x,t,\theta) + A_\theta(x,t,\theta) + m^A(\theta)A(x,t,\theta) = 0,\\
&L(x,t,0) = \lambda S(x,t), \quad A(x,t,0) = \int_0^t \gamma^L(\xi)L(x,t,\xi)d\xi,\\
&S(x_{\min},t) = 0, \quad L(x_{\min},t,\theta) = 0, \quad A(x_{\min},t,\theta) = 0,\\
&S(x,0) = S^0(x), \quad L(x,0,\theta) = 0, \quad A(x,0,\theta) = 0,
\end{aligned} \tag{3.3.1}$$

where $(x,t,\theta) \in [x_{\min}, x_{\max}] \times [0,T] \times [0,T]$. The function $S(x,t)$ represents the density of susceptible individuals with mass x at time t. The function $L(x,t,\theta)$ represents the density of individuals with mass x at time t that have spent θ days in the latent state. Also, the function $A(x,t,\theta)$ represents the density of individuals with mass x at time t that have spent θ days in the acute state.

The functions $m^S(x)$, $m^L(x)$ and $m^A(\theta)$ respectively denote the mortality rate of individuals in the susceptible state, the mortality rate of individuals in the latent state, and the mortality rate of individuals who have spent θ days in the acute state. The function

$\gamma^L(\theta)$ represents the latent to acute rate (the rate at which the shrimp that have spent θ days in the latent state become acutely infected) and the quantity λ denotes the initial infection rate. The initial population density of susceptible shrimp, which is the output from the biomass production model, is given by $S^0(x)$.

Using the method of characteristics, we solve the vaccine production system for $S(x,t)$, $L(x,t,\theta)$, and $A(x,t,\theta)$ as detailed in [1]. Those solutions are given explicitly as follows:

- If $x \geq G^{-1}(t)$,

$$S(x,t) = S^0(\pi^S(x,t))\frac{g^S(\pi^S(x,t))}{g^S(x)} \exp\left(-\int_{\pi^S(x,t)}^{x} \frac{m^S(y)}{g^S(y)}\,dy\right)\exp(-\lambda t) \tag{3.3.2}$$

  and if $x < G^{-1}(t)$,

$$S(x,t) = 0 \tag{3.3.3}$$

  where $\pi^S(x,t) = G^{-1}(G(x)-t)$, and $G(x) = \displaystyle\int_0^x \frac{1}{g^S(s)\,ds}$.

- Then, if $x \geq G^{-1}(\theta)$,

$$\begin{aligned} L(x,t,\theta) = \quad & \lambda S(\pi^L(x,\theta), t-\theta)\frac{g^L(\pi^L(x,\theta))}{g^L(x)} \exp\left(-\int_0^\theta \gamma^L(y)\,dy\right) \\ & \cdot \exp\left(\int_x^{\pi^L(x,\theta)} \frac{m^S(y)}{g^S(y)}\,dy\right) \end{aligned} \tag{3.3.4}$$

  and if $x < G^{-1}(\theta)$,

$$L(x,t,\theta) = 0 \tag{3.3.5}$$

  where $\pi^L(x,t) = G^{-1}(G(x)-t)$, and $G(x) = \displaystyle\int_0^x \frac{1}{g^L(s)\,ds}$.

- Lastly, if $x = x_{\min}$,

$$A(x,t,\theta) = 0, \tag{3.3.6}$$

  otherwise for $x > x_{\min}$,

$$A(x,t,\theta) = \left(\int_0^{t-\theta} \gamma^L(y) L(x,t-\theta,y)\,dy\right)\exp\left(-\int_0^\theta m^A(y)\,dy\right). \tag{3.3.7}$$

3.3.1 Sensitivity Analysis

There are several factors which strongly affect the total acutely infected population density, including the acute mortality $m^A(\theta)$ and the latent-to-acute rate function $\gamma^L(\theta)$. It is then prudent to consider the sensitivities of the population density with respect to these factors. We formally show that the solutions obtained by heuristically taking the derivatives of the vaccine production system and then solving with the method of characteristics are correct.

Acute Mortality Rate $m^A(\theta)$

We now analyze the sensitivity of the population density of the acute state with respect to the acute mortality $m^A(\theta)$. We first verify that the Gateaux derivative (see Definition 3.2.1),

$$dA(m^A, h^m) := \lim_{\varepsilon \to 0} \frac{A(x,t,\theta; m^A + \varepsilon h^m) - A(x,t,\theta; m^A)}{\varepsilon}$$

exists, where h^m, $m^A \in \mathcal{M}$, the set of all possible mortality rates. Using (3.3.7), we see that

$$\begin{aligned} dA(m^A, h^m) &= \lim_{\varepsilon \to 0} \frac{1}{\varepsilon} \Bigg[\left(\int_0^{t-\theta} \gamma^L(y) L(x, t-\theta, y)\, dy \right) \exp\left(- \int_0^{\theta} (m^A + \varepsilon h^m)(y)\, dy \right) \\ &\qquad - \left(\int_0^{t-\theta} \gamma^L(y) L(x, t-\theta, y)\, dy \right) \exp\left(- \int_0^{\theta} m^A(y)\, dy \right) \Bigg] \\ &= \int_0^{t-\theta} \gamma^L(y) L(x, t-\theta, y)\, dy \, \exp\left(- \int_0^{\theta} m^A(y)\, dy \right) \\ &\qquad \times \lim_{\varepsilon \to 0} \frac{1}{\varepsilon} \left[\exp\left(-\varepsilon \int_0^{\theta} h^m(y)\, dy \right) - 1 \right], \end{aligned}$$

and by substitution,

$$dA(m^A, h^m) = A(x,t,\theta) \cdot \lim_{\varepsilon \to 0} \frac{1}{\varepsilon} \left[\exp\left(-\varepsilon \int_0^{\theta} h^m(y)\, dy \right) - 1 \right].$$

We now apply the rule

$$\lim_{h \to 0} \frac{a^h - 1}{h} = \ln a \tag{3.3.8}$$

to our problem, where we see that

$$\begin{aligned}\lim_{\varepsilon\to 0}\frac{1}{\varepsilon}\left[\exp\left(-\varepsilon\int_0^\theta h^m(y)\,dy\right)-1\right] &= \ln\left(\exp\left(-\int_0^\theta h^m(y)\,dy\right)\right)\\ &= -\int_0^\theta h^m(y)\,dy.\end{aligned}$$

Consequently,

$$dA(m^A,h^m) = -A(x,t,\theta)\int_0^\theta h^m(y)\,dy. \tag{3.3.9}$$

Computationally, (3.3.9) can be implemented in several ways. First, we could solve for $A(x,t,\theta)$, and then use a quadrature to approximate

$$-\int_0^\theta h^m(y)\,dy.$$

Alternately, we consider a partial differential equation corresponding to (3.3.9). We couple the PDE with the vaccine production model (3.3.1) and use a finite difference scheme to approximate the corresponding solutions. Before we numerically implement this method, we formally verify that the system

$$\begin{aligned}&M_t(x,t,\theta)+M_\theta(x,t,\theta)+m^A(\theta)M(x,t,\theta)+h^m(\theta)A(x,t,\theta)=0,\\ &M(x,t,0)=0,\qquad M(x_{\min},t,\theta)=0,\qquad M(x,0,\theta)=0,\end{aligned} \tag{3.3.10}$$

obtained by taking the derivative of (3.3.1) with respect to m^A in the direction h^m, has the solution (3.3.9). We let $M(x,t,\theta)$ denote the derivative of A with respect to m^A in the direction h^m.

We solve (3.3.10) explicitly using the method of characteristics with the characteristic equations

$$\tilde{t}(s)=t+s,\quad \tilde{\theta}(s)=\theta+s,\quad \tilde{x}(s)=x.$$

We now consider the solution $M(x,t,\theta)$ along the characteristic curve

$$\frac{dM(\tilde{x}(s),\tilde{t}(s),\tilde{\theta}(s))}{ds} = -m^A(\tilde{\theta}(s))M(\tilde{x}(s),\tilde{t}(s),\tilde{\theta}(s)) - h^m(\tilde{\theta}(s))A(\tilde{x}(s),\tilde{t}(s),\tilde{\theta}(s))$$

and use the integrating factor

$$\exp\left(\int_0^s m^A(\tilde{\theta}(z))\,dz\right)$$

to get the relation

$$\left[\exp\left(\int_0^s m^A(\tilde{\theta}(z))\,dz\right) M(\tilde{x}(s),\tilde{t}(s),\tilde{\theta}(s))\right]'$$
$$= -\exp\left(\int_0^s m^A(\tilde{\theta}(z))\,dz\right) h^m(\tilde{\theta}(s))A(\tilde{x}(s),\tilde{t}(s),\tilde{\theta}(s)).$$

From this we see that

$$\begin{aligned} M(x,t,\theta) &= M(\tilde{x}(s),\tilde{t}(s),\tilde{\theta}(s))\exp\left(\int_0^s m^A(\tilde{\theta}(z))\,dz\right) \\ &\quad + \int_0^s \exp\left(\int_0^\tau m^A(\tilde{\theta}(z))\,dz\right) h^m(\tilde{\theta}(\tau))A(\tilde{x}(\tau),\tilde{t}(\tau),\tilde{\theta}(\tau))\,d\tau. \end{aligned}$$

However, the initial and boundary conditions

$$M(x,t,0)=0, \qquad M(x_{\min},t,\theta)=0, \qquad M(x,0,\theta)=0,$$

imply that the first term is zero, and then

$$M(x,t,\theta) = \int_0^s \exp\left(\int_0^\tau m^A(\tilde{\theta}(z))\,dz\right) h^m(\tilde{\theta}(\tau))A(\tilde{x}(\tau),\tilde{t}(\tau),\tilde{\theta}(\tau))\,d\tau.$$

For every $s\in\mathbb{R}$, it is clear that $\tilde{\theta}(s)\le\tilde{t}(s)$ and therefore we obtain $s=-\theta$. It follows that

$$M(x,t,\theta) = -\int_0^\theta \exp\left(-\int_0^\tau m^A(\theta-z)\,dz\right) h^m(\theta-\tau)A(x,t-\tau,\theta-\tau)\,d\tau,$$

which simplifies to be

$$M(x,t,\theta) = -\int_0^\theta \exp\left(-\int_{\theta-\tau}^\theta m^A(y)\,dy\right) h^m(\theta-\tau)A(x,t-\tau,\theta-\tau)\,d\tau.$$

However,

$$A(x,t-\tau,\theta-\tau) = \left(\int_0^{t-\theta}\gamma^L(y)L(x,t-\theta,y)\,dy\right)\exp\left(-\int_0^{\theta-\tau} m^A(y)\,dy\right), \qquad (3.3.11)$$

and by substituting (3.3.11) into $M(x,t,\theta)$ and simplifying, we get

$$\begin{aligned} M(x,t,\theta) &= -\int_0^\theta \exp\left(-\int_{\theta-\tau}^\theta m^A(y)\,dy\right) h^m(\theta-\tau) \\ &\qquad \times\left[\int_0^{t-\theta}\gamma^L(y)L(x,t-\theta,y)\,dy\,\exp\left(-\int_0^{\theta-\tau} m^A(y)\,dy\right)\right]d\tau \\ &= -\left(\int_0^{t-\theta}\gamma^L(y)L(x,t-\theta,y)\,dy\right)\exp\left(-\int_0^\theta m^A(y)\,dy\right)\int_0^\theta h^m(\theta-\tau)\,d\tau \\ &= -A(x,t,\theta)\int_0^\theta h^m(\theta-\tau)\,d\tau. \end{aligned}$$

This reduces to

$$M(x,t,\theta) = -A(x,t,\theta)\int_0^\theta h^m(y)\,dy,$$

which is precisely (3.3.9), and hence we see that

$$M(x,t,\theta) = dA(m^A, h^m).$$

Latent to Acute Rate Function $\gamma^L(\theta)$

We next analyze the sensitivity of the population density of the latent and acute states with respect to $\gamma^L(\theta)$. Due to the dependence of the acute state on the latent state, we begin with the latent state in order to accurately obtain the necessary derivatives as well as verify their correctness.

Gateaux Derivatives

We first verify that the Gateaux derivative (see Definition 3.2.1),

$$dL(\gamma^L, h^\gamma) := \lim_{\varepsilon\to 0}\frac{L(x,t,\theta;\gamma^L+\varepsilon h^\gamma) - L(x,t,\theta;\gamma^L)}{\varepsilon}$$

exists, where h^γ, $\gamma^L \in \Gamma$, the set of all possible latent-to-acute rates. Using (3.3.4), we see that

$$\begin{aligned} dL(\gamma^L, h^\gamma) &= \lim_{\varepsilon\to 0}\frac{1}{\varepsilon}\Bigg[\Bigg(\lambda S(\pi^L(x,\theta), t-\theta)\frac{g^L(\pi^L(x,\theta))}{g^L(x)}\exp\left(-\int_0^\theta(\gamma^L+\varepsilon h^\gamma)(y)\,dy\right) \\ &\quad\times\exp\left(\int_x^{\pi^L(x,\theta)}\frac{m^S(y)}{g^S(y)}\,dy\right)\Bigg) - \Bigg(\lambda S(\pi^L(x,\theta), t-\theta)\frac{g^L(\pi^L(x,\theta))}{g^L(x)} \\ &\quad\times\exp\left(-\int_0^\theta\gamma^L(y)\,dy\right)\exp\left(\int_x^{\pi^L(x,\theta)}\frac{m^S(y)}{g^S(y)}\,dy\right)\Bigg)\Bigg]. \end{aligned}$$

We can rewrite this as

$$\begin{aligned} dL(\gamma^L, h^\gamma) &= \lambda S(\pi^L(x,\theta), t-\theta)\frac{g^L(\pi^L(x,\theta))}{g^L(x)}\exp\left(\int_x^{\pi^L(x,\theta)}\frac{m^S(y)}{g^S(y)}\,dy\right) \\ &\quad\times\lim_{\varepsilon\to 0}\frac{1}{\varepsilon}\left[\exp\left(-\int_0^\theta(\gamma^L+\varepsilon h^\gamma)(y)\,dy\right) - \exp\left(-\int_0^\theta\gamma^L(y)\,dy\right)\right] \\ &= \lambda S(\pi^L(x,\theta), t-\theta)\frac{g^L(\pi^L(x,\theta))}{g^L(x)}\exp\left(\int_x^{\pi^L(x,\theta)}\frac{m^S(y)}{g^S(y)}\,dy\right) \\ &\quad\times\exp\left(-\int_0^\theta\gamma^L(y)\,dy\right)\lim_{\varepsilon\to 0}\frac{1}{\varepsilon}\left[\exp\left(-\varepsilon\int_0^\theta h^\gamma(y)\,dy\right) - 1\right], \end{aligned}$$

where substitution yields

$$dL(\gamma^L, h^\gamma) = L(x,t,\theta) \cdot \lim_{\varepsilon \to 0} \frac{1}{\varepsilon} \left[\exp\left(-\varepsilon \int_0^\theta h^\gamma(y)\, dy \right) - 1 \right].$$

We again apply (3.3.8) to our problem and see that

$$\lim_{\varepsilon \to 0} \frac{1}{\varepsilon} \left[\exp\left(-\varepsilon \int_0^\theta h^\gamma(y)\, dy \right) - 1 \right] = -\int_0^\theta h^\gamma(y)\, dy.$$

Therefore,

$$dL(\gamma^L, h^\gamma) = -L(x,t,\theta) \int_0^\theta h^\gamma(y)\, dy. \tag{3.3.12}$$

We next verify that the Gateaux derivative

$$dA(\gamma^L, h^\gamma) := \lim_{\varepsilon \to 0} \frac{A(x,t,\theta;\gamma^L + \varepsilon h^\gamma) - A(x,t,\theta;\gamma^L)}{\varepsilon}$$

exists. Using (3.3.4) and (3.3.7), we may expand $A(x,t,\theta)$ as

$$\begin{aligned} A(x,t,\theta) &= \left(\int_0^{t-\theta} \gamma^L(y) L(x, t-\theta, y)\, dy \right) \exp\left(-\textstyle\int_0^\theta m^A(y)\, dy \right) \\ &= \left(\int_0^{t-\theta} \gamma^L(y) \left[\lambda S(\pi^L(x,y), t-\theta-y) \frac{g^L(\pi^L(x,y))}{g^L(x)} \exp\left(-\int_0^y \gamma^L(z)\, dz \right) \right.\right. \\ &\quad \left.\left. \times \exp\left(\int_x^{\pi^L(x,y)} \frac{m^S(z)}{g^S(z)}\, dz \right) \right] dy \right) \exp\left(-\textstyle\int_0^\theta m^A(y)\, dy \right). \end{aligned} \tag{3.3.13}$$

Then we express the Gateaux derivative of $A(x,t,\theta)$ as

$$\begin{aligned} dA(\gamma^L, h^\gamma) &= \lim_{\varepsilon \to 0} \frac{1}{\varepsilon} \left[\left(\int_0^{t-\theta} (\gamma^L + \varepsilon h^\gamma)(y) \left[\lambda S(\pi^L(x,y), t-\theta-y) \frac{g^L(\pi^L(x,y))}{g^L(x)} \right.\right.\right. \\ &\quad \left.\left.\left. \times \exp\left(-\int_0^y (\gamma^L + \varepsilon h^\gamma)(z)\, dz \right) \exp\left(\int_x^{\pi^L(x,y)} \frac{m^S(z)}{g^S(z)}\, dz \right) \right] dy \right) \\ &\quad \times \exp\left(-\int_0^\theta m^A(y)\, dy \right) - \left(\int_0^{t-\theta} \gamma^L(y) \left[\lambda S(\pi^L(x,y), t-\theta-y) \right.\right. \\ &\quad \left.\left. \times \frac{g^L(\pi^L(x,y))}{g^L(x)} \exp\left(-\int_0^y \gamma^L(z)\, dz \right) \exp\left(\int_x^{\pi^L(x,y)} \frac{m^S(z)}{g^S(z)}\, dz \right) \right] dy \right) \\ &\quad \left. \times \exp\left(-\int_0^\theta m^A(y)\, dy \right) \right], \end{aligned}$$

which can be rewritten as

$$\begin{aligned} dA(\gamma^L, h^\gamma) = \; & \exp\left(-\int_0^\theta m^A(y)\,dy\right) \lim_{\varepsilon\to 0}\frac{1}{\varepsilon}\Bigg[\int_0^{t-\theta} \lambda S(\pi^L(x,y), t-\theta-y)\cdot \frac{g^L(\pi^L(x,y))}{g^L(x)} \\ & \times \exp\left(\int_x^{\pi^L(x,y)} \frac{m^S(z)}{g^S(z)}\,dz\right)\Bigg[(\gamma^L+\varepsilon h^\gamma)(y)\exp\left(-\int_0^y (\gamma^L+\varepsilon h^\gamma)(z)\,dz\right) \\ & - \gamma^L(y)\exp\left(-\int_0^y \gamma^L(z)\,dz\right)\Bigg]\,dy\Bigg]. \end{aligned} \tag{3.3.14}$$

This is exactly

$$\begin{aligned} dA(\gamma^L, h^\gamma) = \; & \exp\left(-\int_0^\theta m^A(y)\,dy\right) \lim_{\varepsilon\to 0}\frac{1}{\varepsilon}\Bigg[\int_0^{t-\theta} \lambda S(\pi^L(x,y), t-\theta-y)\cdot \frac{g^L(\pi^L(x,y))}{g^L(x)} \\ & \times \exp\left(\int_x^{\pi^L(x,y)} \frac{m^S(z)}{g^S(z)}\,dz\right)\exp\left(-\int_0^y \gamma^L(z)\,dz\right)\Bigg[(\gamma^L+\varepsilon h^\gamma)(y) \\ & \times \exp\left(-\varepsilon\int_0^y h^\gamma(z)\,dz\right) - \gamma^L(y)\Bigg]\,dy\Bigg] \end{aligned} \tag{3.3.15}$$

and substitution of (3.3.4)–(3.3.5) into (3.3.15) yields

$$\begin{aligned} dA(\gamma^L, h^\gamma) \;=\; & \exp\left(-\int_0^\theta m^A(y)\,dy\right)\cdot \lim_{\varepsilon\to 0}\frac{1}{\varepsilon}\Bigg[\int_0^{t-\theta} L(x, t-\theta, y) \\ & \times\Bigg[\gamma^L(y)\left(\exp\left(-\varepsilon\int_0^y h^\gamma(z)\,dz\right)-1\right)+\varepsilon h^\gamma(y)\exp\left(-\varepsilon\int_0^y h^\gamma(z)\,dz\right)\Bigg]\,dy\Bigg]. \end{aligned}$$

By choosing

$$a = \exp\left(-\int_0^y h^\gamma(z)\,dz\right)$$

and using (3.3.8) we see that

$$\begin{aligned} dA(\gamma^L, h^\gamma) \;&=\; \exp\left(-\int_0^\theta m^A(y)\,dy\right)\lim_{\varepsilon\to 0}\int_0^{t-\theta} L(x,t-\theta,y)\left[\gamma^L(y)\frac{a^\varepsilon-1}{\varepsilon}+h^\gamma(y)a^\varepsilon\right]dy \\ &=\; \exp\left(-\int_0^\theta m^A(y)\,dy\right)\int_0^{t-\theta} L(x,t-\theta,y)\left[\gamma^L(y)\ln(a)+h^\gamma(y)\right]dy. \end{aligned}$$

This is just

$$dA(\gamma^L, h^\gamma) = \exp\left(-\int_0^\theta m^A(y)\,dy\right)\int_0^{t-\theta} L(x,t-\theta,y)\Big[-\gamma^L(y)\int_0^y h^\gamma(z)\,dz + h^\gamma(y)\Big]\,dy. \tag{3.3.16}$$

System of Partial Differential Equations

Computationally, (3.3.12) and (3.3.16) can be implemented in several ways. We could solve for $L(x,t,\theta)$, and then use a quadrature to approximate the remaining components of each equation. Alternately, we consider a PDE system corresponding to (3.3.12) and (3.3.16), coupled with the vaccine production model (3.3.1). Then we can approximate the solution and sensitivities using a finite difference scheme.

Before we numerically implement this method, we formally verify that the system

$$\begin{aligned}
&R_t(x,t,\theta) + (g^L(x)R(x,t,\theta))_x + R_\theta(x,t,\theta) + m^L(x)R(x,t,\theta) \\
&\quad = -\gamma^L(\theta)R(x,t,\theta) - h^\gamma(\theta)L(x,t,\theta), \\
&P_t(x,t,\theta) + P_\theta(x,t,\theta) + m^A(\theta)P(x,t,\theta) = 0, \\
&R(x,t,0) = 0, \quad P(x,t,0) = \textstyle\int_0^t \left(\gamma^L(\xi)R(x,t,\xi) + h^\gamma(\xi)L(x,t,\xi)\right)\, d\xi, \\
&R(x_{\min},t,\theta) = 0, \quad P(x_{\min},t,\theta) = 0, \\
&R(x,0,\theta) = 0, \quad P(x,0,\theta) = 0.
\end{aligned} \tag{3.3.17}$$

obtained by taking the derivative of (3.3.1) with respect to γ^L in the direction h^γ, has the solutions given by (3.3.12) and (3.3.16). We let $R(x,t,\theta)$ and $P(x,t,\theta)$ denote the derivatives of L and A, respectively, with respect to γ^L in the direction h^γ.

We first examine the sensitivity in the latent state, thereby reducing the system (3.3.17) to

$$\begin{aligned}
&R_t(x,t,\theta) + (g^L(x)R(x,t,\theta))_x + R_\theta(x,t,\theta) + m^L(x)R(x,t,\theta) \\
&\quad = -\gamma^L(\theta)R(x,t,\theta) - h^\gamma(\theta)L(x,t,\theta),
\end{aligned} \tag{3.3.18}$$

with initial and boundary conditions

$$R(x,t,0) = 0, \quad R(x_{\min},t,\theta) = 0, \quad R(x,0,\theta) = 0. \tag{3.3.19}$$

We solve (3.3.18) for $R(x,t,\theta)$ using the method of characteristics, and employ the characteristic equations

$$\tilde{t}(s) = t + s, \quad \tilde{\theta}(s) = \theta + s, \quad \tilde{x}(s) = G^{-1}(G(x) + s),$$

and setting $G(x) = \displaystyle\int_0^x \frac{1}{g^L(z)}\, dz$.

We now consider the solution $R(x,t,\theta)$ along the characteristic curve,

$$\begin{aligned}\frac{dR(\tilde{x}(s),\tilde{t}(s),\tilde{\theta}(s))}{ds} = & -\Big(\gamma^L(\tilde{\theta}(s)) + g_x^L(\tilde{x}(s)) + m^L(\tilde{x}(s))\Big) R(\tilde{x}(s),\tilde{t}(s),\tilde{\theta}(s)) \\ & -h^\gamma(\tilde{\theta}(s)) L(\tilde{x}(s),\tilde{t}(s),\tilde{\theta}(s)).\end{aligned}$$

Utilizing the integrating factor:

$$\exp\left(\int_0^s \gamma^L(\tilde{\theta}(z)) + g_x^L(\tilde{x}(z)) + m^L(\tilde{x}(z))\,dz\right)$$

we get

$$\begin{aligned}&\left[\exp\left(\int_0^s \gamma^L(\tilde{\theta}(z)) + g_x^L(\tilde{x}(z)) + m^L(\tilde{x}(z))\,dz\right) R(\tilde{x}(s),\tilde{t}(s),\tilde{\theta}(s))\right]' \\ &\qquad = -h^\gamma(\tilde{\theta}(s)) \exp\left(\int_0^s \gamma^L(\tilde{\theta}(z)) + g_x^L(\tilde{x}(z)) + m^L(\tilde{x}(z))\,dz\right) L(\tilde{x}(s),\tilde{t}(s),\tilde{\theta}(s)).\end{aligned}$$

From this we have

$$\begin{aligned}R(x,t,\theta) = {} & R(\tilde{x}(s),\tilde{t}(s),\tilde{\theta}(s)) \exp\left(\int_0^s \gamma^L(\tilde{\theta}(z)) + g_x^L(\tilde{x}(z)) + m^L(\tilde{x}(z))\,dz\right) \\ & + \int_0^s h^\gamma(\tilde{\theta}(\tau)) \exp\left(\int_0^\tau \gamma^L(\tilde{\theta}(z)) + g_x^L(\tilde{x}(z)) + m^L(\tilde{x}(z))\,dz\right) L(\tilde{x}(\tau),\tilde{t}(\tau),\tilde{\theta}(\tau))\,d\tau.\end{aligned} \tag{3.3.20}$$

Recalling the initial and boundary conditions (3.3.19) we see that the first term of (3.3.20) is zero, yielding

$$\begin{aligned}R(x,t,\theta) = {} & \int_0^s h^\gamma(\tilde{\theta}(\tau)) \exp\left(\int_0^\tau \gamma^L(\tilde{\theta}(z)) + g_x^L(\tilde{x}(z)) + m^L(\tilde{x}(z))\,dz\right) \\ & \times L(\tilde{x}(\tau),\tilde{t}(\tau),\tilde{\theta}(\tau))\,d\tau.\end{aligned} \tag{3.3.21}$$

Further, $\tilde{\theta}(s) \le \tilde{t}(s)$ for every $s \in \mathbb{R}$, implying that we can make the substitution $s = -\theta$ and rewrite (3.3.21) as

$$\begin{aligned}R(x,t,\theta) = {} & -\int_0^\theta \left[h^\gamma(\theta-\tau) \exp\left(\int_0^{-\tau} \gamma^L(\tilde{\theta}(z)) + g_x^L(\tilde{x}(z)) + m^L(\tilde{x}(z))\,dz\right)\right. \\ & \left. \times L(\tilde{x}(-\tau), t-\tau, \theta-\tau)\right] d\tau.\end{aligned}$$

We can rewrite the exponential component as

$$\begin{aligned}
&\exp\left(\int_0^{-\tau} \gamma^L(\tilde{\theta}(z)) + g_x^L(\tilde{x}(z)) + m^L(\tilde{x}(z))\,dz\right) \\
&\quad = \exp\left(-\int_0^{\tau} \gamma^L(\theta - z)\,dz\right) \exp\left(-\int_0^{\tau} g_x^L(\tilde{x}(-z)) + m^L(\tilde{x}(-z))\,dz\right) \\
&\quad = \exp\left(\int_{\theta}^{\theta-\tau} \gamma^L(z)\,dz\right) \exp\left(\int_x^{\tilde{x}(-\tau)} \frac{g_x^L(z)}{g^L(z)} + \frac{m^L(z)}{g^L(z)}\,dz\right) \\
&\quad = \frac{g^L(\tilde{x}(-\tau))}{g^L(x)} \exp\left(-\int_{\theta-\tau}^{\theta} \gamma^L(z)\,dz\right) \exp\left(\int_x^{\tilde{x}(-\tau)} \frac{m^L(z)}{g^L(z)}\,dz\right).
\end{aligned}$$

Then,

$$\begin{aligned}
R(x,t,\theta) \;=\; & -\int_0^{\theta} \left[h^{\gamma}(\theta-\tau) L(\pi^L(x,\tau), t-\tau, \theta-\tau) \frac{g^L(\pi^L(x,\tau))}{g^L(x)}\right. \\
& \left. \times \exp\left(-\int_{\theta-\tau}^{\theta} \gamma^L(z)\,dz\right) \exp\left(\int_x^{\pi^L(x,\tau)} \frac{m^L(z)}{g^L(z)}\,dz\right)\right] d\tau
\end{aligned}$$

where $\pi^L(x,\tau) = \tilde{x}(-\tau) = G^{-1}(G(x) - \tau)$. Note that

$$\begin{aligned}
L(\pi^L(x,\tau), t-\tau, \theta-\tau) \;=\; & \lambda S(\pi^L(\pi^L(x,\tau), \theta-\tau), t-\theta) \left(\frac{g^L(\pi^L(x,\theta))}{g^L(\pi^L(x,\tau))}\right) \\
& \times \exp\left(-\int_0^{\theta-\tau} \gamma^L(y)\,dy\right) \exp\left(\int_{\pi^L(x,\tau)}^{\pi^L(x,\theta)} \frac{m^S(y)}{g^S(y)}\,dy\right),
\end{aligned}$$

and

$$\begin{aligned}
\pi^L(\pi^L(x,\tau), \theta-\tau) &= G^{-1}(G(G^{-1}(G(x) - \tau)) - \theta + \tau) \\
&= G^{-1}(G(x) - \tau - \theta + \tau) \\
&= G^{-1}(G(x) - \theta) \\
&= \pi^L(x,\theta).
\end{aligned}$$

Hence,

$$\begin{aligned}
R(x,t,\theta) \;=\; & -\int_0^{\theta} \left[h^{\gamma}(\theta-\tau) \left[\lambda S(\pi^L(x,\theta), t-\theta) \left(\frac{g^L(\pi^L(x,\theta))}{g^L(\pi^L(x,\tau))}\right)\right.\right. \\
& \left. \times \exp\left(-\int_0^{\theta-\tau} \gamma^L(y)\,dy\right) \exp\left(\int_{\pi^L(x,\tau)}^{\pi^L(x,\theta)} \frac{m^S(y)}{g^S(y)}\,dy\right)\right] \frac{g^L(\pi^L(x,\tau))}{g^L(x)} \\
& \left. \times \exp\left(-\int_{\theta-\tau}^{\theta} \gamma^L(z)\,dz\right) \exp\left(\int_x^{\pi^L(x,\tau)} \frac{m^L(z)}{g^L(z)}\,dz\right)\right] d\tau
\end{aligned}$$

which simplifies to

$$\begin{aligned} R(x,t,\theta) &= -\lambda S(\pi^L(x,\theta), t-\theta)\frac{g^L(\pi^L(x,\theta))}{g^L(x)} \exp\left(-\int_0^\theta \gamma^L(y)\,dy\right) \\ &\quad \times \exp\left(\int_x^{\pi^L(x,\theta)} \frac{m^S(y)}{g^S(y)}\,dy\right)\int_0^\theta h^\gamma(\theta-\tau)\,d\tau \\ &= -L(x,t,\theta)\int_0^\theta h^\gamma(\theta-\tau)\,d\tau. \end{aligned}$$

By substituting $y = \theta - \tau$, we have

$$R(x,t,\theta) = -L(x,t,\theta)\int_0^\theta h^\gamma(y)\,dy, \tag{3.3.22}$$

which is just (3.3.12), and therefore we see that

$$R(x,t,\theta) = dL(\gamma^L, h^\gamma).$$

We next examine the sensitivity in the acute state, reducing the system (3.3.17) to

$$P_t(x,t,\theta) + P_\theta(x,t,\theta) + m^A(\theta)P(x,t,\theta) = 0, \tag{3.3.23}$$

with initial and boundary conditions

$$\begin{aligned} &P(x,t,0) = \int_0^t \left(\gamma^L(\xi)R(x,t,\xi) + h^\gamma(\xi)L(x,t,\xi)\right)\,d\xi, \\ &P(x_{\min},t,\theta) = 0, \quad P(x,0,\theta) = 0. \end{aligned} \tag{3.3.24}$$

Using the method of characteristics we solve (3.3.23) by implementing the characteristic equations

$$\tilde{t}(s) = t + s, \quad \tilde{\theta}(s) = \theta + s, \quad \tilde{x}(s) = x.$$

We now consider the solution $P(x,t,\theta)$ along the characteristic curve,

$$\frac{dP(\tilde{x}(s),\tilde{t}(s),\tilde{\theta}(s))}{ds} = -m^A(\tilde{\theta}(s))P(\tilde{x}(s),\tilde{t}(s),\tilde{\theta}(s))$$

with solution

$$P(x,t,\theta) = P(\tilde{x}(s),\tilde{t}(s),\tilde{\theta}(s))\exp\left(\int_0^s m^A(\tilde{\theta}(s))\,ds\right).$$

Again, note that $\tilde{\theta}(s) \le \tilde{t}(s)$ for every $s \in \mathbb{R}$, and by making the substitution $s = -\theta$, we get

$$P(x,t,\theta) = P(x,t-\theta,0)\exp\left(\int_0^{-\theta} m^A(\theta+s)\,ds\right).$$

Lastly, we use our initial θ condition from (3.3.24) and have

$$P(x,t,\theta) = \int_0^{t-\theta} \gamma^L(y)R(x,t-\theta,y)+h^\gamma(y)L(x,t-\theta,y)\,dy \exp\left(-\int_0^\theta m^A(z)\,dz\right). \quad (3.3.25)$$

We substitute (3.3.22) into (3.3.25), which results in

$$\begin{aligned} P(x,t,\theta) &= -\int_0^{t-\theta} \gamma^L(y)L(x,t-\theta,y)\left(\int_0^y h^\gamma(z)\,dz\right) + h^\gamma(y)L(x,t-\theta,y)\,dy \\ &\quad \times \exp\left(-\int_0^\theta m^A(z)\,dz\right), \end{aligned}$$

and we write this as

$$\begin{aligned} P(x,t,\theta) &= \int_0^{t-\theta} L(x,t-\theta,y)\left[-\gamma^L(y)\int_0^y h^\gamma(z)\,dz + h^\gamma(y)\right] dy \\ &\quad \times \exp\left(-\int_0^\theta m^A(z)\,dz\right). \end{aligned} \quad (3.3.26)$$

We see that this is exactly (3.3.16), and thus

$$P(x,t,\theta) = dA(\gamma^L, h^\gamma).$$

3.3.2 Numerical Scheme and Results

Now we couple the sensitivity systems (3.3.10) and (3.3.17) with the vaccine production model (3.3.1) in order to solve for the sensitivities $M(x,t,\theta)$, $R(x,t,\theta)$ and $P(x,t,\theta)$. We will also approximate these systems using finite differences. In order to produce computational results, we use the following function values in our numerical schemes: we consider x ranging from 0 to 10 grams with a uniform step size of 0.02, and t ranges from 0 to 10 days with a uniform step size of 0.01. Additionally, we let the class age θ range from 0 to 7 days for both the latent and acute states. The initial population density for the susceptible state is

$$S^0(x) = 10x^3(10-x)$$

with an infection rate of $\lambda = 1.5$. Here we define the susceptible and latent growth functions as

$$g^S(x) = .2 - .02x \quad \text{and} \quad g^L(x) = .5g^S(x)$$

and give the corresponding mortality rates as

$$m^S = 0.0014 \quad \text{and} \quad m^L = 0.0028.$$

For this example the acute mortality rate is given by

$$m^A(\theta) = \frac{1}{\left(1 + \frac{1}{1.1}\left|\theta - 3\right|\right)^2},$$

as shown in Figure 3.8(a). We observe that most of the shrimp die from infection within approximately three days after entering the acute state. In Figure 3.8(b) we have the cumulative acute mortality rate, given as

$$1 - \exp\left(-\int_0^\theta m^A(\tau)\, d\tau\right),$$

and we note that only around 93% of the acutely infected popluation die from infection after spending seven days in the acute state. This reflects the idea that some shrimp become resistant to the infection and survive for long periods of time after the infection (chronic state). However, recall that our goal is to harvest the shrimp population before they have either become resistant to the infection or expired. For our numerical simulations we consider the sensitivity of the acute population density with respect to m^A in the direction of h^m, where $h^m = 2m^A$.

The latent to acute rate function is given by

$$\gamma^L(\theta) = \frac{2}{1 + \exp(-5(\theta - 4))}.$$

We observe in Figure 3.9(a) that the shrimp generally spend at least three days in the latent state before progressing into the acute state. In Figure 3.9(b), we see the cumulative latent

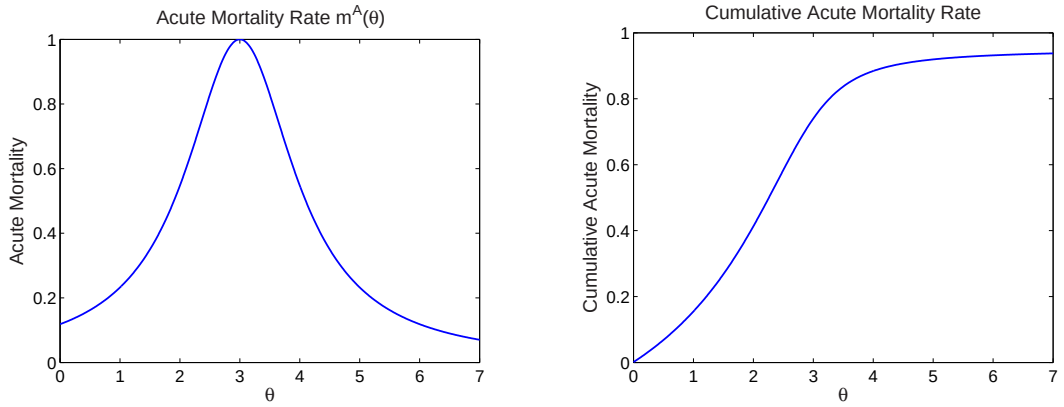

(a) (b)

Figure 3.8: (a) The acute mortality rate $m^A(\theta)$ and (b) the cumulative acute mortality rate.

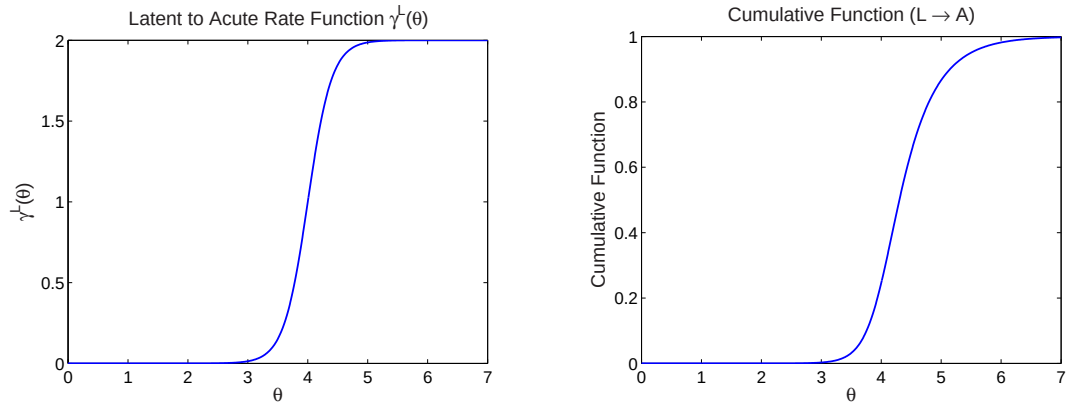

(a) (b)

Figure 3.9: (a) The latent to acute rate function $\gamma^L(\theta)$ and (b) the cumulative latent to acute rate function.

to acute rate function given as

$$1 - \exp\left(-\int_0^\theta \gamma^L(\tau)\, d\tau\right).$$

For this example, almost 100% of the latently infected popluation have become acutely infected after spending seven days in the latent state. We will consider the sensitivities of the latent and acute population densities with respect to the latent-to-acute rate function γ^L in the direction of h^γ, where $h^\gamma = 2\gamma^L$.

Numerical Scheme

As in Subsection 3.2.2, we numerically approximate the solution to the vaccine production model (3.3.1) using a finite difference scheme. We begin by dividing the x interval $[x_{\min}, x_{\max}]$ into n_x equal subintervals, where $\Delta x = \dfrac{x_{\max} - x_{\min}}{n_x}$. We then have $n_x + 1$ points $x_j = j\Delta x$ for $j = 0, 1, 2, \ldots, n_x$. We similarly divide the t interval $[0, T]$ into n_t equal subintervals with $n_t + 1$ points $t_k = k\Delta t$ for $\Delta t = \dfrac{T}{n_t}$, and $k = 0, 1, 2, \ldots, n_t$. Lastly we divide the θ interval $[0, T]$ into n_θ equal subintervals, with $n_\theta + 1$ points, $\theta_l = l\Delta\theta$ for $\Delta\theta = \dfrac{T}{n_\theta}$, and $l = 0, 1, 2, \ldots, n_\theta$. Let the notations

$$S_j^k \approx S(x_j, t_k), \qquad L_j^{k,l} \approx L(x_j, t_k, \theta_l), \qquad A_j^{k,l} \approx A(x_j, t_k, \theta_l),$$

represent the susceptible, latent, and acute states at mass x_j, time t_k, and class age θ_l. Also,

$$g_j^S = g^S(x_j), \quad g_j^L = g^L(x_j), \quad \gamma^{L,l} = \gamma^L(\theta_l),$$

$$m_j^S = m^S(x_j), \quad m_j^L = m^L(x_j), \quad m^{A,l} = m^A(\theta_l).$$

We will discretize the vaccine production model (3.3.1) using the implicit finite difference scheme [1] as follows.

For $j = 1, \ldots, n_x$, $k = 0, \ldots, n_t - 1$, and $l = 0, \ldots, n_\theta - 1$ we have

$$\begin{aligned}
&(i) \quad \frac{S_j^{k+1} - S_j^k}{\Delta t} + \frac{g_j^S S_j^{k+1} - g_{j-1}^S S_{j-1}^{k+1}}{\Delta x} + m_j^S S_j^{k+1} = -\lambda S_j^{k+1},\\
&(ii) \quad \frac{L_j^{k+1,l+1} - L_j^{k,l+1}}{\Delta t} + \frac{g_j^L L_j^{k+1,l+1} - g_{j-1}^L L_{j-1}^{k+1,l+1}}{\Delta x} + \frac{L_j^{k+1,l+1} - L_j^{k+1,l}}{\Delta \theta}\\
&\qquad + m_j^L L_j^{k+1,l+1} = -\gamma^{L,l+1} L_j^{k+1,l+1},\\
&(iii) \quad \frac{A_j^{k+1,l+1} - A_j^{k,l+1}}{\Delta t} + \frac{A_j^{k+1,l+1} - A_j^{k+1,l}}{\Delta \theta} + m^{A,l+1} A_j^{k+1,l+1} = 0,\\
&(iv) \quad S_0^{k+1} = 0,\\
&(v) \quad L_0^{k+1,l+1} = 0,\ L_j^{0,l+1} = 0,\ L_j^{k+1,0} = \lambda S_j^{k+1},\\
&(vi) \quad A_0^{k+1,l+1} = 0,\ A_j^{0,l+1} = 0,\ A_j^{k+1,0} = \sum_{l=1}^{\tilde{n}_{\theta,k+1}} \gamma^{L,l} L_j^{k+1,l} \Delta\theta,
\end{aligned} \tag{3.3.27}$$

where $\tilde{n}_{\theta,k} = [t_k/\Delta\theta]$ with $[z]$ being the usual greatest integer part of z.

We additionally use the following notation to denote the finite difference approximations used in the numerical schemes for the sensitivities:

$$M_j^{k,l} \approx M(x_j, t_k, \theta_l), \qquad R_j^{k,l} \approx R(x_j, t_k, \theta_l), \qquad P_j^{k,l} \approx P(x_j, t_k, \theta_l),$$

where we recall that M is the sensitivity of the acute state with respect to the acute mortality rate, R is the sensitivity of the latent state with respect to the latent-to-acute function γ^L, and P is the sensitivity of the acute state with respect to γ^L. Also,

$$h^{m,l} = h^m(\theta_l) \quad \text{and} \quad h^{\gamma,l} = h^\gamma(\theta_l).$$

We discretize the system (3.3.10) governing the sensitivity of the acute state with respect to the acute mortality rate m^A using an implicit finite difference scheme as follows.

For $j = 1, \ldots, n_x$, $k = 0, \ldots, n_t - 1$, and $l = 0, \ldots, n_\theta - 1$ we have

$$\begin{aligned}
(i) \quad & \frac{M_j^{k+1,l+1} - M_j^{k,l+1}}{\Delta t} + \frac{M_j^{k+1,l+1} - M_j^{k+1,l}}{\Delta \theta} + m^{A,l+1} M_j^{k+1,l+1} \\
& + h^{m,l+1} A_j^{k+1,l+1} = 0, \qquad (3.3.28) \\
(ii) \quad & M_0^{k+1,l+1} = 0, \quad M_j^{0,l+1} = 0, \quad M_j^{k+1,0} = 0.
\end{aligned}$$

We will similarly discretize the system (3.3.17) governing the sensitivity of the latent and acute states with respect to the latent to acute rate function γ^L using the following implicit finite difference scheme.

For $j = 1, \ldots, n_x$, $k = 0, \ldots, n_t - 1$, and $l = 0, \ldots, n_\theta - 1$ we have

$$\begin{aligned}
(i) \quad & \frac{R_j^{k+1,l+1} - R_j^{k,l+1}}{\Delta t} + \frac{g_j^L R_j^{k+1,l+1} - g_{j-1}^L R_{j-1}^{k+1,l+1}}{\Delta x} + \frac{R_j^{k+1,l+1} - R_j^{k+1,l}}{\Delta \theta} \\
& + m_j^L R_j^{k+1,l+1} = -\gamma^{L,l+1} R_j^{k+1,l+1} - h^{\gamma,l+1} L_j^{k+1,l+1}, \\
(ii) \quad & \frac{P_j^{k+1,l+1} - P_j^{k,l+1}}{\Delta t} + \frac{P_j^{k+1,l+1} - P_j^{k+1,l}}{\Delta \theta} + m^{A,l+1} P_j^{k+1,l+1} = 0, \\
(iii) \quad & R_0^{k+1,l+1} = 0,\ R_j^{0,l+1} = 0,\ R_j^{k+1,0} = 0, \\
(iv) \quad & P_0^{k+1,l+1} = 0,\ P_j^{0,l+1} = 0,\ P_j^{k+1,0} = \sum_{l=1}^{\tilde{n}_{\theta,k+1}} \left(\gamma^{L,l} R_j^{k+1,l} + h^{\gamma,l} L_j^{k+1,l} \right) \Delta \theta, \qquad (3.3.29)
\end{aligned}$$

where $\tilde{n}_{\theta,k} = [t_k / \Delta \theta]$.

Computational Results

In Figure 3.10 we see plots of $S(x,t)$, $\mathcal{L}(x,t)$, and $\mathcal{A}(x,t)$ where

$$\mathcal{L}(x,t) = \int_0^T L(x,t,\theta)\, d\theta \quad \text{and} \quad \mathcal{A}(x,t) = \int_0^T A(x,t,\theta)\, d\theta,$$

which are the population densities for each viral state over all age classes. We note that the shrimp progress from the susceptible to latent state and then latent to acute state after remaining in each for a few days. To see the transition more clearly, we plot the total number of individuals in each state as a function of time. Then,

$$N^S(t) = \int_{x_{\min}}^{x_{\max}} S(x,t)\, dx, \quad N^L(t) = \int_{x_{\min}}^{x_{\max}} \mathcal{L}(x,t)\, dx, \quad \text{and} \quad N^A(t) = \int_{x_{\min}}^{x_{\max}} \mathcal{A}(x,t)\, dx$$

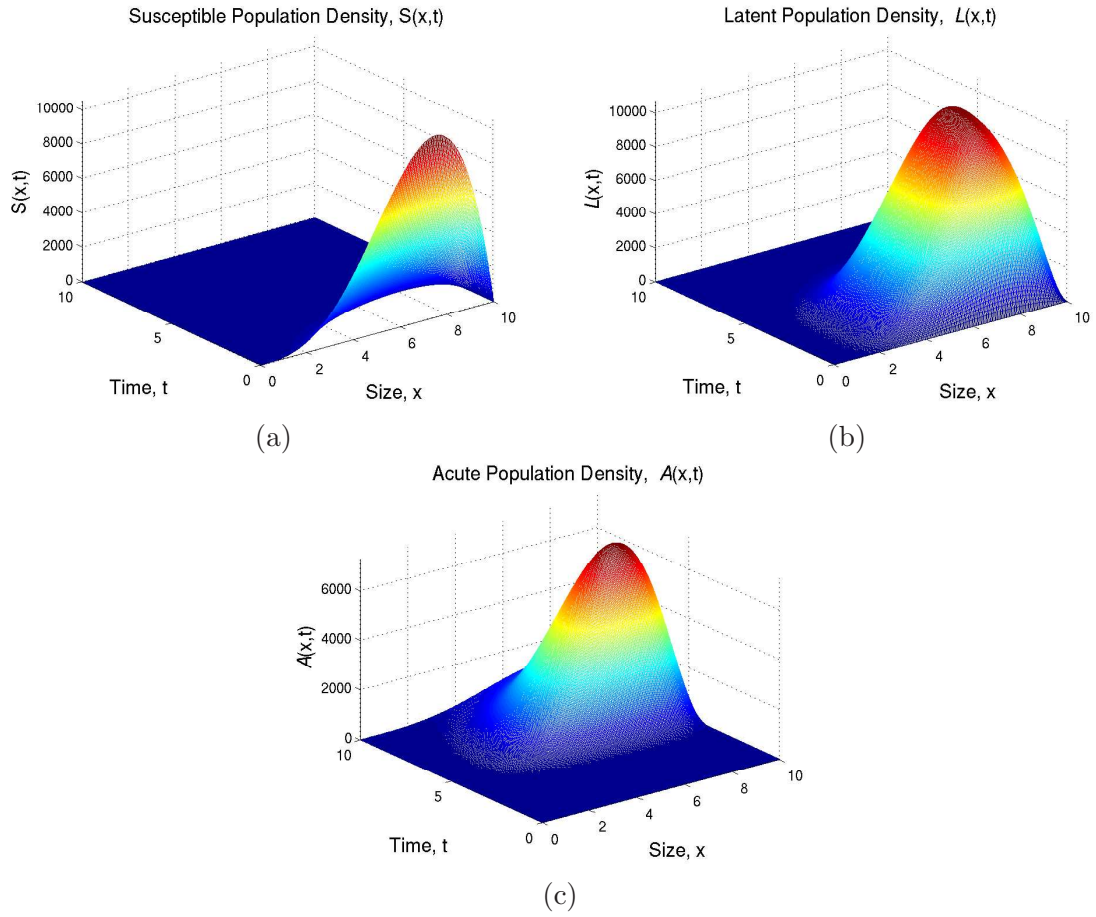

Figure 3.10: (a) The susceptible, (b) latent, and (c) acute population densities.

as seen in Figure 3.11. After two days, the predominance of the susceptible population has become latently infected, while some of the population has transitioned to the acute state.

In Figure 3.12(a) we see the plot of

$$\mathcal{M}(x,t) = \int_0^T M(x,t,\theta)\, d\theta$$

which represents the sensitivity of the acute population density with respect to the acute mortality rate m^A over all acute class ages θ. $\mathbf{M}(t)$, displayed in Figure 3.12(b) represents the sensitivity for all sizes x at time t and is given by

$$\mathbf{M}(t) = \int_{x_{\min}}^{x_{\max}} \mathcal{M}(x,t)\, dx.$$

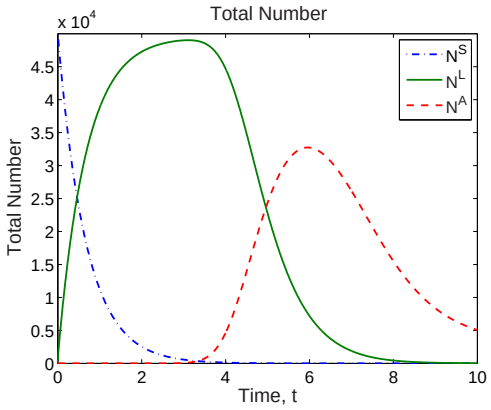

Figure 3.11: The total number of individuals for the susceptible, latent, and acute populations, as a function of time. These numbers are represented as N^S, N^L and N^A, respectively.

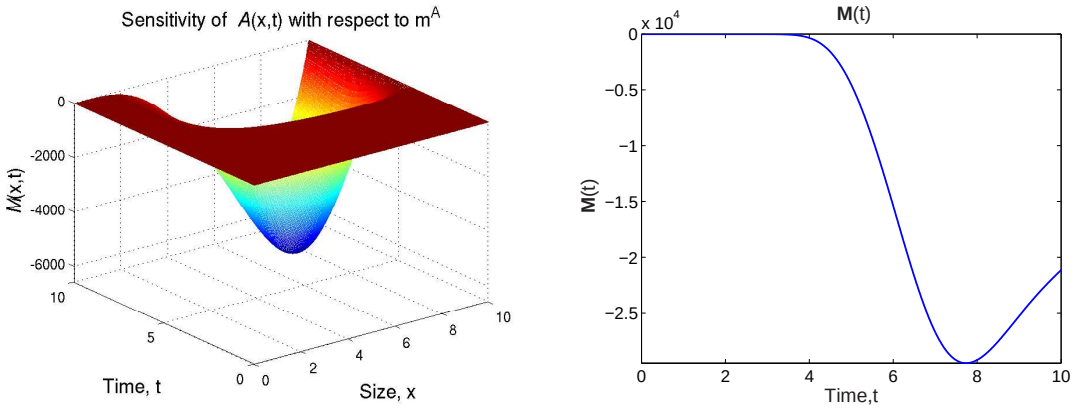

(a) (b)

Figure 3.12: The sensitivity of the acute population with respect to m^A in the direction $h^m = 2m^A$ (a) as a function of size and time, $\mathcal{M}(x,t)$ and (b) as a function of time, $\mathbf{M}(t)$.

Similarly, $\mathcal{R}(x,t)$ and $\mathbf{R}(t)$ respectively represent the sensitivities of the latent population density with respect to the latent-to-acute rate function γ^L over all latent class ages θ, and the sensitivity for all sizes x at time t. These are given as

$$\begin{aligned} \mathcal{R}(x,t) &= \int_0^T R(x,t,\theta)\,d\theta \\ \mathbf{R}(t) &= \int_{x_{\min}}^{x_{\max}} \mathcal{R}(x,t)\,dx \end{aligned}$$

and are shown in Figure 3.13.

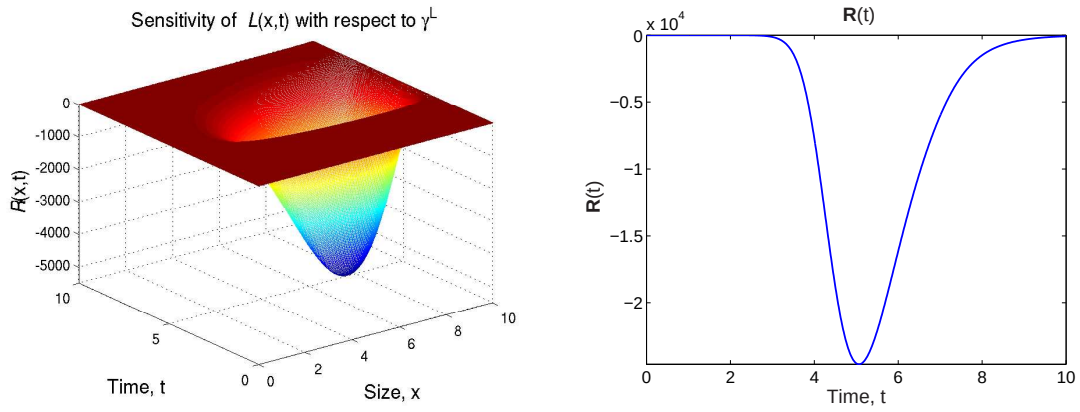

(a) (b)

Figure 3.13: The sensitivity of the latent population with respect to γ^L in the direction $h^\gamma = 2\gamma^L$ (a) as a function of size and time, $\mathcal{R}(x,t)$ and (b) as a function of time, $\mathbf{R}(t)$.

Likewise,

$$\begin{aligned} \mathcal{P}(x,t) &= \int_0^T P(x,t,\theta)\,d\theta \\ \mathbf{P}(t) &= \int_{x_{\min}}^{x_{\max}} \mathcal{P}(x,t)\,dx, \end{aligned}$$

respectively, represent the sensitivity of the acute population density with respect to γ^L over all acute class ages θ, and the sensitivity for all sizes x at time t. The corresponding plots are given in Figure 3.14.

We observe in Figures 3.13(a) and 3.14(a) that both $\mathcal{R}(x,t)$ and $\mathcal{P}(x,t)$ reach their highest magnitude near the fifth day in the latent state. This corresponds to the time when the rate of change of the cumulative latent-to-acute rate function decreases. This is more obvious when we consider the functions $\mathcal{R}(t)$ and $\mathbf{P}(t)$ in Figures 3.13(b) and 3.14(b), respectively. We notice in Figure 3.14 that $\mathcal{P}(x,t)$ and consequently $\mathbf{P}(t)$ have zero sensitivity when the values of both curves change from positive to negative. We readily observe this behavior in Figure 3.14(b) when t nears 6.3. We must determine whether this zero value occurs due to insensitivity or due to equivalent positive and negative contributions from the class ages at $t \approx 6.3$. It follows that we consider a new set of equations:

$$\mathcal{P}_{\text{abs}}(x,t) = \int_0^T |P(x,t,\theta)|\,d\theta \tag{3.3.30}$$

$$\mathbf{P}_{\text{abs}}(t) = \int_{x_{\min}}^{x_{\max}} \mathcal{P}_{\text{abs}}(x,t)\,dx. \tag{3.3.31}$$

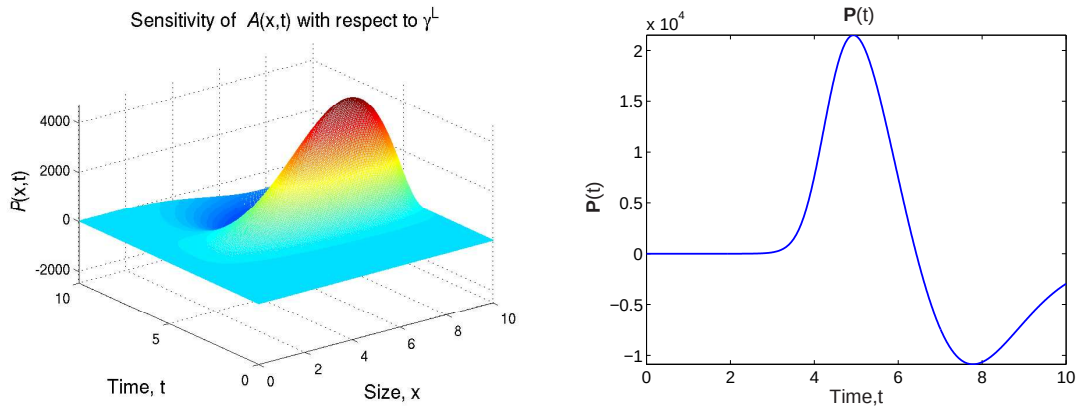

(a) (b)

Figure 3.14: The sensitivity of the acute population with respect to γ^L in the direction $h^\gamma = 2\gamma^L$ (a) as a function of size and time, $\mathcal{P}(x,t)$ and (b) as a function of time, $\mathbf{P}(t)$.

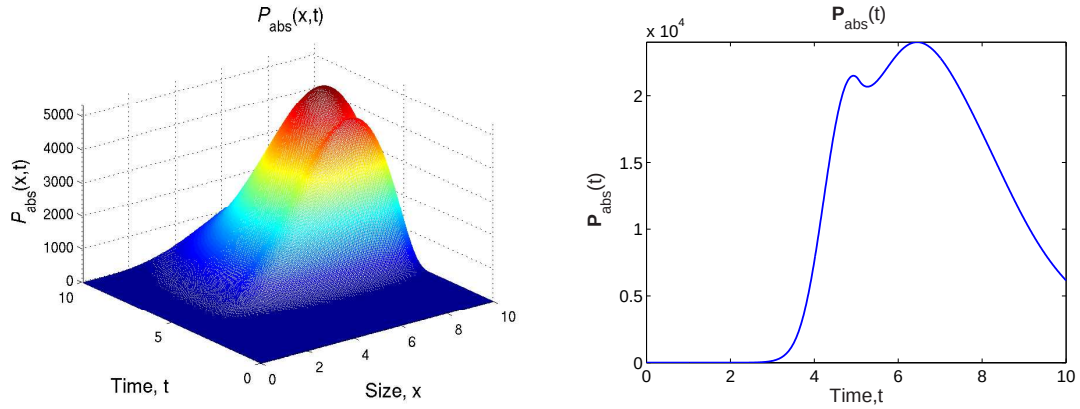

(a) (b)

Figure 3.15: The absolute sensitivity of the acute population with respect to γ^L in the direction $h^\gamma = 2\gamma^L$ (a) as a function of size and time, $\mathcal{P}_{\text{abs}}(x,t)$ and (b) as a function of time, $\mathbf{P}_{\text{abs}}(t)$.

We can see the graphs of (3.3.30) and (3.3.31) in Figure 3.15 where it is made clear that the zero value is due to adding positive and negative values at each time point.

3.3.3 Concluding Vaccine Production Remarks

In this section, we considered the multi-stage vaccine production model (3.3.1), which is the second component in our hybrid Sinko-Streifer model. We derived the partial

differential equations for the sensitivity of the population density with respect to the latent-to-acute rate function γ^L and the acute mortality m^A. Then, we verified that the systems of differential equations could be numerically represented with finite difference schemes in order to sufficiently approximate the analytical solutions, which in most cases are difficult or impossible to attain.

Due to our investigations, we see that the correct sensitivity equations can be formally obtained by differentiating the population equation of interest with respect to each rate function. This will be essential when investigating the sensitivities pertaining to realistic inputs and rates for a model such as in the case with the shrimp biomass/vaccine production system.

3.4 Environmental Conditions affecting the Biomass Model

By studying the Pacific white shrimp (Litopenaeus vannamei), we determined the primary factors contributing to the growth and mortality of healthy shrimp. We can use this information to determine the conditions in which the Pacific white shrimp can be raised within a certain time period to achieve maximum growth potential, given a certain initial distribution. Additionally, through our study of the Taura Syndrome Virus (TSV), we learned about the additional influences of growth and mortality factors on the shrimp when infected by a virus.

Water quality affects the growth and mortality of the Pacific white shrimp. In this section we consider the main affecting factors of the water quality, and determine how sensitive the biomass system is to each one. The factors that we are considering include the temperature $\left(q^H\right)$, dissolved oxygen level $\left(q^{do}\right)$, pH level $\left(q^{ph}\right)$, salinity (q^s), nitrite level (q^n), and amount of un-ionized ammonia (q^{ua}), collectively represented by

$$\mathbf{q} = \left(q^H, q^{do}, q^{ph}, q^s, q^n, q^{ua}\right).$$

Because the water quality changes with time, the water must be regularly monitored to ensure properly regulated levels.

Growth and Mortality

In order to demonstrate the importance of each environmental factor, we create an example of potential growth and mortality functions. We represent the growth function

by

$$g(x,\mathbf{q}) = 0.25\, g^H\left(x,q^H\right) g^{do}\left(q^{do}\right) g^{ph}\left(q^{ph}\right) g^s\left(q^s\right) g^n\left(q^n\right) g^{ua}\left(q^{ua}\right), \tag{3.4.1}$$

with each of the individual growth functions given by the formulae listed in this section. The mortality function is similarly given by

$$m(\mathbf{q}) = 0.0014 + m^H\left(q^H\right) + m^{do}\left(q^{do}\right) + m^{ph}\left(q^{ph}\right) + m^s\left(q^s\right) + m^n\left(q^n\right) + m^{ua}\left(q^{ua}\right), \tag{3.4.2}$$

where 0.0014 is approximately the natural mortality rate of the shrimp [1, 13].

Sensitivity

We consider the sensitivity of the biomass system (3.2.2) with respect to each parameter. We will use q to denote the water quality factor of interest. Then by choosing an initial value q_0 we have

$$\frac{\partial}{\partial t}\left(\frac{\partial u}{\partial q}(x,t;q_0)\right) + \frac{\partial}{\partial x}\left(\frac{\partial g}{\partial q}(x;q_0)\, u_0 + g_0 \frac{\partial u}{\partial q}(x,t;q_0)\right) = -\frac{\partial m}{\partial q}(x;q_0)\, u_0 - m_0 \frac{\partial u}{\partial q}(x,t;q_0)$$

where u_0, g_0, and m_0 represent the state as well as the growth and mortality functions evaluated at q_0. By allowing $v = \frac{\partial u}{\partial q}(x,t;q_0)$, we have

$$\frac{\partial v}{\partial t} + \frac{\partial}{\partial x}\left(\frac{\partial g}{\partial q}(x;q_0)\, u_0 + g_0 v\right) = -\frac{\partial m}{\partial q} u_0 - m_0 v$$

which is just

$$\frac{\partial v}{\partial t} + \frac{\partial}{\partial x}(g_0 v) = -m_0 v - \frac{\partial}{\partial x}\left(\frac{\partial g}{\partial q} u_0\right) - \frac{\partial m}{\partial q} u_0.$$

We then have two systems to solve:

$$\frac{\partial u_0}{\partial t} + \frac{\partial}{\partial x}(g_0 u_0) = -m_0 u_0, \qquad u_0(0,x) = \Phi(x), \qquad u_0(t,0) = 0, \tag{3.4.3}$$

and

$$\frac{\partial v}{\partial t} + \frac{\partial}{\partial x}(g_0 v) = -m_0 v + F(u_0), \qquad v(0,x) = 0, \qquad v(t,0) = 0, \tag{3.4.4}$$

where

$$F(u_0) = -\frac{\partial}{\partial x}\left(\frac{\partial g}{\partial q} u_0\right) - \frac{\partial m}{\partial q} u_0. \tag{3.4.5}$$

The initial input $u_0(0,x) = \Phi(x)$ is chosen to be a smooth function which peaks at one gram,

$$\Phi(x) = 25231 e^{-20(x-1)^2}. \tag{3.4.6}$$

and represents a scenario of about 1000 shrimp of size near one gram initially placed in the raceway, or

$$\int_0^{25} \Phi(x)\,dx = 1000.$$

3.4.1 Dissolved Oxygen Level

Shrimp require oxygen to metabolize food, making the dissolved oxygen (DO) level a very important component of water quality. If the oxygen level is too low, the shrimp will have reduced food conversion and growth rates. Shrimp growth rates are at their best when the oxygen level is maintained above 80% of the saturation level of the water [39]. Oxygen depletion can cause mass mortality of shrimp if they are exposed to low concentrations of oxygen for extended periods of time.

Growth and Mortality

We now determine the dependency of the growth and mortality functions on the DO level. We begin with the growth function,

$$g^{do}\left(q^{do}\right) = \frac{1}{1 + e^{-2.25\left(q^{do} - 3.75\right)}},$$

created based on the available literature [40], as shown in Figure 3.16(a). Here, the dissolved oxygen level, q^{do}, ranges from 1.5 to 10 ppm. The shrimp exhibit stress below 2 ppm DO,

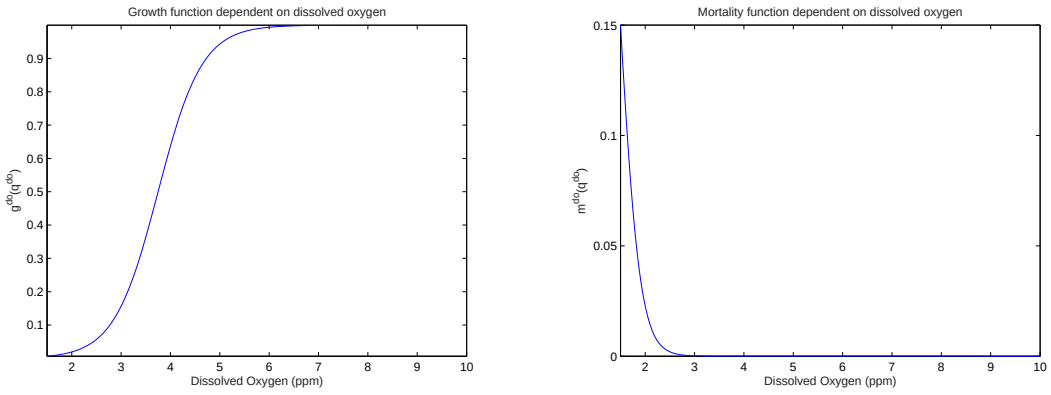

(a) (b)

Figure 3.16: (a) Dissolved oxygen dependent growth function and (b) mortality function.

and values less than 1.5 ppm can be lethal. Hence, we only consider values as low as 1.5 ppm, although dissolved oxygen levels as low as 3 ppm can be inadequate for maximum growth [13]. Additionally, the solubility of oxygen in water as a function of temperature and salinity is given as

$$\phi\left(q^H, q^s\right) = \frac{1418 - 17q^H}{120} + \frac{q^s\left(q^H - 70\right)}{1050}$$

and is an approximation to data provided in [39], see Figure 3.17. Incorporating this constraint means that we restrict the level of dissolved oxygen to be no greater than the solubility level. We consider the following

$$q^{do} = a^{do}\phi\left(q^H, q^s\right),$$

where a^{do} is a value ranging from 0.26 to 1, bounding q^{do} between 1.5 and 10 ppm. The DO mortality rate increases as the amount of DO decreases, since a certain DO level must be maintained for shrimp survival. This function is given by

$$m^{do}\left(q^{do}\right) = \frac{.3}{1 + e^{5\left(q^{do} - 1.5\right)}}$$

and can be seen in Figure 3.16(b).

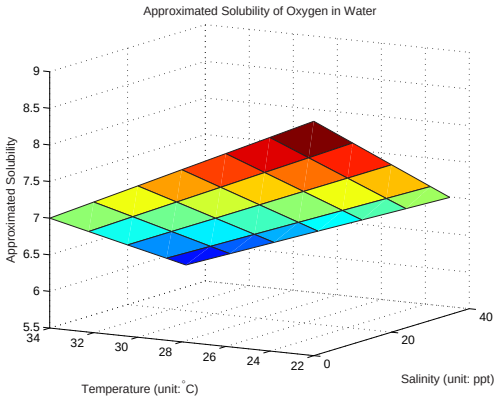

Figure 3.17: Solubility of oxygen as a function of temperature and salinity.

Sensitivity

In order to observe the effects of the dissolved oxygen without regard for the other environmental conditions, we allow the growth function (3.4.1) to have a contribution of

one from each of the remaining individual growth functions, i.e.,

$$g^H\big(x, q^H\big) = g^{ph}\big(q^{ph}\big) = g^s\big(q^s\big) = g^n\big(q^n\big) = g^{ua}\big(q^{ua}\big) = 1.$$

Similarly for the mortality function (3.4.2), the individual mortality functions for the other factors have zero contribution, with

$$m^H\big(q^H\big) = m^{ph}\big(q^{ph}\big) = m^s\big(q^s\big) = m^n\big(q^n\big) = m^{ua}\big(q^{ua}\big) = 0.$$

Then we see that

$$g\big(q^{do}\big) = .25 g^{do}\big(q^{do}\big) \quad \text{and} \quad m\big(q^{do}\big) = m^{do}\big(q^{do}\big) + 0.0014. \tag{3.4.7}$$

We solve system (3.4.3) using the dissolved oxygen growth and mortality functions (3.4.7). Since $g^{do}\left(q^{do}\right)$ and $m^{do}\left(q^{do}\right)$ are not dependent on x, we can use the method of characteristics to solve this system easily, which is given by

$$u_0\big(x, t; q_0^{do}\big) = \Phi\left(x - g\big(q_0^{do}\big)t\right) e^{-m\left(q_0^{do}\right)t}$$

for a fixed dissolved oxygen level given by q_0^{do}. Then the forcing function (3.4.5) used to solve the sensitivity system (3.4.4) is given by

$$F\Big(u_0\big(x, t; q_0^{do}\big)\Big) = -\left(\frac{\partial g}{\partial q}\big(q_0^{do}\big)\Phi'\Big(x - g\big(q_0^{do}\big)t\Big) + \frac{\partial m}{\partial q}\big(q_0^{do}\big)\Phi\Big(x - g\big(q_0^{do}\big)t\Big)\right) e^{-m\left(q_0^{do}\right)t}$$

where $\frac{\partial g}{\partial q}\big(q_0^{do}\big)$ and $\frac{\partial m}{\partial q}\big(q_0^{do}\big)$ are both constants. Then, using the method of characteristics we obtain

$$\begin{aligned} v &= F\left(u_0\big(x, t; q_0^{do}\big)\right) t \\ &= -\left(\frac{\partial g}{\partial q}\big(q_0^{do}\big)\Phi'\left(x - g\big(q_0^{do}\big)t\right) + \frac{\partial m}{\partial q}\big(q_0^{do}\big)\Phi\left(x - g\big(q_0^{do}\big)t\right)\right) te^{-m\left(q_0^{do}\right)t}. \end{aligned}$$

Numerical simulations are performed using (3.4.6) as the initial function with a set value for q_0^{do}. To show a sample population density and sensitivity that are dependent on our dissolved oxygen growth and mortality functions, we performed simulations corresponding to 2.2688 ppm DO, where

$$g\big(q_0^{do}\big) = 0.0077 \quad \text{and} \quad m\big(q_0^{do}\big) = 0.0086.$$

This amount of dissolved oxygen gives us a non-zero contribution from both the growth and mortality functions. In Figure 3.18, the corresponding sample population density and

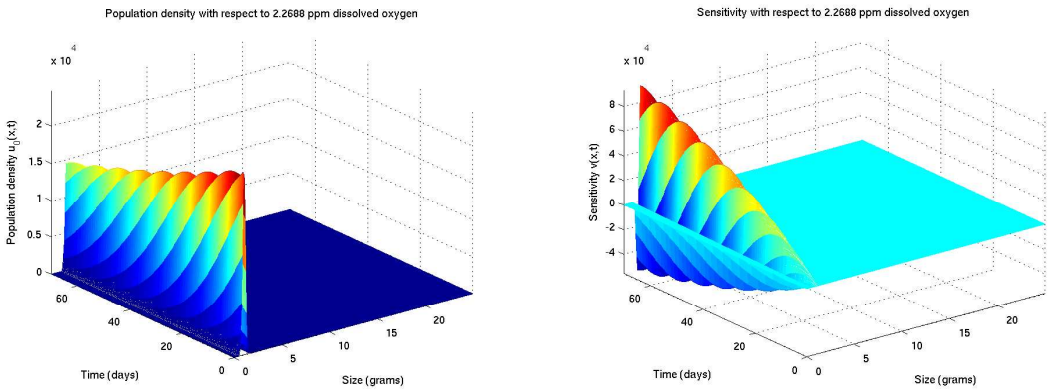

(a) (b)

Figure 3.18: (a) Population density and (b) sensitivity with 2.2688 ppm dissolved oxygen.

sensitivity are displayed. We see that $u\big(x,t;q^{do}\big)$ is not sensitive to q^{do} when the population density is low, and is less sensitive to the parameter near the initial time, where the initial function is dependent on x and not $\mathbf{q}$. As time progresses, we see that the sensitivity to the parameter q^{do} grows linearly. We note that there are positive and negative contributions in the sensitivity function, and the true magnitude of the sensitivity would be reflected if we included only the absolute value of each contribution. Regardless, the magnitude of the sensitivity is large (on the order of 10^4), which is not unreasonable when considering the magnitude of the population density.

3.4.2 pH Level

The pH level is another factor which contributes heavily to the water quality. We note that the pH level affects the ammonia levels in the water, and consequently the pH range must be closely monitored. Additionally, shrimp cannot tolerate very acidic or basic water, as the gills of the shrimp will be affected, causing reduced growth rates.

Growth and Mortality

We now consider a pH-dependent growth function, $g^{ph}\big(q^{ph}\big)$ where q^{ph} represents the pH level, which ranges from 5 to 9.5. The growth function is given by

$$g^{ph}\big(q^{ph}\big) = \frac{1}{\Big(1+e^{-4\left(q^{ph}-6.9\right)}\Big)\Big(1+e^{8\left(q^{ph}-8.8\right)}\Big)}$$

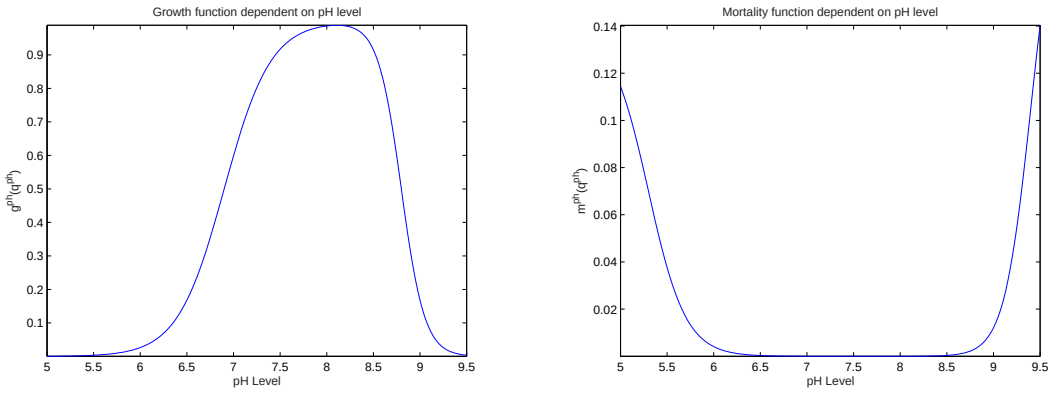

(a) (b)

Figure 3.19: (a) Growth and (b) mortality functions dependent on pH level.

and is shown in Figure 3.19(a). From [40] we know that the pH-dependent growth function should peak between 7.5 and 9.0, as water with pH levels in this range is generally suitable for shrimp production. The growth rate decreases if the pH falls below 5.0, and pH values greater than 9.5 may also be harmful to shrimp growth and survival. The corresponding mortality rate increases if the pH Level is outside of the proper range. This is indicated by the function

$$m^{ph}\left(q^{ph}\right) = \frac{.21}{1+e^{-7\left(q^{ph}-9.4\right)}} + \frac{.14}{1+e^{5\left(q^{ph}-5.3\right)}}$$

seen in Figure 3.19(b).

Sensitivity

To observe the effects of the pH level without considering the other contributing factors, we restrict the growth function (3.4.1) with a contribution of one from each of the remaining individual growth functions, as before. Similarly for the mortality function (3.4.2), the individual mortality functions for the other factors have zero contribution. Then we have

$$g\left(q^{ph}\right) = .25g^{ph}\left(q^{ph}\right) \quad \text{and} \quad m\left(q^{ph}\right) = m^{ph}\left(q^{ph}\right) + 0.0014. \tag{3.4.8}$$

We solve system (3.4.3) using the pH growth and mortality functions (3.4.8), and because $g^{ph}\left(q^{ph}\right)$ and $m^{ph}\left(q^{ph}\right)$ are not dependent on x, we can use the method of characteristics

to solve this system easily. The solution is given by

$$u_0\big(x,t;q_0^{ph}\big) = \Phi\left(x - g\big(q_0^{ph}\big)t\right) e^{-m\left(q_0^{ph}\right)t}$$

for a fixed pH level q_0^{ph}. The forcing function (3.4.5) used to solve the sensitivity system (3.4.4) is given by

$$F\Big(u_0\big(x,t;q_0^{ph}\big)\Big) = -\left(\frac{\partial g}{\partial q}\big(q_0^{ph}\big)\Phi'\Big(x - g\big(q_0^{ph}\big)t\Big) + \frac{\partial m}{\partial q}\big(q_0^{ph}\big)\Phi\Big(x - g\big(q_0^{ph}\big)t\Big)\right) e^{-m\left(q_0^{ph}\right)t}$$

where $\frac{\partial g}{\partial q}\big(q_0^{ph}\big)$ and $\frac{\partial m}{\partial q}\big(q_0^{ph}\big)$ are constant values. Then, using the method of characteristics, we obtain

$$\begin{aligned} v &= F\left(u_0\big(x,t;q_0^{ph}\big)\right)t \\ &= -\left(\frac{\partial g}{\partial q}\big(q_0^{ph}\big)\Phi'\left(x - g\big(q_0^{ph}\big)t\right) + \frac{\partial m}{\partial q}\big(q_0^{ph}\big)\Phi\left(x - g\big(q_0^{ph}\big)t\right)\right) te^{-m\left(q_0^{ph}\right)t}. \end{aligned}$$

We perform numerical simulations using the initial function (3.4.6) for a set value $q_0^{ph} = 9.093$. The corresponding growth and mortality functions,

$$g\big(q_0^{ph}\big) = 0.0219 \quad \text{and} \quad m\big(q_0^{ph}\big) = 0.0233$$

are displayed in Figure 3.20. This pH level gives us a non-zero contribution from both the growth and mortality. We see that $u\big(x,t;q^{ph}\big)$ is less sensitive to q^{ph} near the initial time, as $\Phi(x)$ is dependent on x and not $\mathbf{q}$. We see that as time progresses, the sensitivity to

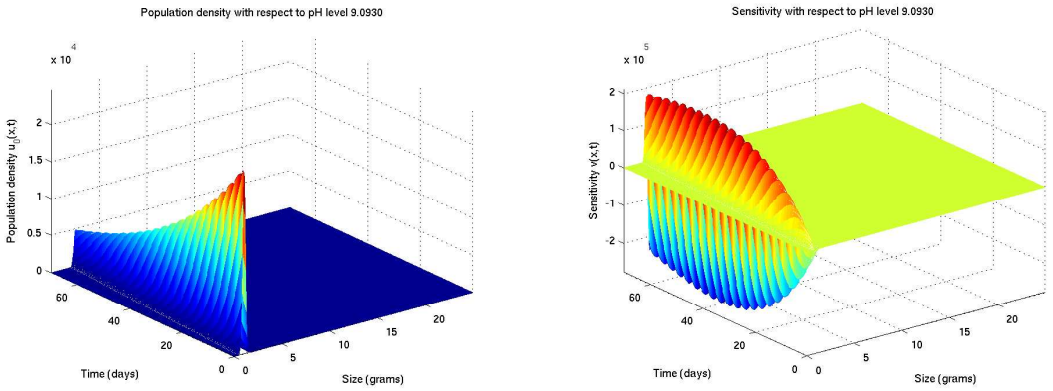

(a) (b)

Figure 3.20: (a) Population density and (b) sensitivity with pH level of 9.093.

the parameter q^{ph} seems to grow at an inversely proportional rate to that of the population density. We note that there are positive and negative contributions in the sensitivity function, and the true magnitude of the sensitivity would be reflected if we included only the absolute value of each contribution. Regardless, the magnitude of the sensitivity is large (on the order of 10^5), which is reasonable when considering the magnitude of the population density.

3.4.3 Salinity

Salinity is a measure of the concentration of salts in the water (i.e. the salinity of seawater is generally in the range 28-35 ppt). Shrimp gain the ability to regulate their internal salt and water balance as they grow out of the postlarval stage. Adult penaeid shrimp can tolerate a broad range in salinity; however, it is best that the salinity level not fluctuate heavily. In addition to temperature, the salinity levels in the water directly affect the solubility of oxygen [39].

Growth and Mortality

We now consider the dependency of the growth and mortality functions on salinity. Based on literature ([28, 33, 40]), we have created a growth function,

$$g^s\left(q^s\right) = \frac{1.009}{\left(1+e^{-1.5(q^s-9.5)}\right)\left(1+e^{0.45(q^s-24.5)}\right)},$$

where q^s ranges from 0.5 to 45 ppt. While the shrimp tolerate these levels of salinity, they grow best in the 7 to 34 ppt range, peaking near 15 ppt. This function is displayed in Figure 3.21(a). We represent the effects of salinity on the mortality of the shrimp in

$$m^s(q^s) = \frac{.1092}{1+e^{3.5(q^s-1.4)}}.$$

This function can be seen in Figure 3.21(b).

Sensitivity

To observe the effects of salinity alone, we allow the growth function (3.4.1) to have a contribution of one from each of the remaining individual growth functions. Likewise, when considering the mortality function (3.4.2), the individual mortality rates corresponding

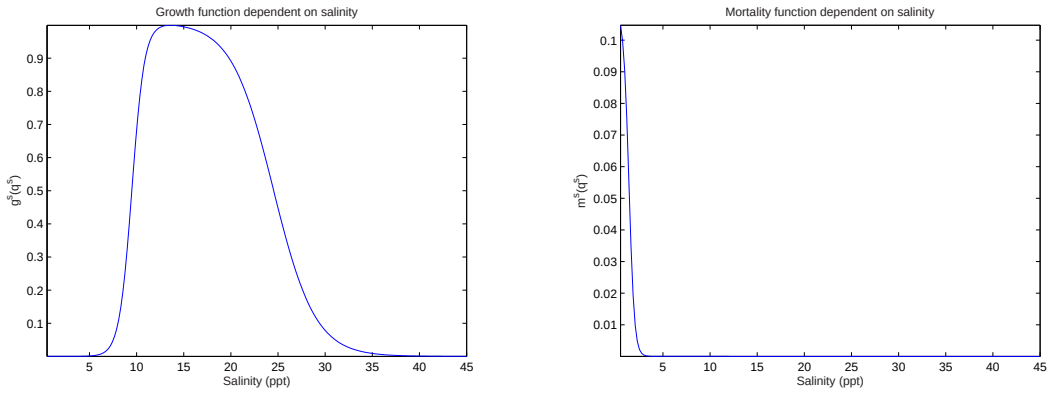

(a) (b)

Figure 3.21: (a) Growth and (b) mortality functions dependent on the salinity level.

to the other factors have zero contribution. Then we have

$$g(q^s) = .25g^s(q^s) \quad \text{and} \quad m(q^s) = m^s(q^s) + 0.0014. \tag{3.4.9}$$

We solve system (3.4.3) using the salinity growth and mortality functions (3.4.9), and since $g^s(q^s)$ and $m^s(q^s)$ are independent of x, we use the method of characteristics to solve this system easily. The population density is given as

$$u_0\left(x,t;q_0^s\right) = \Phi\left(x - g\left(q_0^s\right)t\right)e^{-m\left(q_0^s\right)t}$$

for a fixed amount of salinity given by q_0^s. Then the forcing function (3.4.5) used in the sensitivity system (3.4.4) is given by

$$F\left(u_0\left(x,t;q_0^s\right)\right) = -\left(\frac{\partial g}{\partial q}\left(q_0^s\right)\Phi'\left(x - g\left(q_0^s\right)t\right) + \frac{\partial m}{\partial q}\left(q_0^s\right)\Phi\left(x - g\left(q_0^s\right)t\right)\right)e^{-m\left(q_0^s\right)t}$$

with constant values $\frac{\partial g}{\partial q}\left(q_0^s\right)$ and $\frac{\partial m}{\partial q}\left(q_0^s\right)$. Then, using the method of characteristics again, we obtain the sensitivity

$$\begin{aligned} v &= F\left(u_0\left(x,t;q_0^s\right)\right)t \\ &= -\left(\frac{\partial g}{\partial q}\left(q_0^s\right)\Phi'\left(x - g\left(q_0^s\right)t\right) + \frac{\partial m}{\partial q}\left(q_0^s\right)\Phi\left(x - g\left(q_0^s\right)t\right)\right)te^{-m\left(q_0^s\right)t}. \end{aligned}$$

Using initial function (3.4.6) with a set value for q_0^s we can perform the numerical simulations. Initially, we allow $q_0^s = 0.5$ ppt, which yields a nonzero contribution from the mortality function. For this simulation,

$$g\left(q_0^s\right) = 0 \quad \text{and} \quad m\left(q_0^s\right) = 0.1061$$

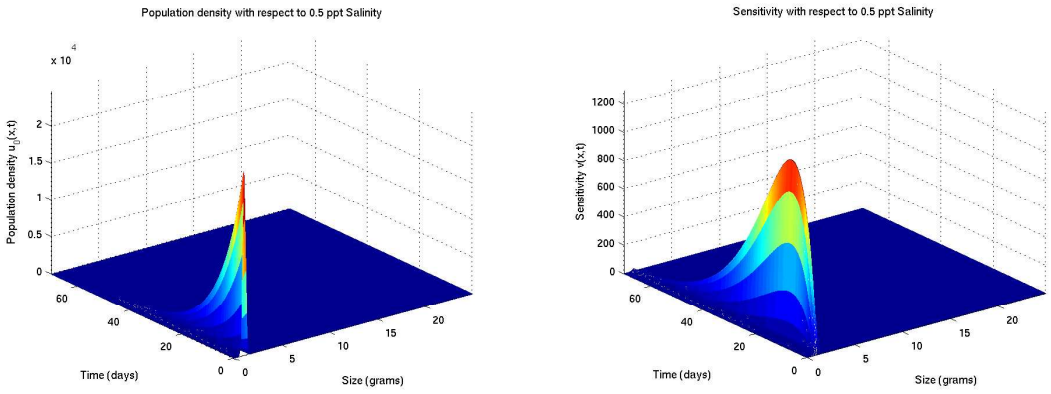

(a) (b)

Figure 3.22: (a) Population density and (b) sensitivity with 0.5 ppt salinity.

where the resulting population density and sensitivity plots can be viewed in Figure 3.22. We observe that $u(x,t;q^s)$ is less sensitive to the parameter near the initial time, as the initial function $\Phi(x)$ is not dependent $\mathbf{q}$. By choosing such a low amount of salinity, we have forced the population to respond poorly, and hence we see a rapid decline in the biomass, with no growth. The magnitude of the sensitivity is much lower than in the other sensitivity equations we have observed as a consequence of the reduced population density.

We also ran simulations corresponding to 15.0352 ppt salinity, where

$$g\left(q_0^s\right) = .2487 \quad \text{and} \quad m\left(q_0^s\right) = 0.0014,$$

and these plots can be seen in Figure 3.23. Then, as time progresses the sensitivity to the parameter q^s grows linearly. As with dissolved oxygen and pH level, we note that there are positive and negative contributions in the sensitivity function. The true magnitude of the sensitivity would be reflected if we included only the absolute value of each contribution. Regardless, the magnitude of the sensitivity is nearly seven times larger than the sensitivity displayed in Figure 3.22(b), which seems much more reasonable since the population density is not declining in this case.

3.4.4 Ammonia Levels

Ammonia can be both un-ionized (NH_3) and ionized (NH_4). While both forms are generally present in the water, only the un-ionized form is toxic to shrimp [40]. Con-

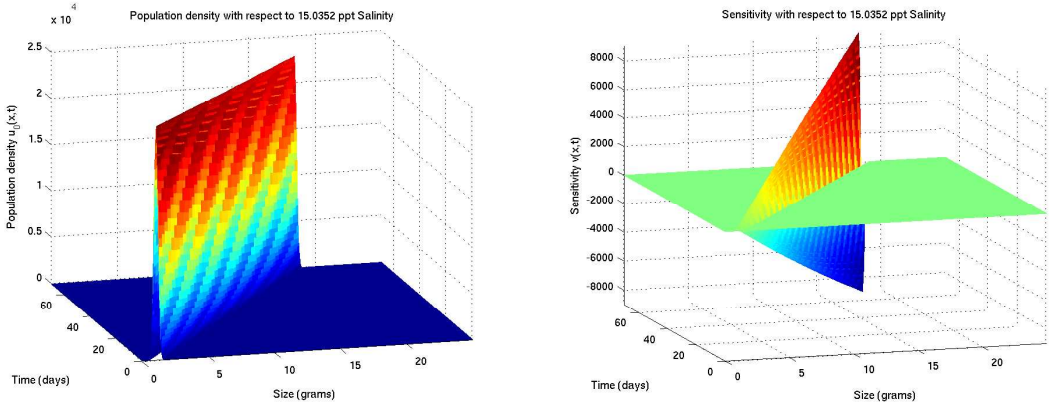

(a) (b)

Figure 3.23: (a) Population density and (b) sensitivity with 15.0352 ppt salinity.

centrations above 0.1 ppm are considered to be moderately lethal, although non-lethal concentrations above 0.03 ppm will still produce undesirable effects on shrimp, including reduced growth rates, swollen gills, low tolerance of low dissolved oxygen concentrations, and lower resistance to disease [39]. Generally, high concentrations of un-ionized ammonia can be reduced to safer levels by using a biofilter.

Growth and Mortality

We consider the effects that the amount of un-ionized ammonia has on the growth and mortality functions of the shrimp, and begin by creating a growth function,

$$g^{ua}(q^{ua}) = \frac{1}{1 + e^{70(q^{ua} - 0.06)}}$$

which is shown in Figure 3.24(a). In this function, q^{ua} represents the amount of un-ionized ammonia nitrogen, which ranges from 0 to 1.3 ppm. We want the growth to peak very close to 0 ppm [40]. We measure the total amount of ammonia nitrogen (TAN), represented here by q^a, while only the un-ionized ammonia is toxic to shrimp. The proportion of TAN that is un-ionized is dependent upon the temperature as well as the pH level, and is given by the function $A\left(q^H, q^{ph}\right)$. Hence, $q^{ua} = q^a A\left(q^H, q^{ph}\right)$, where

$$A\left(q^H, q^{ph}\right) = \left(\frac{0.0193\left(q^H + 24.7681\right)}{1 + e^{-2.4369\left(q^{ph} - 8.8614\right)}}\right) - \frac{0.2129}{\left(1 + e^{-2.97\left(q^{ph} - 8.44\right)}\right)\left(1 + e^{3.7\left(q^{ph} - 9.85\right)}\right)}.$$

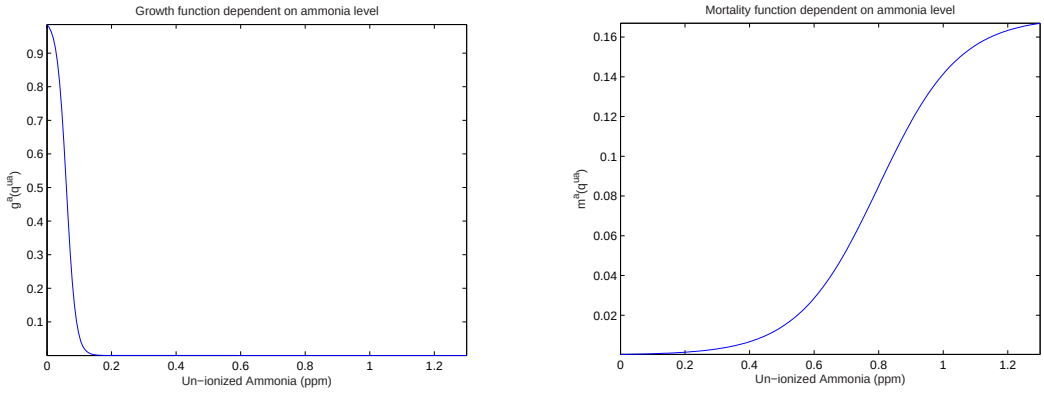

(a) (b)

Figure 3.24: (a) Growth and (b) mortality functions dependent on the un-ionized ammonia level.

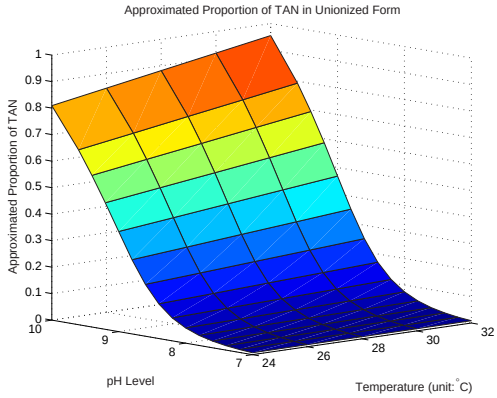

Figure 3.25: Proportion of TAN in the un-ionized form as a function of temperature and pH.

This is an approximation to data provided in [39], and is shown in Figure 3.25. When we combine the growth functions, we have $g^{ua}\big(q^a A\big(q^H, q^{pH}\big)\big) = g^{ua}\big(q^{ua}\big)$. The effects that the ammonia levels have on the mortality of the shrimp are represented in

$$m^{ua}(q^{ua}) = \frac{0.17}{1 + e^{-8(q^{ua} - 0.8)}},$$

and can be seen in Figure 3.24(b).

Sensitivity

In order to observe the effects of the un-ionized ammonia on the shrimp without regard for the other environmental factors, we allow the growth function (3.4.1) to have a contribution of one from each of the remaining individual growth functions, as before. Similarly, for the mortality function (3.4.2), the individual mortality functions for the other factors have zero contribution. Then we see that

$$g(q^{ua}) = .25g^{ua}(q^{ua}) \quad \text{and} \quad m(q^{ua}) = m^{ua}(q^{ua}) + 0.0014. \tag{3.4.10}$$

We solve system (3.4.3) using the ammonia growth and mortality functions (3.4.10), and we use the method of characteristics to solve this system easily. The population density is

$$u_0\left(x,t;q_0^{ua}\right) = \Phi\left(x - g\left(q_0^{ua}\right)t\right)e^{-m\left(q_0^{ua}\right)t}$$

for a fixed un-ionized ammonia concentration given by q_0^{ua}. Then the forcing function (3.4.5) used in the sensitivity system (3.4.4) is given by

$$F\left(u_0\left(x,t;q_0^{ua}\right)\right) = -\left(\frac{\partial g}{\partial q}\left(q_0^{ua}\right)\Phi'\left(x - g\left(q_0^{ua}\right)t\right) + \frac{\partial m}{\partial q}\left(q_0^{ua}\right)\Phi\left(x - g\left(q_0^{ua}\right)t\right)\right)e^{-m\left(q_0^{ua}\right)t}$$

with $\frac{\partial g}{\partial q}\left(q_0^{ua}\right)$ and $\frac{\partial m}{\partial q}\left(q_0^{ua}\right)$ as constants. Using the method of characteristics, we then obtain

$$\begin{aligned} v &= F\left(u_0\left(x,t;q_0^{ua}\right)\right)t \\ &= -\left(\frac{\partial g}{\partial q}\left(q_0^{ua}\right)\Phi'\left(x - g\left(q_0^{ua}\right)t\right) + \frac{\partial m}{\partial q}\left(q_0^{ua}\right)\Phi\left(x - g\left(q_0^{ua}\right)t\right)\right)te^{-m\left(q_0^{ua}\right)t}. \end{aligned}$$

We perform numerical simulations using (3.4.6) as the initial function for a set value for q_0^{ua}. We ran simulations corresponding to 0 ppm un-ionized ammonia present, where

$$g\left(q_0^{ua}\right) = 0.2463 \quad \text{and} \quad m\left(q_0^{ua}\right) = 0.0017$$

as well as 1.2608 ppm, where

$$g\left(q_0^{ua}\right) = 0 \quad \text{and} \quad m\left(q_0^{ua}\right) = 0.1672,$$

and these plots can be seen in Figures 3.26 and 3.27, respectively.

With 0 ppm un-ionized ammonia, there is maximal growth and minimal mortality, and when there is 1.2608 ppm un-ionized ammonia, there is minimal growth and maximal mortality. With 0 ppm un-ionized ammonia, we see that $u\left(x,t;q^{ua}\right)$ is not sensitive to q^{ua}

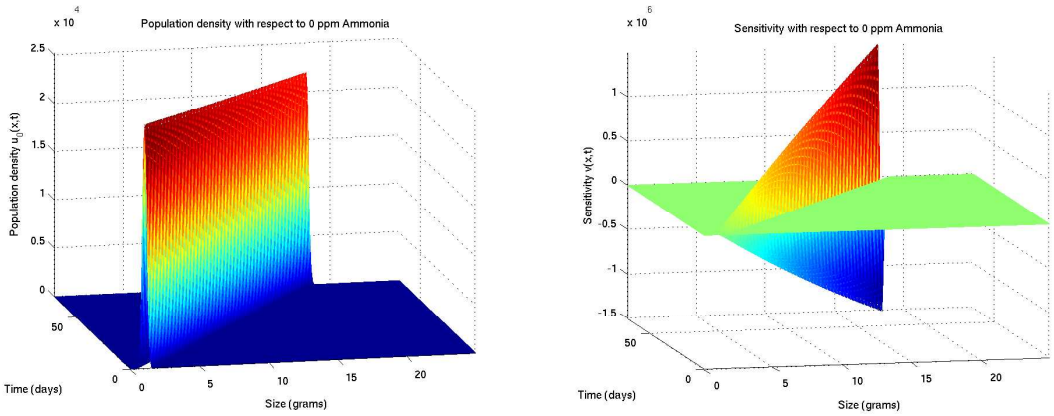

(a) (b)

Figure 3.26: (a) Population density and (b) sensitivity with un-ionized ammonia level of 0 ppm.

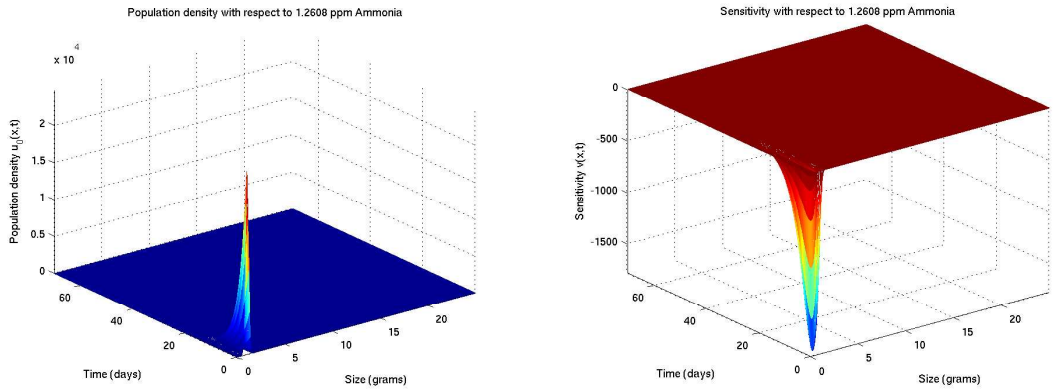

(a) (b)

Figure 3.27: (a) Population density and (b) sensitivity with un-ionized ammonia level of 1.2608 ppm.

when the population density is low, and is less sensitive to the parameter near the initial time, where the initial function is not dependent on **q**. Then we see that as time progresses the sensitivity to the parameter q^{ua} grows linearly, see Figure 3.26(b). There are again positive and negative contributions in the sensitivity function, and the true magnitude of the sensitivity would be reflected if we included only the absolute value of each contribution. Regardless, the magnitude of the sensitivity is large (on the order of 10^5), which is not unreasonable when considering the magnitude of the population density.

Next, we consider the plots in Figure 3.27 corresponding to 1.2608 ppm un-ionized ammonia. By choosing such a high amount of un-ionized ammonia, we have forced the population to respond poorly, and hence we see a rapid decline in the biomass, with no growth. The magnitude of the sensitivity is much lower (than when we considered 0 ppm un-ionized ammonia) as a consequence of the immediate decay in population density.

3.4.5 Nitrite Level

High levels of nitrite in the water lower the tolerance of shrimp to low dissolved oxygen levels, as well as causing retarded growth and mortalities [23, 39]. As with ammonia, a biofilter is the best means to keep the levels of nitrite low in the water.

Growth and Mortality

We consider the effect that the nitrite level has on the growth and mortality functions of the shrimp. The nitrite levels should remain very low for optimal growth, particularly at low salinities [13]. The shrimp can tolerate levels as high as 20 ppm, however the growth process is halted with nitrite levels higher than 2 ppm. This is reflected in the growth function

$$g^n(q^n) = \frac{1}{1 + e^{6.5(q^n - 0.7)}},$$

which is shown in Figure 3.28(a). In this function, q^n represents the nitrate level and ranges from 0 to 20 ppm. We want the growth to peak very close to 0 ppm.

Based on [39], we have constructed a nitrite-dependent mortality function given by

$$m^n(q^n) = \frac{.1733}{1 + e^{-0.6(q^n - 10.8)}}.$$

This function, shown in Figure 3.28(b), represents an increasing rate as the amount of nitrite increases.

Sensitivity

In order to observe the effects from the nitrite alone, we allow the growth function (3.4.1) to have a contribution of one from each of the remaining individual growth functions. Similarly for the mortality function (3.4.2), the individual mortality functions for the other

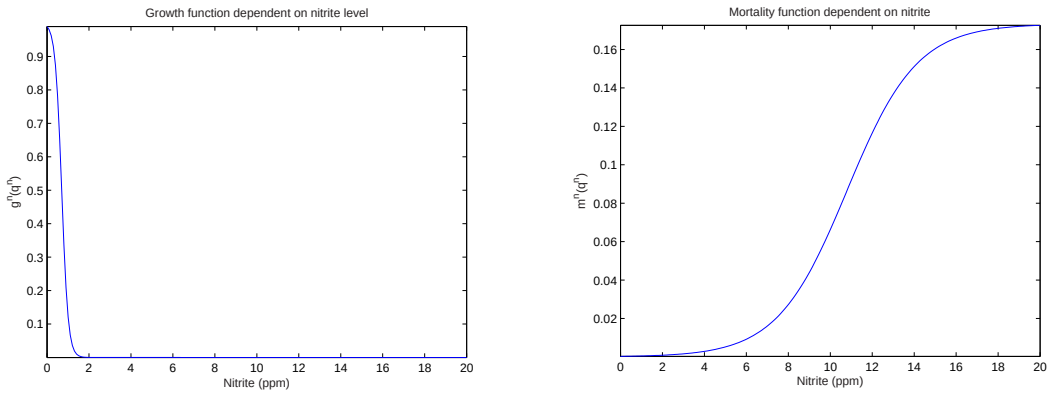

(a) (b)

Figure 3.28: (a) Growth and (b) mortality functions dependent on nitrite level.

factors have zero contribution. Then we see that

$$g(q^n) = .25g^n(q^n) \quad \text{and} \quad m(q^n) = m^n(q^n) + 0.0014. \tag{3.4.11}$$

We solve system (3.4.3) using the nitrite growth and mortality functions (3.4.11), and use the method of characteristics to solve this system. The solution is

$$u_0\left(x,t;q_0^n\right) = \Phi\left(x - g\left(q_0^n\right)t\right)e^{-m\left(q_0^n\right)t}$$

for a nitrite concentration given by q_0^n. Then the forcing function (3.4.5) used for the sensitivity system (3.4.4) is given by

$$F\left(u_0\left(x,t;q_0^n\right)\right) = -\left(\frac{\partial g}{\partial q}\left(q_0^n\right)\Phi'\left(x - g\left(q_0^n\right)t\right) + \frac{\partial m}{\partial q}\left(q_0^n\right)\Phi\left(x - g\left(q_0^n\right)t\right)\right)e^{-m\left(q_0^n\right)t}$$

with constants $\frac{\partial g}{\partial q}\left(q_0^n\right)$ and $\frac{\partial m}{\partial q}\left(q_0^n\right)$. Then, using the method of characteristics, we obtain

$$\begin{aligned} v &= F\left(u_0\left(x,t;q_0^n\right)\right)t \\ &= -\left(\frac{\partial g}{\partial q}\left(q_0^n\right)\Phi'\left(x - g\left(q_0^n\right)t\right) + \frac{\partial m}{\partial q}\left(q_0^n\right)\Phi\left(x - g\left(q_0^n\right)t\right)\right)te^{-m\left(q_0^n\right)t}. \end{aligned}$$

We perform numerical simulations with initial function (3.4.6) for a set value for q_0^n. Initially, we allow $q_0^n = 0$ ppm, which is the value corresponding to the maximum growth value, and the growth and mortality values for this nitrite quantity are given by

$$g\left(q_0^n\right) = 0.2474 \quad \text{and} \quad m\left(q_0^n\right) = 0.0017.$$

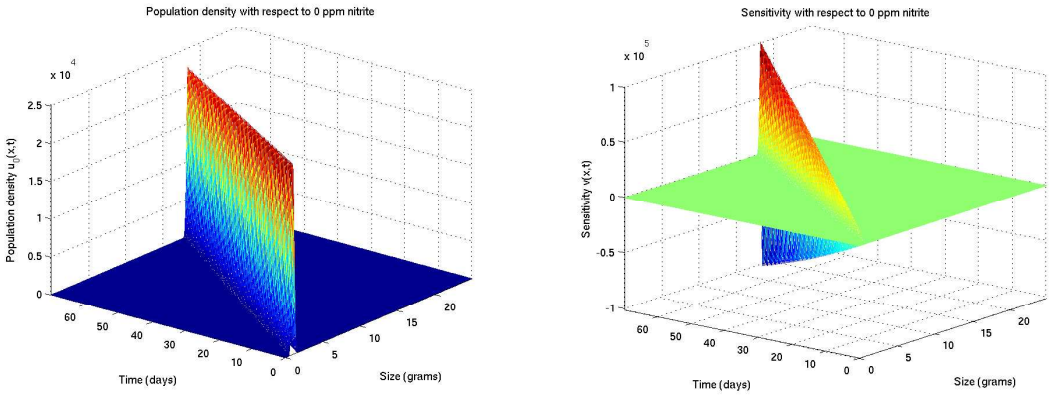

(a) (b)

Figure 3.29: (a) Population density and (b) sensitivity with 0 ppm nitrite.

The resulting population density and sensitivity plots can be viewed in Figure 3.29. We see that $u(x,t;q^n)$ is less sensitive to the parameter q^n when the population density is small, and is also less sensitive to the parameter near the initial time. Then as time progresses the sensitivity to the parameter q^n grows linearly, see Figure 3.29(b). There are again positive and negative contributions in the sensitivity function, and the true magnitude of the sensitivity would be reflected if we included only the absolute value of each contribution. Regardless, the magnitude of the sensitivity is large (on the order of 10^5), which is reasonable when considering the magnitude of the population density.

We also ran simulations corresponding to 20 ppm nitrite, where

$$g\left(q_0^n\right) = 0 \quad \text{and} \quad m\left(q_0^n\right) = 0.1740,$$

and these plots can be seen in Figure 3.30. By choosing such a high amount of nitrite, we have forced the population to respond poorly, and hence we again observe a rapid decline in the biomass, with no growth, see Figure 3.30(a). The magnitude of the sensitivity is much lower than any of the other sensitivities we have observed in this section, and is a consequence of the immediate decay in population density.

3.4.6 Temperature

Water temperature strongly affects the health of the Pacific white shrimp since their internal temperature is environmentally regulated. Temperature also affects other

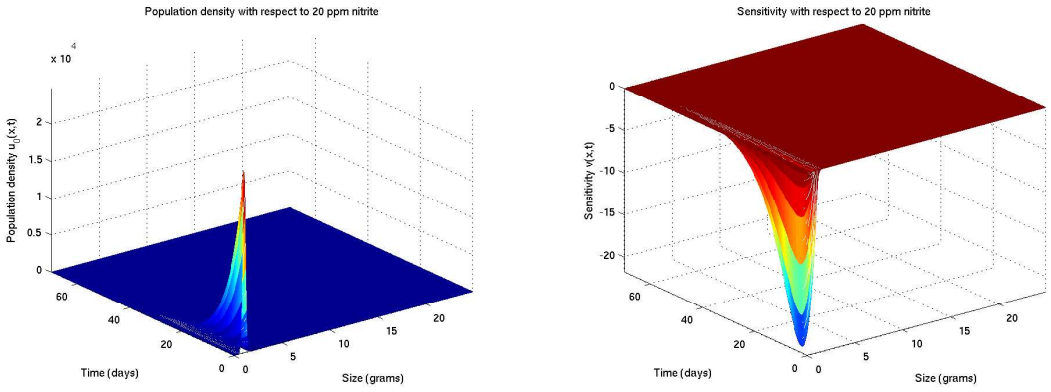

(a) (b)

Figure 3.30: (a) Population density and (b) sensitivity with 20 ppm nitrite.

aspects of the water quality such as the dissolved oxygen level and proportion of un-ionized ammonia.

Growth and Mortality

We consider a growth function which is dependent upon temperature as well as size. The growth function, shown in Figure 3.31, is given as

$$g^H\left(x, q^H\right) = \frac{1.0309}{\left(1 + e^{-0.62\left(q^H - 25 + \frac{53}{250}x\right)}\right)\left(1 + e^{\left(4 - \frac{29}{250}x\right)\left(q^H - 32 + \frac{17}{125}x\right)}\right)}.$$

We consider temperature ranging from 10 to 33 degrees, and size ranging from 0 to 25 grams. We desire the peak growth to occur at approximately 30°C when the shrimp are small (around one gram). We desire the peak growth to occur around 27°C when the shrimp are approximately 12-18 grams [19]. As the degree of peak growth gets further from 33°C, the rate of decrease (where $\frac{\partial g^H}{\partial q^H} < 0$) declines. It is important that the growth rate of the shrimp not decrease to zero before 33°C. The mortality function that is dependent on temperature is not size-dependent, and is given by

$$m^H\left(q^H\right) = \frac{.1}{1 + e^{4(32.5 - q^H)}} + \frac{.14}{1 + e^{(q^H - 12)}},$$

which represents a higher mortality rate as the temperature gets too high or too low, see Figure 3.32.

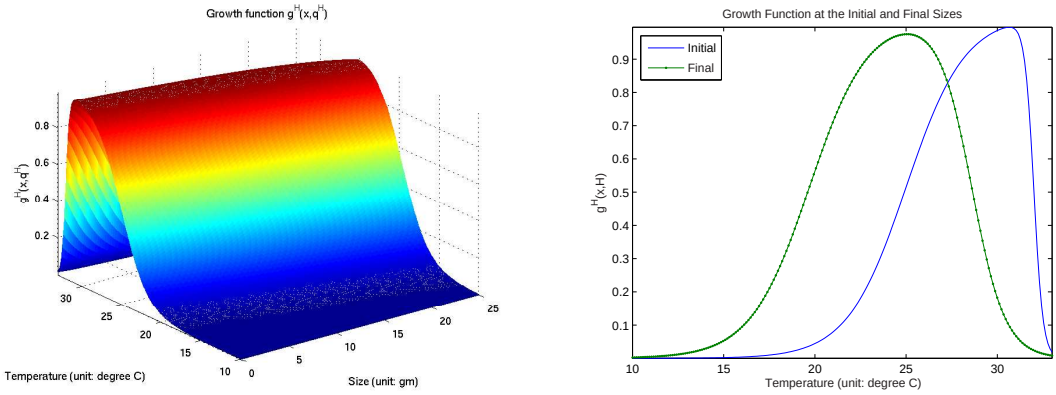

(a) (b)

Figure 3.31: (a) Growth function dependent on size and temperature for all sizes x, and (b) for the initial and final sizes only.

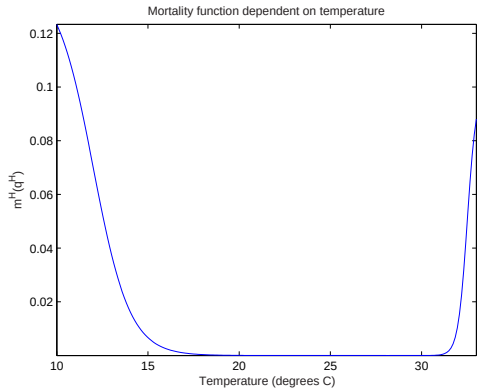

Figure 3.32: Mortality function dependent on temperature.

Sensitivity

In order to observe the effects of the temperature alone, we allow the growth function (3.4.1) to have a contribution of one from each of the remaining individual growth functions. Similarly for the mortality function (3.4.2), the individual mortality functions for the other factors have zero contribution. Then we see that

$$g(x, q^H) = .25 g^H(x, q^H) \quad \text{and} \quad m(q^H) = m^H(q^H) + 0.0014. \tag{3.4.12}$$

We solve system (3.4.3) using the temperature growth and mortality functions (3.4.12), but since $g^H\left(x, q^H\right)$ is dependent on x, we note that this system will be more challenging to solve than the others. We use the method of characteristics as when solving for the population densities in the hybrid model, and we represent the system for a fixed temperature q_0^H as

$$u_0\left(x,t;q_0^H\right) = \Phi(\hat{x}(t))\frac{g(\hat{x}(t))}{g(x)}\exp\left(-\int_{\hat{x}(t)}^{x}\frac{m(\xi)}{g(\xi)}d\xi\right),$$

if $x \geq G^{-1}(t)$, and

$$u_0\left(x,t;q_0^H\right) = 0$$

otherwise. Here, $\hat{x}(t) = G^{-1}(G(x)+t)$ and $G(x) = \displaystyle\int_0^x \frac{1}{g(\xi)}d\xi$. Then, because $v(0,x) = 0$, we have

$$v = e^{-\int_0^t m(\hat{x}(\tau))+g_x(\hat{x}(\tau))\,d\tau}\int_0^t e^{-\int_s^t m(\hat{x}(\tau))+g_x(\hat{x}(\tau))\,d\tau}F\left(u_0\left(x,t;q_0^H\right)\right)\,ds$$

where $F(u_0)$ can be represented as in (3.4.5).

When we previously considered the other environmental factors, we were able to analytically solve for the biomass and the sensitivities. However, in this case, the more complicated growth function prevented us from successfully solving the biomass and sensitivities in this manner. In order to represent the system graphically, we need to use a finite difference scheme; however, this is not currently easy to implement. Due to the sharp spike in the initial condition, the scheme is unable to reasonably approximate the solution curves. In order to represent this well, we would need to implement a moving mesh so that the grid would be refined in the region of interest for better results. This will be left to future work.

3.4.7 Concluding Environmental Condition Remarks

Based on the available literature [23, 28, 33, 39, 40] as well as consultation with biologists in this field [13, 19], we were able to reasonably establish the amount of influence that each environmental factor has on the growth and mortality of non-infected shrimp, given our created growth and mortality functions (3.4.1) and (3.4.2).

In the future we would like to determine a realistic set of growth and mortality functions which include influences from each of the affecting environmental conditions. The affecting factors have varying levels of influence on the shrimp, and we would like to take this into consideration when determining the new rate functions. The factors, listed in the order

of importance, are nitrite, un-ionized ammonia, dissolved oxygen, pH level, temperature, and salinity [13]. By studying the sensitivities associated with each factor, performing extensive searches in the available literature, and consulting further with biologists in this field, we should be able to appropriately weight each influence from the environmental conditions in the creation of new rate functions.

Chapter 4

Conclusions and Future Directions

In summary, we have illustrated the usefulness and feasibility of using sensitivity analysis in parameter estimation and modeling problems.

In Chapter 2 we established that the traditional and generalized sensitivities are both essential tools in parameter estimation and inverse problems. We used the logistic model as a simple example to demonstrate the effectiveness of each type of sensitivity function. Additionally, the we considered properties of the Fisher information matrix as tools for the formulation of data collection for parameter estimation problems. We will continue efforts in numerically implementing the optimal time point distribution methodology as outlined in Section 2.2.3.

In Chapter 3 we considered the hybrid model with components (3.2.1) and (3.3.1), based on the widely used Sinko-Streifer equations for size-structured populations. We derived the partial differential equations for sensitivities of the population density. We then verified that the systems of differential equations could be numerically represented with finite difference schemes in order to approximate the analytical solutions. Due to our investigations, we see that the correct sensitivity equations can be formally obtained by differentiating the population equation of interest with respect to each rate function. This will be essential when investigating the sensitivities pertaining to realistic rates (growth, mortality, latent-to-acute, etc.) for a model such as the shrimp biomass and vaccine production system.

In the hybrid model with components (3.2.1) and (3.3.1), we made the assumption that each shrimp of size x has the same growth rate. In actuality, the shrimp grow at different rates, and hence we would like to incorporate this when modeling the biomass and

vaccine production in the future [3]. Additionally, we would like to determine a realistic set of growth and mortality functions for the Pacific white shrimp which include influences from each of the affecting environmental conditions.

Bibliography

[1] H.T. Banks, V.A. Bokil, S. Hu, A.K. Dhar, R.A. Bullis, C.L. Browdy, and F.C.T. Allnutt. Modeling shrimp biomass and viral infection for production of biological countermeasures. *Mathematical Biosciences and Engineering*, 3(4):635–660, 2006.

[2] H.T. Banks, M. Davidian, and J. Samuels Jr. An inverse problem statistical methodology summary. Center for Research in Scientific Computation Report CRSC-TR07-14, North Carolina State University, August 2007.

[3] H.T. Banks, J.L. Davis, S.L. Ernstberger, S. Hu, E. Artimovich, A.K. Dhar, and C.L. Browdy. Comparison of Probabilistic and Stochastic Formulations in Modeling Growth Uncertainty and Variability. Center for Research in Scientific Computation Report CRSC-TR08-03, North Carolina State University, February 2008; *Journal of Biological Dynamics*, accepted.

[4] H.T. Banks, S. Dediu, and S.L. Ernstberger. Sensitivity functions and their uses in inverse problems. Center for Research in Scientific Computation Report CRSC-TR07-12, North Carolina State University, July 2007; *Journal of Inverse and Ill-posed Problems*, 15(7)683–708, 2007.

[5] H.T. Banks, S. Dediu, and H.K. Nguyen. Sensitivity of dynamical systems to parameters in a convex subset of a topological vector space. *Mathematical Biosciences and Engineering*, 4:403–430, 2007.

[6] H.T. Banks, S.L. Ernstberger, and S.L. Grove. Standard errors and confidence intervals in inverse problems: sensitivity and associated pitfalls. Center for Research in Scientific Computation Report CRSC-TR06-10, North Carolina State University, March 2006; *Journal of Inverse and Ill-posed Problems*, 15(1)1–18, 2007.

[7] H.T. Banks, S.L. Ernstberger, and S. Hu. Sensitivity equations for a size-structured population model. Center for Research in Scientific Computation Report CRSC-TR07-18, North Carolina State University, September 2007; *Quarterly of Applied Mathematics*, accepted.

[8] H.T. Banks and F. Kappel. Transformation semigroups and L^1-approximation for size structured population models. *Semigroup Forum*, 38(1):141–155, 1989.

[9] H.T. Banks, F. Kappel, and C. Wang. Weak solutions and differentiability for size structured population models. *International Series of Numerical Mathematics*, 100:35–50, 1991.

[10] J.J. Batzel, F. Kappel, D. Schneditz, and H.T. Tran. *Cardiovascular and Respiratory Systems: Modeling, Estimation and Control*. Frontiers in Applied Mathematics. SIAM, 2006.

[11] R.E. Bellman and K.L. Cooke. *Differential-Difference equations*. Academic Press, New York, 1963.

[12] J. Borggaard and J. Burns. A PDE sensitivity equation method for optimal aerodynamic design. *Journal of Computational Physics*, 136(2):367–384, 1997.

[13] C.L. Browdy. Personal communication, June 2006.

[14] D.P. Bureau, P.A. Azevedo, M. Tapia-Salazar, and G. Cuzon. Pattern and cost of growth and nutrient deposition in fish and shrimp: Potential implications and applications. *Potential Implications and Applications. Avances en Nutricion Acuicola V: Memorıas del Quinto Simposium Internacional de Nutricion Acucola*, pages 19–22, 2000.

[15] K.P. Burnham and D.R. Anderson. *Model Selection and Multimodel Inference: A Practical Information-theoretic Approach*. Springer, 2002.

[16] À. Calsina and J. Saldaña. A model of physiologically structured population dynamics with a nonlinear individual growth rate. *Journal of Mathematical Biology*, 33(4):335–364, 1995.

[17] G. Casella and R.L. Berger. *Statistical Inference*. Thomson Learning, Pacific Grove, CA, 2002.

[18] M. Davidian and D.M. Giltinan. *Nonlinear Models for Repeated Measurement Data*. Monographs on Statistics and Applied Probability. Chapman & Hall/CRC, 1995.

[19] A.K. Dhar. Personal communication, July 2006.

[20] A.K. Dhar, J.A. Cowley, K.W. Hasson, and P.J. Walker. Genomic organization, biology, and diagnosis of Taura syndrome virus and yellowhead virus of penaeid shrimp. *Advances in Virus Research*, 63:353–421, 2004.

[21] V.V. Fedorov and P. Hackl. *Model-Oriented Design of Experiments*. Lecture Notes in Statistics. Springer, 1997.

[22] H. von Foerster. Some remarks on changing populations. In F. Stohlman Jr., editor, *The Kinetics of Cellular Proliferation*, pages 382–407. Grune and Stratton, New York, 1959.

[23] A. Gross, S. Abutbul, and D. Zilberg. Acute and chronic effects of nitrite on white shrimp, litopenaeus vannamei, cultured in low-salinity brackish water. *Journal of the World Aquaculture Society*, 35(3):315–321, 2004.

[24] E.J. Haug, K.K. Choi, and V. Komkov. *Design Sensitivity Analysis of Structural Systems*. Academic Press, Orlando, FL, 1986.

[25] K. Ito, F. Kappel, and G. Peichl. A fully discretized approximation scheme for size-structured population models. *SIAM Journal of Numerical Analysis*, 28(4):923–954, 1991.

[26] D.H. Jiang, A.L. Lawrence, W.H. Neill, and H. Gong. Effects of temperature and salinity on nitrogenous excretion by Litopenaeus vannamei juveniles. *Journal of Experimental Marine Biology and Ecology*, 253(2):193–209, 2000.

[27] M. Kot. *Elements of Mathematical Ecology*. Cambridge University Press, 2001.

[28] S. Laramore, C.R. Laramore, and J. Scarpa. Effect of low salinity on growth and survival of postlarvae and juvenile *Litopenaeus vannamei*. *Journal of the World Aquaculture Society*, 32(4):385–392, 2001.

[29] J.M. Lotz, A.M. Flowers, and V. Breland. A model of Taura syndrome virus (TSV) epidemics in Litopenaeus vannamei. *Journal of Invertebrate Pathology*, 83(2):168–176, 2003.

[30] A.G. McKendrick. Applications of mathematics to medical problems. *Proceedings of the Edinburgh Mathematical Society*, 44:98–130, 1926.

[31] J.A.J Metz and O. Diekmann. *The Dynamics of Physiologically Structured Populations*, volume 68 of *Lecture Notes in Biomathematics*. Springer-Verlag, 1986.

[32] O. Pironneau. Optimal Shape Design for Elliptic Systems. In *System Modeling and Optimization*, pages 42–66, New York, 1982. IFIP, Springer Berlin/Heidelberg.

[33] J. Ponce-Palafox, C.A. Martinez-Palacios, and L.G. Ross. The effects of salinity and temperature on the growth and survival rates of juvenile white shrimp, *Penaeus vannamei*, boone, 1931. *Aquaculture*, 157:107–115, 1997.

[34] A. Saltelli, K. Chan, and E.M. Scott, editors. *Sensitivity Analysis*. Wiley Series in Probability and Statistics. John Wiley & Sons Ltd., New York, 2000.

[35] G.A.F. Seber and C.J. Wild. *Nonlinear Regression*. Wiley Series in Probability and Statistics. John Wiley & Sons Ltd., New York, 2003.

[36] J.W. Sinko and W. Streifer. A new model for age-size structure of a population. *Ecology*, 48(6):910–918, 1967.

[37] L.G. Stanley and D.L. Stewart. *Design Sensitivity Analysis: Computational Issues of Sensitivity Equation Methods*. Frontiers in Applied Mathematics. SIAM, Philadelphia, 2002.

[38] K. Thomaseth and C. Cobelli. Generalized sensitivity functions in physiological system identification. *Annals of Biomedical Engineering*, 27(5):607–616, 1999.

[39] P. Van Wyk, M. Davis-Hodgkins, C.R. Laramore, K. Main, J. Mountain, and J. Scarpa. Farming marine shrimp in recirculating freshwater production systems: A practical manual. *FDACS Contract*, 4520, 1999.

[40] P. Van Wyk and J. Scarpa. Water quality requirements and management in farming marine shrimp in recirculating freshwater systems. *Harbor Branch Oceanic Institution. Department of Agriculture and Consumer Services, Florida*, 20, 1999.